PONTIFÍCIA UNIVERSIDADE CATÓLICA DO RIO GRANDE DO SUL
FACULDADE DE MEDICINA
PROGRAMA DE PÓS-GRADUAÇÃO EM MEDICINA E CIÊNCIAS DA SAÚDE

LEONARDO ASTOLFI ROSADO

A ENZIMA *CHIQUIMATO QUINASE* (EC 2.7.1.71) DE *MYCOBACTERIUM TUBERCULOSIS* COMO ALVO PARA O DESENVOLVIMENTO DE DROGAS

Porto Alegre
2011

LEONARDO ASTOLFI ROSADO

A ENZIMA *CHIQUIMATO QUINASE* (EC 2.7.1.71) DE *MYCOBACTERIUM TUBERCULOSIS* COMO ALVO PARA O DESENVOLVIMENTO DE DROGAS

Dissertação apresentada ao Programa de Pós-graduação em Medicina e Ciências da Saúde da Pontifícia Universidade Católica do Rio Grande do Sul.
Área de Concentração: Farmacologia e Bioquímica Molecular.

Orientador: Prof. Dr. Diógenes Santiago Santos
Co-orientador: Luiz Augusto Basso

Porto Alegre
2011

LEONARDO ASTOLFI ROSADO

A ENZIMA *CHIQUIMATO QUINASE* (EC 2.7.1.71) DE *MYCOBACTERIUM TUBERCULOSIS* COMO ALVO PARA O DESENVOLVIMENTO DE DROGAS

Dissertação apresentada ao Programa de Pós-graduação em Medicina e Ciências da Saúde da Pontifícia Universidade Católica do Rio Grande do Sul.
Área de Concentração: Farmacologia e Bioquímica Molecular.

Aprovada em 23 de fevereiro de 2011.

BANCA EXAMINADORA:

Dr. Maria Lucia Bianconi (UFRJ)

_____

Dr. Osmar Norberto de Souza (PUCRS)

_____

Dr. Walter Filgueira de Azevedo Jr (PUCRS)

_____

The world ain't all sunshine and rainbows. It's a very mean and nasty place and I don't care how tough you are it will beat you to your knees and keep you there permanently if you let it. You, me, or nobody is gonna hit as hard as life. But it ain't about how hard you hit. It's about how hard you can get hit and keep moving forward. How much you can take and keep moving forward.

- Rocky Balboa

Agradecimentos

Primeiramente eu gostaria de agradecer aos meus orientadores, os professores Diógenes Santigo Santos e Luiz Augusto Basso pelo apoio durante os anos em que este projeto se desenvolveu, sempre incentivando e orientando em busca do conhecimento cientifico e na minha formação como pesquisador e pessoa.

Eu gostaria de agradecer a todos os meus colegas de laboratório pela ajuda, incentivo, amizade e companheirismo, principalmente aos colegas Christiano Ev Neves, Daniel Lorenzini, José Eduardo Nunes, Leonardo Martinelli, Rodrigo Ducati, Thiago Milech e Valnês Jr.

Eu quero agradecer aos meus amigos de fora do meio acadêmico (a galera do futebol), que sempre estiveram do meu lado mesmo antes deste projeto e sempre me incentivaram e estiveram presentes durante os momentos bons e ruins.

Eu não poderia deixar de salientar a importância de algumas pessoas, pois elas foram fundamentais durante o desenvolvimento desta dissertação, pois sempre estiveram por perto, ajudando e principalmente descontraindo nos momentos difíceis, Ardala Breda, Diana Rostirola e Claudia Paiva Nunes, um muito obrigado pelas risadas e momentos de descontração.

Não esquecendo a pessoa que sempre esteve ao meu lado, ajudando, incentivando, com carinho e dedicação, a minha namorada Daiana Renck, que mesmo nos momentos mais complicados me ajudou a achar uma resposta para as minhas duvidas, tanto no meio pessoal como profissional, sempre amável e compreensiva. Não tenho palavras pra dizer tudo que gostaria, então, resumidamente, eu te amo.

E por fim, mas não menos importante, eu gostaria de agradecer a minha família, que sempre me apoiou incondicionalmente e sempre esteve ao meu lado. Alguns problemas de saúde familiar ocorreram durante o desenvolvimento deste projeto, porem eles serviram pra salientar o quão importante vocês são pra mim e o quanto eu amo vocês. Pai, Mãe e Irmão, Muito obrigado por tudo.

Resumidamente, obrigado a todos!

Resumo

A tuberculose prevalece como uma das principais causas de morte no mundo ocasionadas por um único agente infeccioso, o *Mycobacterium tuberculosis*. A enzima Chiquimato Quinase (*Mt*SK) codificada pelo gene *aroK* de *M. tuberculosis*, quinta enzima da via do chiquimato, catalisa a transferência de um grupo fosfato do ATP para o carbono 3 do grupo hidroxila do chiquimato, formando chiquimato-3-fosfato e ADP. A interrupção do gene *aroK* demonstrou que a enzima *Mt*SK é essencial para a viabilidade do *M. tuberculosis*. Neste trabalho, apresentamos a purificação da enzima *Mt*SK até a homogeneidade, análise por espectrometria de massa, sequenciamento de aminoácidos da porção N-Terminal, determinação do estado oligomérico da enzima em solução, cinética em estado estacionário, espectroscopia de fluorescência e calorimetria de titulação isotérmica. Os resultados encontrados sugerem que a reação catalisada pela enzima monomérica *Mt*SK segue um mecanismo em equilíbrio-rápido aleatório para a adição dos substratos e uma liberação ordenada dos produtos, onde a liberação do chiquimato-3-fosfato é seguida pela liberação do ADP, resultando na enzima na sua forma livre. Os resultados de calorimetria demonstraram uma grande diferença de calor gerada na associação da enzima livre aos seus ligantes, revelando assinaturas termodinâmicas de interações não-covalentes para cada processo de ligação. Estes resultados ajudaram a compreender melhor o modo de ação da enzima *Mt*SK e podem subsequentemente serem úteis para guiar o desenho racional de inibidores relacionados a esta enzima e que possam ser avaliados posteriormente como drogas anti-TB.

Abstract

Tuberculosis (TB) still remains as one of main cause of mortality worldwide due to a single infectious agent, *Mycobacterium tuberculosis*. The *aroK*-encoded *M. tuberculosis* Shikimate Kinase (*Mt*SK), the fifth enzyme of the shikimate pathway, catalyzes phosphate transfer from ATP to the carbon-3 hydroxyl group of shikimate, yielding shikimate 3-phosphate and ADP. Disruption of *aroK* gene has demonstrated that *Mt*SK is essential for the viability of *M. tuberculosis*. Here we present purification of *Mt*SK to homogeneity, mass spectrometry analysis, N-terminal amino acid sequencing, and oligomeric state determination of the recombinant protein. Steady-state kinetics, and studies on ligand binding by fluorescence spectroscopy and isothermal titration calorimetry (ITC) suggest that the chemical reaction catalyzed by monomeric *Mt*SK follows a rapid-equilibrium random order of substrate binding, and ordered product release in which shikimate-3-phosphate release is followed by ADP dissociation to yield free enzyme. ITC results showed significant heat changes upon ligand binding to free *Mt*SK enzyme, thereby providing thermodynamic signatures of non-covalent interactions to each binding process. These results provide a better understanding of the mode of action of *Mt*SK that should be useful to guide the rational design of inhibitors of this enzyme that can be further be evaluated as anti-TB drugs.

Lista de Abreviaturas e Siglas

ADP, adenosina 5'-difosfato;

ATP, adenosina 5'-trifosfato;

***Ec*SK**, SK de *Erwinia chrysanthemi* codificada pelo gene *aroL*;

E4P, D-eritrose 4-fosfato;

ESI-MS, espectrometria de massa com ionização por *eletrospray*;

HEPES, do inglês *N-2-hydroxyethylpiperazyne-N'-2-ethanesulfonic acid*;

ITC, calorimetria de titulação isotérmica;

LDH, L-lactato desidrogenase;

MDR-TB, infecção humana causada por cepas de *M. tuberculosis* multirresistentes;

***Mt*SK**, Chiquimato Quinase de *Mycobacterium tuberculosis*;

NADH, nicotinamida adenina dinucleotídeo reduzido;

NMP, nucleotídeo monofosfato;

PEP, fosfoenolpiruvato;

PK, piruvato quinase;

SDS-PAGE, do inglês *sodium dodecyl sulfate-polyacrylamide gel eletrophoresis*;

SKH, chiquimato, [3*R*-(3α,4α,5β)]3,4,5-trihidroxi-1-ciclohexano-1-ácido carboxílico;

S3P, chiquimato 3-fosfato;

TB, tuberculose;

TDR-TB, infecção humana causada por cepas de *M. tuberculosis* totalmente resistentes;

Tris, tris(hidroximetil) aminometano;

XDR-TB, infecção humana causada por cepas de *M. tuberculosis* extremamente resistentes.

Lista de Ilustrações

SUMÁRIO

Capítulo 01

Introdução

1. INTRODUÇÃO

1.1 A Tuberculose

Dentre as doenças infecto-contagiosas que afligem o homem, a tuberculose é uma das mais preocupantes devido a sua alta taxa de incidência, prevalência e mortalidade (Zahrt, 2003), segundo a OMS (WHO, 2009). Atualmente, epidemiologistas estimam que um terço da população do planeta esteja infectada pelo bacilo da tuberculose, com uma taxa anual de aproximadamente 9.2 milhões de novos casos e 1.7 milhões de mortes por ano ocorrendo em todo o mundo. A infecção se dá preferencialmente pelas vias aéreas e se desenvolve de acordo com a **Figura 1**.

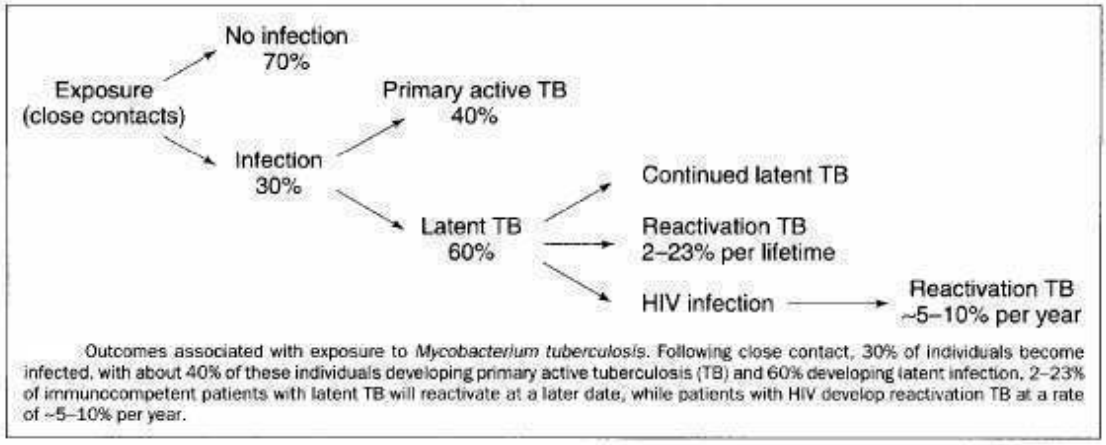

Outcomes associated with exposure to *Mycobacterium tuberculosis*. Following close contact, 30% of individuals become infected, with about 40% of these individuals developing primary active tuberculosis (TB) and 60% developing latent infection. 2–23% of immunocompetent patients with latent TB will reactivate at a later date, while patients with HIV develop reactivation TB at a rate of ~5–10% per year.

Figura 1. Estágios de infecção do *M.tuberculosis* (Mechanisms of latency in *Mycobacterium tuberculosis* Nikki M. Parrish et al.).

Aproximadamente 95% destes casos ocorrem nas nações em desenvolvimento, onde estão relacionados aos poucos recursos disponíveis para garantir um tratamento adequado e onde a infecção pelo vírus da imunodeficiência humana (HIV) é comum. O aumento da resistência a drogas, causada pelo surgimento de novas linhagens, tem levado a uma maior necessidade em compreender os mecanismos moleculares de ação das drogas e a resistência do bacilo as mesmas. Ainda, o custo do tratamento de

pacientes com tuberculose resistente a múltiplas drogas pode assumir valores muito mais altos que o de pacientes com tuberculose susceptível as drogas de uso comum.

Robert Koch, em 1882, identificou uma bactéria álcool-ácido resistente, *Mycobacterium tuberculosis* (MTB), como o agente causador da tuberculose. Em 1921, a vacina BCG foi utilizada pela primeira vez como um agente profilático contra a infecção causada pelo MTB, e é a vacina utilizada no mundo atualmente. O descobrimento das propriedades antibacterianas de algumas drogas de primeira linha levaram a quimioterapias efetivas que diminuíram a taxa de mortalidade no mundo, e a posterior introdução de algumas outras ao arsenal utilizado para combater a tuberculose parecem ter provido um número adequado de efetivos agentes antimicrobianos (Goodman & Gilman *et al*, 2006).

A quimioterapia efetiva contra tuberculose deve incluir uma ação primária bactericida contra organismos em rápido crescimento e uma subseqüente esterilização da população de bacilos dormentes. As drogas de primeira linha exibem uma atividade bactericida contra bacilos metabolicamente ativos e as drogas bacteriostáticas de segunda linha são reservadas para fortalecer tratamentos com resistência presente. A moderna terapia padrão de curta duração para tuberculose está baseada em um regime de quatro drogas que deve ser estritamente seguido para prevenir resistência a drogas e relapso, e a observação direta da complacência do paciente é o melhor meio de garantir um tratamento efetivo e prevenir a aquisição de resistência. Micobactérias demonstram um alto grau de resistência intrínseca à maioria dos antibióticos e agentes quimioterápicos devido à baixa permeabilidade da parede celular (Cole *et al*, 1998). Entretanto, a barreira formada pela parede celular, sozinha, não pode produzir níveis significativos de resistência a drogas. Mutantes de MTB resistentes a uma droga qualquer estão naturalmente presentes em qualquer grande população bacteriana,

independentemente a exposição a drogas. A freqüência de mutantes resistentes a rifampicina e isoniazida é relativamente alta e, portanto, a grande população extracelular de bacilos metabolicamente ativos e com rápido crescimento em lesões cavitárias conterá organismos resistentes a pelo menos uma das drogas. Conseqüentemente, a monoterapia ou a terapia de duas drogas impropriamente administrada selecionará mutantes resistentes a drogas que podem conferir resistência a toda população de bacilos. Em 2006, 500.000 casos de cepas resistentes foram reportados, demonstrando assim a atual situação e a gravidade do problema. Existem duas formas de tuberculose altamente perigosas para a saúde humana; a MDR é resistente a pelo menos isoniazida e rifampicina e requer um tratamento quimioterápico mais extensivo com quimioterápicos de segunda linha; e a XDR se mostra resistente aos quimioterápicos tanto de primeira quanto de segunda linha, indicando assim uma necessidade de desenvolver novos quimioterápicos contra a tuberculose (Hargreaves, 2008).

1.2 *Mycobacterium tuberculosis*

O *Mycobacterium tuberculosis*, principal agente causador da tuberculose, é uma bactéria gram-positiva com um alto conteúdo genômico de G+C. Esta bactéria se apresenta em forma de bacilo mostrando dimensões que variam de 0,3 a 0,6 μm de largura e de 1 a 4 μm de altura, possuindo uma alta complexidade em seu envelope celular e crescimento lento.

1.3 A Via do acido chiquímico

A via do acido chiquímico (**Figura 2**) é constituída por sete passos enzimáticos cada um catalisado por uma enzima diferente e cada enzima é codificada por um único gene (Ducati,2007).

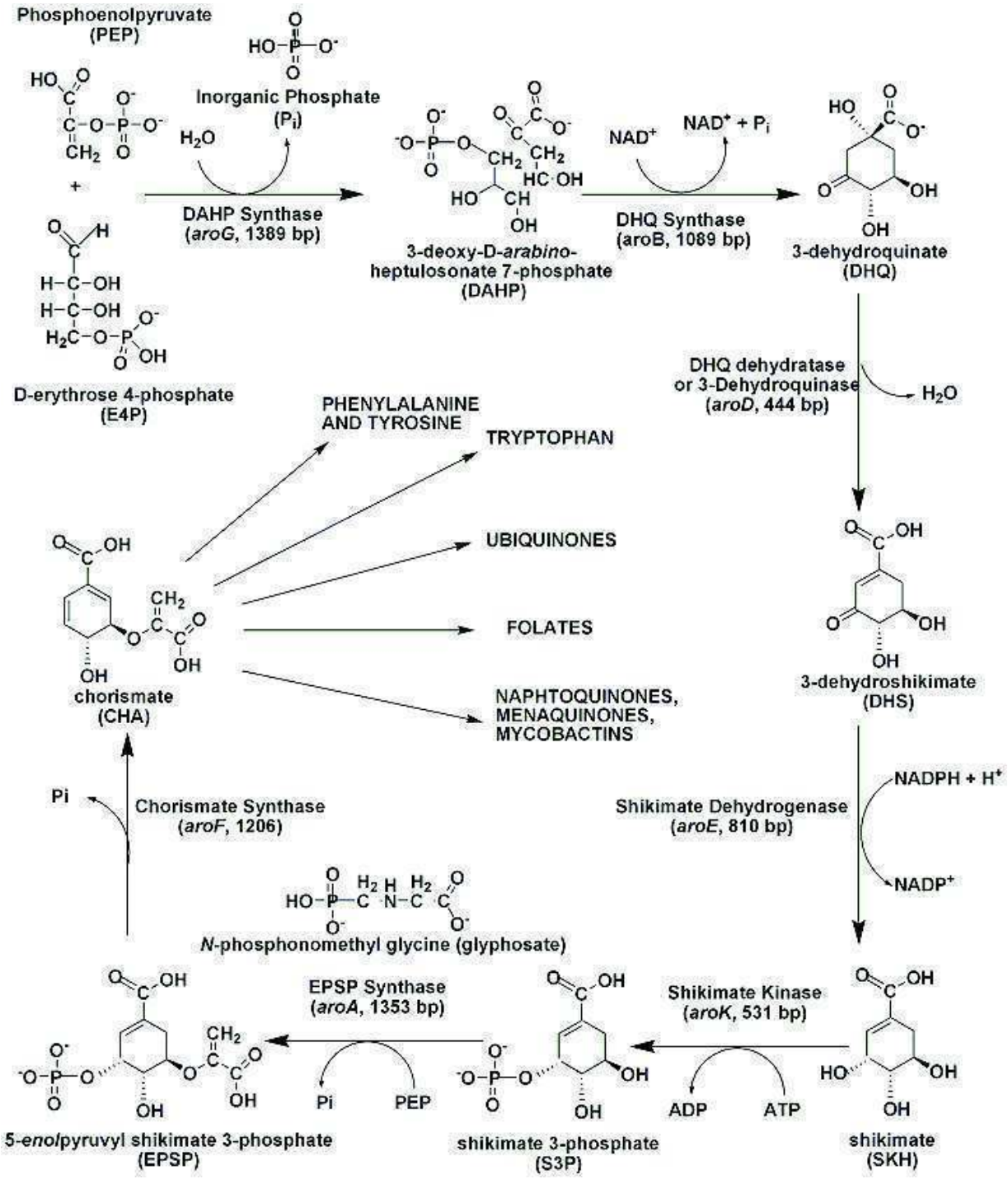

Figura 2. A via do acido chiquímico

Esta via é essencial para a vida de plantas, organismos do filo apicomplexa, parasitas e bactérias (R. Bentley, 1990; Campbell, 2004; Roberts, 2002; Roberts, 1998; Keeling, 1999; McConkey, 1999; McConkey, 2004;), incluindo o MTB (Parish, 2002), porem é ausente no homem, o que a torna um alvo atrativo para o descobrimento de novos fármacos contra a tuberculose. No bacilo causador da tuberculose, a via do acido chiquímico tem como substratos iniciais o fosfoenolpiruvato e D-eritrose 4-fosfato, tendo como produto final o corismato, que é um importante componente na síntese das vitaminas E e K, folato, ubiquinona, menaquinonas, mycobactinas, naftoquinonas e dos aminoácidos aromáticos (Hermann, 1999).

1.4 Chiquimato quinase

A enzima *chiquimato quinase* é codificada pelo gene *aroK*, composto por 531pb que resultam em uma proteína de 176 aa com peso molecular teórico de 18451Da. Esta enzima catalisa a quinta reação da via do ácido chiquímico, convertendo adenosina trifosfato (ATP) e chiquimato em adenosina difosfato e chiquimato-3-fosfato, utilizando magnésio como co-fator, realizando uma transferência de um fosfato do doador (ATP) para o carbono três do anel do acido chiquímico (**Figura 3**).

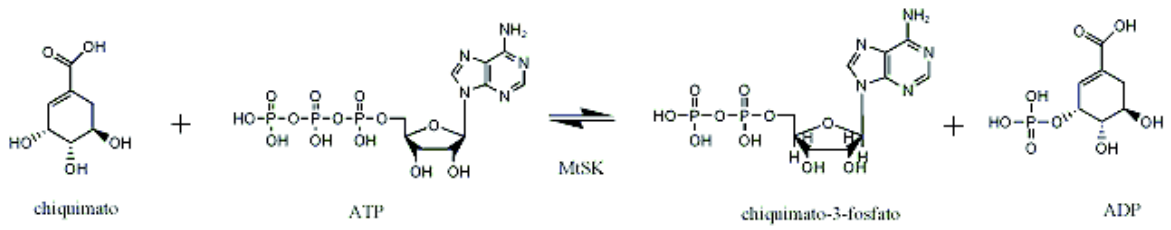

Figura 3. Reação enzimática catalisada pela enzima chiquimato quinase.

Esta enzima pertence à família de enzimas Nucleosídeo Monofosfato Quinase, sendo um importante grupo de enzimas que catalisa a transferência reversível de um

fosfato, pertencente a um nucleosídeo trifosfato, para um nucleosídeo difosfato específico (Yan, 1999). O produto desta reação é subseqüentemente fosforilado, resultando em precursores dos ácidos nucléicos. Esta família possui três domínios conservados: o domínio Core contendo cinco folhas-β paralelas e o P-loop que formam o sítio de ligação dos nucleotídeos; o domínio LID, que se move sobre o sítio ativo e possui resíduos essênciais para a ligação do ATP; e o sítio de ligação NMP, que reconhece e se liga ao nucleosídeo monofosfato. No caso da chiquimato quinase, esse sítio reconhece e se liga ao chiquimato, que é o substrato da reação.

Capítulo 02

Justificativa

2. JUSTIFICATIVA

A tuberculose é uma doença que demonstra índices preocupantes em relação à incidência, prevalência e mortalidade em todos os continentes do mundo, o que a torna uma preocupação mundial. A rifampicina e a isoniazida, descobertas em 1966 e 1952 respectivamente, são os antibióticos mais poderosos utilizados atualmente contra a tuberculose, entretanto, o surgimento de novas cepas resistentes ao tratamento atual e as altas taxas de incidência estão indicando a necessidade do desenvolvimento de novos agentes contra a tuberculose, a fim de impedir a proliferação destas cepas resistentes, o que tornaria ainda mais difícil a luta contra esta doença. A enzima alvo deste trabalho pertence à via do ácido chiquímico, que é uma via muito interessante para o estudo de novos inibidores, já que esta é inexistente em seu hospedeiro, o homem, o que nos remete ao princípio da toxicidade seletiva. Se o produto final desta via, o corismato, for impedido de ser produzido, o bacilo da tuberculose não conseguirá sobreviver, pois o corismato é um dos precursores na síntese do folato, ubiquinonas, vitamina E, vitamina K e dos aminoácidos aromáticos que são essenciais para a sobrevivência do bacilo.

Capítulo 03

Objetivos

Objetivo Geral
Objetivos Específicos

3. OBJETIVOS

3.1 Objetivo Geral

Este trabalho se refere a uma etapa para o desenvolvimento de um possível inibidor relacionado à enzima chiquimato quinase a partir de ensaios de atividade e afinidade entre a enzima e os seus substratos/produtos a fim de elucidar o mecanismo enzimático abrindo o caminho para o desenvolvimento racional de um possível agente contra o bacilo da tuberculose.

3.2 Objetivos Específicos

De modo mais concreto, esta proposta abrange os seguintes objetivos específicos:

- Purificação da enzima chiquimato quinase de *M. tuberculosis (MtSK)*
- Análise por espectrometria de massa com ionização por *eletrospray*
- Sequenciamento dos aminoácidos da porção N-terminal
- Determinação do estado oligomérico
- Cinética em estado estacionário
- Espectroscopia de fluorescencia em equilíbrio
- Calorimetria de titulação isotérmica

Capítulo 04

Materiais e Métodos

4. MATERIAIS E MÉTODOS.

4.1 Purificação da enzima Chiquimato quinase de *M. tuberculosis (MtSK)*

A enzima recombinante foi expressa em células hospedeiras *Escherichia coli* BL21(DE3), como previamente descrito (Oliveira, 2001). Aproximadamente 6 g de células foram ressuspendidas em 24 mL de Tris-HCl 50 mM pH 7.6, rompidas por sonicação, e a fração insolúvel foi removida por centrifucação (48,000*g* for 60 min). $MgCl_2$ foi adicionado ao sobrenadante em uma concentração final de 10 mM seguido pela adição de DNAse (1 mg), agitado durante 30 min a 4 °C, e centrifugado (10,000*g* por 30 min).

A adição de $MgCl_2$ resultou na precipitação da enzima *Mt*SK mantendo outras proteínas no sobrenadante. A utilização deste passo teve dois propósitos no protocolo de purificação: a lise do DNA pela DNAse, e a precipitação da enzima *Mt*SK. O precipitado foi ressuspendido em Tris-HCl 50 mM pH 7.6 contendo KCl 500 mM, e centrifugado (10,000*g* por 15 min). Esta solução foi concentrada para volume aproximado de 20 mL, com posterior adição de 20 mL de Tris-HCl 50mM pH 7.6 contendo KCl 500 mM e $(NH_4)_2SO_4$ 2M, resultando em uma solução com concentração final igual a 1M $(NH_4)_2SO_4$.

O sobrenadante foi injetado em uma coluna Phenyl Sepharose 16/10 (GE HealthCare) previamente equilibrada com o tampão A (Tris-HCl 50mM, KCl 500mM, $(NH_4)_2SO_4$ 1M, pH 7.6) e o material que interagiu com a coluna foi eluído em um gradiente linear contendo o tampão B (Tris-HCl 50mM, KCl 500mM, pH 7.6), com fluxo de 1 mL min^{-1}. As frações contendo a proteína *Mt*SK foram agrupadas e injetadas em uma coluna Sephacryl S-100 HR (GE HealthCare) e eluídas em gradiente isocrático de tampão B a um fluxo de 0.25 mL min^{-1}. As frações contendo a proteína recombinante homogênea *Mt*SK foram agrupadas e armazenadas em 85 % $(NH_4)_2SO_4$. A expressão e purificação da proteína recombinante *Mt*SK foi confirmada por eletroforese em gel de

acrilamida 12 % (SDS-PAGE) corado com Coomassie Brilliant Blue (Laemmli, 1970). A concentração de proteína foi determinada pelo método de Bradford *et al*. (Bradford, 1976).

4.2 Análise por espectrometria de massa com ionização por *eletrospray*

A homogeneidade da proteína recombinante foi observada utilizando espectrometria de massa com ionização por *eletrospray* (ESI-MS), em protocolo adaptado de Chassaigne and Lobinski (Chassaigne, 1998)). A amostra foi analisada em um espectrômetro de massa triplo quadrupolo (modelo QUATTRO II) equipado com uma sonda de *eletrospray* padrão (ESI-Micromass, Altrincham, United Kingdom), e ajustado a um fluxo de 250 µL min^{-1}. A temperatura (80 °C) e a voltagem da agulha (3.6 kV) foram mantidas constantes durante a coleta de dados, aplicando um gás secante (nitrogênio) a um fluxo de 200 L h^{-1} e um gás nebulizante a um fluxo de 20 L h^{-1}. O espectrômetro de massa foi calibrado com mioglobina de coração de cavalo intacta. A subunidade molecular da proteína recombinante *Mt*SK foi determinada por ESI-MS, ajustando o espectrômetro de massa para fornecer um pico com a metade da altura de 1 unidade de massa, e a voltagem da lente de transferência de íons foi ajustada para 38 V. Cerca de 50 pmol (10 µL) de amostra foi injetada no solvente de transporte. O espectro de ESI foi obtido no modo de aquisição multicanal, escaneando entre 500 e 1.800 *m*/*z* em um intervalo de 7 s. O espectrômetro de massa é equipado com MassLynx and Transform software para a aquisição e manejo do espectro.

4.3 Sequenciamento dos aminoácidos da porção N-terminal

Os aminoácidos da porção N-terminal da proteína recombinante MtSK homogênea foram identificados pelo método de degradação de Edman (Edman, 1949) utilizando um sequenciador PPSQ 21A gas-phase (Shimadzu).

4.4 Determinação do estado oligomérico

O estado oligomérico da proteína *Mt*SK homogênea foi determinado utilizando cromatografia líquida de separação por tamanho em uma coluna Superdex 200 (HR 10/30-GE HealthCare). A coluna foi pré-equilibrada com 50 mM Tris-HCl pH 7.5 contendo 200 mM NaCl a um fluxo de of 0.4 mL min^{-1} (4 °C), com detecção por UV a 280 nm. A curva de calibração foi construída utilizando as seguintes proteínas como padrão: ribonuclease A (13.7 kDa), quimotripsinogenio (25 kDa), ovalbumina (43 kDa), albumina (67 kDa), aldolase (158 kDa), catalase (232 kDa), and ferritina (440 kDa). Os volumes de eluição (V_e) foram utilizados para calcular os respectivos coeficientes de partição. (K_{av}, **Eq. 1**). Blue dextran foi utilizado para determinar o volume percolado pela fase móvel da coluna (V_o). V_t corresponde ao volume total da coluna. O volume de 100 µL da proteína recombinante foi injetado na coluna de gel filtração para se obter o V_e da proteína *Mt*SK. O valor de K_{av} para cada proteína foi plotado contra a sua massa molecular correspondente.

$$K_{av} = (V_e - V_o)/(V_t - V_o) \qquad \textbf{Eq. 1}$$

4.5 Cinética em estado estacionário

A atividade da proteína recombinante *Mt*SK foi ensaiada no sentido direto acoplando o produto ADP com a enzima piruvato quinase (PK; EC 2.7.1.40) e lactato desidrogenase (LDH; EC 1.1.1.27), a reação seguiu o protocolo previamente descrito

(Oliveira, 2001 e Millar, 1986). A oxidação chiquimato dependente do NADH foi continuamente monitorada a 340 nm (ε = 6.22 $\times$ 10^3 M^{-1} cm^{-1}). Todas as reações foram realizadas a 25 °C e iniciadas com a adição da proteína recombinante *Mt*SK (1 µg mL^{-1}). A mistura de reação era composta de 100 mM Tris HCl, pH 7.6, 100 mM KCl, 5 mM $MgCl_2$, 1.5 mM PEP, 0.2 mM NADH, 6 U mL^{-1} PK, e 5 U mL^{-1} LDH. As velocidades iniciais em estado estacionário foram calculadas a partir da porção linear da curva de reação nas condições experimentais em que menos de 5% do substrato foi consumido. Os parâmetros cinéticos verdadeiros em estado estacionário foram determinados a partir das medidas da velocidade inicial em concentrações variáveis de SKH (37 - 4800 µM) em presença de diferentes concentrações de ATP (9 - 1200 µM).

Os valores dos parâmetros da cinética em estado estacionário e seus respectivos erros foram obtidos adequando os resultados as equações apropriadas utilizando a função de regressão não linear do software SigmaPlot 9.0 (SPSS, Inc). As curvas hiperbólicas de saturação construídas a partir da velocidade inicial em concentrações fixas de um substrato e variáveis do outro foram adequadas a equação de Michaelis-Menten (**Eq. 2**) (Segel,1975 e Cook, 2007).

$$v = VA/(K + A) \qquad \textbf{Eq. 2}$$

4.6 Espectroscopia de Fluorescência em Equilíbrio

O monitoramento da fluorescência intrínseca da proteína *Mt*SK foi realizado a fim de determinar a ordem de adição dos substratos, de liberação dos produtos e suas respectivas afinidades em relação ao sítio catalítico proporcionando assim um maior entendimento do mecanismo cinético da reação catalisada pela enzima. Como a proteína *Mt*SK não possui resíduos de triptofano, as mudança de fluorescência das tirosinas encontradas foram monitoradas em relação a adição dos ligantes (a cadeia polipeptídica

na enzima *Mt*SK possui 3 resíduos de tirosina). As medidas de fluorescência foram realizadas em um Espectrofluorofotometro RF-5301 PC (Shimadzu) a 25 °C. Os comprimentos de onda de excitação e emissão foram, respectivamente, 280 e 315 nm. Os slits de excitação foram 5 nm. Como as tirosinas tipicamente possuem uma sensibilidade baixa (baixa absorbância máxima e baixa emissão de fluorescência), a concentração da enzima *Mt*SK nos experimentos de ligação foi de 10 µM. As titulações para a formação do complexo binário foram realizadas adicionando 1 microlitro do seguintes compostos em 2 mL de solução contendo 10 µM *Mt*SK in 100 mM Tris-HCl, 100 mM KCl, 5 mM $MgCl_2$, pH 7.6: 120 mM SKH solução estoque (10 – 1100 µM concentração final); 120 mM S3P solução estoque (59.97-952.3 µM concentração final). Experimentos de controle foram realizados nas mesmas condições experimentais exceto pela ausência de adição do ligante, e estes valores foram subtraídos dos valores encontrados na presença do ligante. Devido ao grande efeito de filtro interno encontrado, as reações de ligação entre ATP e ADP não puderam ser determinadas por espectroscopia de fluorescência.

Os valores encontrados nos ensaios de espectroscopia de fluorescência foram adequados a **Eq. 3**, em que F é a florescência encontrada, F_0 é a fluorescência inicial, ΔF é a mudança de fluorescência, e K_D representa a constante de dissociação em equilíbrio em relação à formação do complexo binário proteína:ligante.

$$F = F_0 + \Delta F[ligante]/(K_D + [ligante]) \qquad \textbf{Eq. 3}$$

4.7 Calorimetria de Titulação Isotérmica (ITC)

Os experimentos de calorimetria foram realizados em um Microcalorimetro iTC_{200} Microcalorimeter (Microcal, Inc., Northampton, MA). As células de referência e de reação possuem um volume total de 200 µL e a seringa possui um volume total de 39 µL. Os

ensaios calorimétricos foram realizados com os substratos (SKH e ATP), e com os produtos (S3P e ADP) a 25 °C. A célula de referência (200 µL) foi preenchida com água durante todos os experimentos e a célula de amostra (200 µL) foi preenchida com a enzima *Mt*SK em uma concentração de 100 µM nos experimentos de ligação com ATP e ADP, e 130 µM nos ensaios de ligação com SKH e S3P. A seringa de injeção (39 µL) foi preenchida com os substratos ou produtos em diferente concentrações: ATP e ADP a 6 mM, e SKH e S3P a 4.2 mM. Devido a alta entalpia de ionização do tampão Tris usado nos ensaio de cinética em estado estacionário e espectroscopia de fluorescencia (Fukada, 1998), todos os experimentos de ITC foram realizados em HEPES 50 mM, KCl 50 mM e $MgCl_2$ 5mM, pH 7.5. A reação de ligação foi iniciada com uma injeção de 0.5 µL do ligante seguida de 17 injeções de 2.26 µL em intervalos de 180 s, chegando a um volume final injetado de 39 µL com uma velocidade de agitação de 500 RPM. A variação de calor foi monitorada dentro da célula, permitindo a determinação da entalpia de ligação do processo (ΔH) e a constante de associação em equilíbrio (K_a). Todos os valores de entalpia relacionados à ligação dos substratos se mostraram exotérmicas. Titulações de controle foram realizadas a fim de subtrair o calor de diluição e de mistura para cada experimento.

O ΔG (Energia livre de Gibbs) de ligação foi calculado usando a relação descrita na **Eq. 4**, em que R é a constante dos gases (8.314 J K^{-1} mol^{-1}), T é a temperatura em Kelvin (T = °C + 273.15), e K_a é a constante de associação em equilíbrio. A entropia de ligação (ΔS) pode também ser determinada por esta formula matemática. O modelo matemático em que se espera um grupo de sítios com a mesma afinidade e assinatura termodinâmica foi utilizado para determinar a ligação e as constantes termodinâmicas. O valor inicial de estequiometria (n) foi fixado em 1, sabendo-se que a enzima *Mt*SK se encontra como um monômero em solução, e estimativas de K_a e ΔH foram refinados

pelo método de regressão não linear padrão de Marquardt fornecido pelo software Origin 7 SR4 software.

$$\Delta G^{o} = -RT\ln K_{a} = \Delta H^{o} - T\Delta S^{o} \qquad \textbf{Eq. 4}$$

Capítulo 05

Resultados e Discussão

5. RESULTADOS E DISCUSSÃO

5.1 Purificação da enzima Chiquimato quinase de *M. tuberculosis (MtSK)*

A proteína recombinante *Mt*SK foi purificada até sua homogeneidade utilizando um protocolo de purificação contendo três passos, sendo eles: precipitação do estrato bruto, cromatografia de troca hidrofóbica (Phenyl Sepharose) seguido por cromatografia de separação por tamanho (Sephacryl S-100). A utilização de $MgCl_2$, em uma concentração final de 10 mM, foi extremamente eficiente mantendo a proteína na fração insolúvel e outras proteínas contaminantes na fração solúvel, permitindo assim sua separação. (**Figura 4**). Trabalhos na área bioquímica já demonstraram que interações íon-macromolécula, tais como interação com moléculas de água da primeira camada de hidratação representam um papel fundamental nos efeitos de Hofmeister (Zhang, 2006). As séries de Hofmeister graduam a influência relativa de íons no comportamento físico de uma grande variedade de processos aquosos, abrangendo desde agrupamentos coloidais até a organização estrutural de proteínas. Usualmente, os efeitos iônicos específicos relatados pelas séries de Hofmeister são mais evidentes em relação a ânions do que cátions (Zhang, 2006). O ânion Cl^- está situado na linha divisória entre espécies cosmostrópicos ("*water structure makers*", alto grau de hidratação, com efeito estabilizador e de solubilização sobre proteínas – *salting-out*) e caotrópicos ("*water structure breakers*", efeito de desestabilização de proteínas enoveladas e sua precipitação – *salting-in*). O íon Mg^{2+} tem efeito caotrópico (*salting-in*), podendo explicar o efeito de *salting-out* de 10 mM $MgCl_2$ na *Mt*SK. Entretanto, recentemente foi descrito que o transporte de cátions é maior que outros cátions biológicos, e a velocidade de troca com o solvente é 3 ordens de magnitude menor que outros cátions de ocorrência comum (Maguire, 2002). Este passo de precipitação foi seguido por dois passos cromatográficos (interação hidrofóbica e exclusão por tamanho), resultando em

aproximadamente 20 mg de proteina *Mt*SK homogênea e funcional a cada 1.5 L de cultura de células. A proteína *Mt*SK recombinante foi armazenada em 85 % $(NH_4)_2SO_4$ a 4°C, sem perda de atividade.

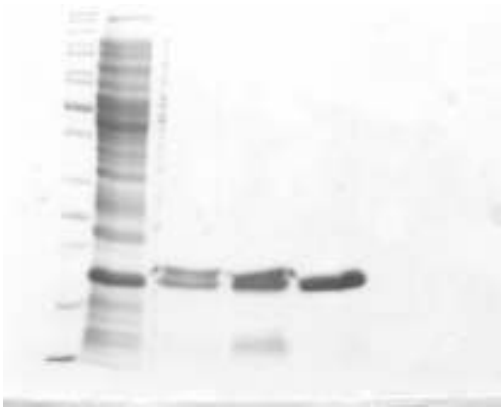

Figura 4. Analise por SDS-PAGE12% dos passos de purificação da enzima *Mt*SK. Canaleta 1, Marcador de peso molecular (Fermentas); Canaleta 2, Extrato solúvel de *E. coli* BL21 (DE3) [pET-23a(+)::*aroK*]; Canaleta 3, Proteínas solúveis após a precipitação com 10 mM $MgCl_2$; Canaleta 4, Eluido da coluna Phenyl Sepharose 16/10 ; e canaleta 5, Eluido da coluna Sephacryl S-100 HR.

5.2 Análise por espectrometria de massa com ionização por *eletrospray*

O valor de 18,451 Da, para a massa molecular da subunidade da proteína recombinante *Mt*SK foi determinada por ESI-MS. Este resultado é consistente com a remoção pós-traducional da metionina na porção N-terminal (131.2 Da) do tamanho total do produto de tradução (18,583 Da). O resultado não encontrou picos de massa relativos à enzima Chiquimato Quinase I (19,526 Da), codificada pelo gene *aroK* e para enzima Chiquimato Quinase II (18,998 Da), codificada pelo gene *aroL* de *E. coli* SK (Whipp, 1989), fornecendo então suporte para a identificação da proteína recombinante.

5.3 Sequenciamento dos aminoácidos da porção N-terminal

Os 8 primeiros resíduos de aminoácidos da proteína recombinante *Mt*SK foram identificados pelo método de degradação de Edman (APKAVLGL). Este resultado

demonstrou que a proteína purificada corresponde à *Mt*SK, uma vez que a sequência N-terminal da enzima Chiquimato Quinase I, codificada pelo gene *aroK*, e a enzima Chiquimato Quinase II, codificada pelo gene *aroL* de *E. coli* são, respectivamente, MAEKRNIFLV e MTQPLFLIGP. Os resultados encontrados pelo método de degradação de Edman também confirmaram a retirada da metionina na porção N-terminal, e esta de acordo com a estrutura cristalográfica do complexo ternário *Mt*SK:MgADP:SKH (Pereira, 2004). A retirada da metionina da porção N-terminal é uma modificação pos-traducional comum que ocorre em proteínas que foram sintetizadas no citoplasma de células procarióticas. A clivagem da metionina iniciadora é usualmente direcionada pelo penúltimo resíduo de aminoácido com a menor liberdade de rotação da sua cadeia lateral (Gli, Ala, Ser, Thr, Pro, Val, e Cis) (Hirel, 1989). A remoção da metionina da porção N-terminal da cadeia polipeptídica da proteína recombinante *Mt*SK está de acordo com esta regra, já que encontramos uma alanina como penúltimo resíduo de aminoácido.

5.4 Determinação do estado oligomérico

O valor de 20.72 ± 0.5 kDa encontrado para a massa molecular da proteína homogênea recombinante *Mt*SK foi estimado por cromatografia líquida de gel filtração. Este resultado demonstrou que a enzima *Mt*SK é um monômero em solução, desde que, a análise por ESI-MS sugeriu o valor de 18,451 Da por subunidade de proteína.

5.5 Cinética em estado estacionário

A velocidade inicial hiperbólica em função da concentração de substrato (ATP ou SKH) foi plotado em uma função linear duplo-recíproca (velocidade inicial vs concentração de substrato – gráfico de Lineweaver-Burk). Estes resultados permitiram a determinação dos parâmetros cinéticos verdadeiros em estado estacionário e o

mecanismo enzimático. Os gráficos de duplo-recíprocos demonstraram uma família de retas que se intersectam a esquerda do eixo y (**Figura 5**), que é consistente com a formação do complexo ternário e um mecanismo seqüencial. Este padrão de retas permitiu a exclusão dos mecanismos tipo *ping-pong* (retas paralelas), estado estacionário aleatório (gráficos de duplos-recíprocos não lineares) e equilíbrio rápido ordenado (uma das retas deveria cruzar o eixo y em um valor único).

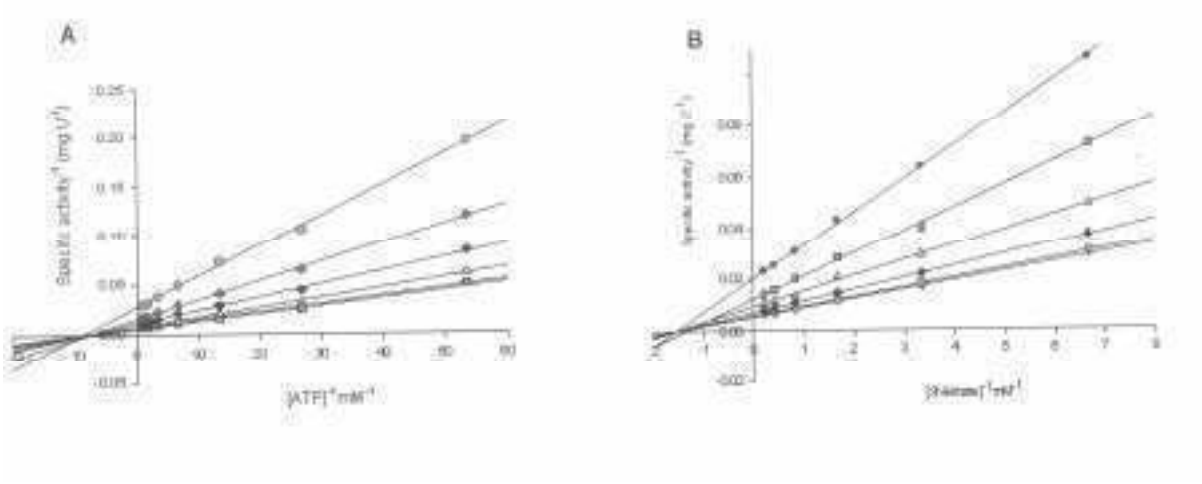

Figura 5. Grafico dos duplo reciprocos referentes aos valores de cinética em estado estacionário da enzima *Mt*SK, utilizando ATP (**A**) ou SKH (**B**) como substrato variavel. Cada curva representa concentrações variaveis-fixas dos substratos, em um intervalo de 37 a 4800 µM para SKH e 9 a 1200 µM para o ATP.

Entretanto, estes dados sozinhos não são capazes de distinguir entre os mecanismos equilíbrio rápido aleatório e estado estacionário compulsório ordenado bi bi. Os resultados encontrados pelo gráfico duplo-reciproco foram adequados à equação de velocidade inicial seqüencial (**Eq. 5**), fornecendo os seguintes valores para as constantes cinéticas verdadeiras (**Tabela 1**): k_{cat} = 60 (± 8) s^{-1}, K_{MgATP} = 112 (± 4) µM, K_{SKH} = 650 (± 28) µM, k_{cat}/K_{MgATP} = 5.4 (± 0.7) x 10^5 $M^{-1}s^{-1}$, and k_{cat}/K_{SKH} = 0.9 (± 0.1) x 10^5 $M^{-1}s^{-1}$. *E. coli* possui duas enzimas Chiquimato Quinase : SK I, codificada pelo gene *aroK*, e SK II codificada pelo gene *aroL* (Pittard, 1996). Os valores de K_{SKH} para *E. coli* SK I (20 mM) são significantemente maiores do que os valores encontrados para *E. coli* SK II (200 µM)

(**Tabela 1**). Entretanto, o sequenciamento completo do genoma de MTB foi identificado por homologia de sequências na presença do gene *aroK*, que codifica a enzima SK I (Cole, 1998), os parâmetros cinéticos encontrados aqui e previamente descritos (Gu, 2002), também demonstram que a *Mt*SK deveria ser mais apropriadamente descrita como uma enzima do tipo II codificada pelo gene *aroL*.

$$v = VAB/(K_{ia}K_b + K_aB + K_bA + AB) \qquad \textbf{Eq. 5}$$

Tabela 1 – Constantes cinéticas em estado estacionário de enzimas Chiquimato quinases de diferentes organismos.

	*Mt*SK[1]	*Mt*SK[2]	*E. coli* SKI[2]	*E. coli* SKII[2]	EcSK[2,3]
$k_{cat}(s^{-1})$	60 (± 8)	44 (± 2)		32	35
K_{MgATP} (μM)	112 (± 4)	83 (± 4)		160	620
K_{SKH} (μM)	650 (± 28)	410 (± 20)	20×10^3	200	310
k_{cat}/K_{MgATP} (M^{-1} s^{-1})	5.4 (± 0.7) x 10^5	5.3 x 10^5		2.0 x 10^5	5.6 x 10^4
k_{cat}/K_{SKH} (M^{-1} s^{-1})	0.9 (± 0.1) x 10^5	1.1 x 10^5		1.6 x10^5	1.1 x10^5

[1] Constantes cinéticas verdadeiras em estado estacionário produzidos neste trabalho.
[2]Constantes cinéticas aparentes em estado estacionário adaptados da referencia (Gu, 2002).
[3] Adaptado da referencia (Gu, 2002).
[4] SK de *Erwinia chrysanthemi*.

5.6 Espectroscopia de Fluorescência em Equilíbrio

Nos experimentos de formação do complexo binário, foi monitorado uma mudança de emissão de fluorescência em relação à ligação da proteína com o SKH e S3P. O padrão de titulação entre a enzima *Mt*SK e o SKH se mostrou hiperbólico (**Figura 6**), e foi adequado a **Eq. 3**, resultando em um valor de 124 (± 7) μM para a constante de dissociação em equilibrio do SKH (K_D). Não foi monitorada mudança na fluorescência intrinsica da proteína quando feito a titulação com o S3P. Entretanto, não podemos assumir que não ocorreu a formação do complexo binário *Mt*SK:S3P e sim que não ocorreu mudança de fluorescência durante a titulação, podendo ser devido a não formação do complexo binário ou pela ausência de alteração na emissão de fluorescencia em decorrência da ligação do S3P ao sítio ativo da enzima.

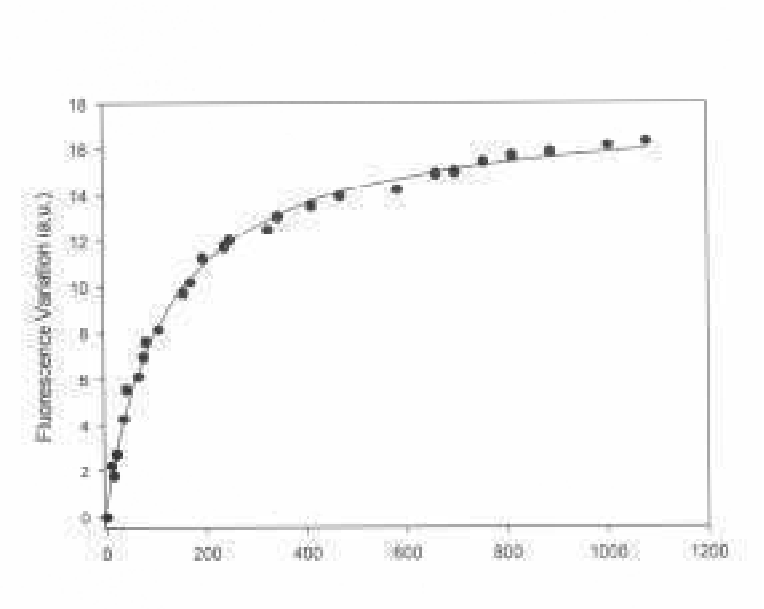

Figura 6. – Espectroscopia de fluorescência em equilibrio referente a ligação entre SKH e *Mt*SK, monitorando a diferença na fluorescencia intrinsica da proteina em relação ao aumento na concentração de SKH.

5.7 Calorimetria de Titulação Isotérmica (ITC)

Os experimentos de calorimetria de titulação isotérmica foram realizados a fim de determinar a ordem de adição dos substratos e liberação dos produtos, resultando na enzima livre regenerada após cada ciclo catalítico. Em concordância com os experimentos de fluorescência, não foi observada ligação do S3P à enzima livre por ITC. Experimentos de ITC também demonstraram a interação entre o SKH, Mg^{2+}ATP e Mg^{2+}ADP e a *Mt*SK livre (**Figura 7** e **Tabela 2**). Estes resultados confirmam o mecanismo em que a ligação dos substratos (SKH e ATP) na enzima *Mt*SK é aleatório, e a liberação do S3P é seguida pela liberação do ADP, resultando na regeneração da enzima livre. O valor da constante de equilíbrio encontrado por espectroscopia de fluorescência (124 μM) está de acordo com o valor determinado por ITC (181 μM). Como os resultados de cinética em estado estacionário não foram capazes, isoladamente, de distinguir o mecanismo verdadeiro da reação catalisada pela enzima, os ensaios de espectroscopia de fluorescência e ITC, em conjunto, indicaram que o mecanismo bi bi

da enzima *Mt*SK é um mecanismo de equilíbrio rápido ordenado na adição de substratos. Baseado em uma série de estruturas cristalográficas, foi proposto que a ligação dos substratos é aleatória (Hartmann, 2006), em concordância com os resultados aqui apresentados. Entretanto, quando o mecanismo de uma enzima é de equilíbrio rápido ou estado estacionário, ele não pode ser determinado por cristalografia. A estrutura cristalográfica sugere que o produto ADP é liberado seguido da liberação do S3P, gerando a enzima livre (Hartmann, 2006). Neste presente trabalho, é demonstrado claramente que o S3P é o primeiro produto da reação liberado, seguido pela dissociação do ADP do complexo binário *Mt*SK:ADP regenerando a enzima livre para o próximo ciclo de catálise.

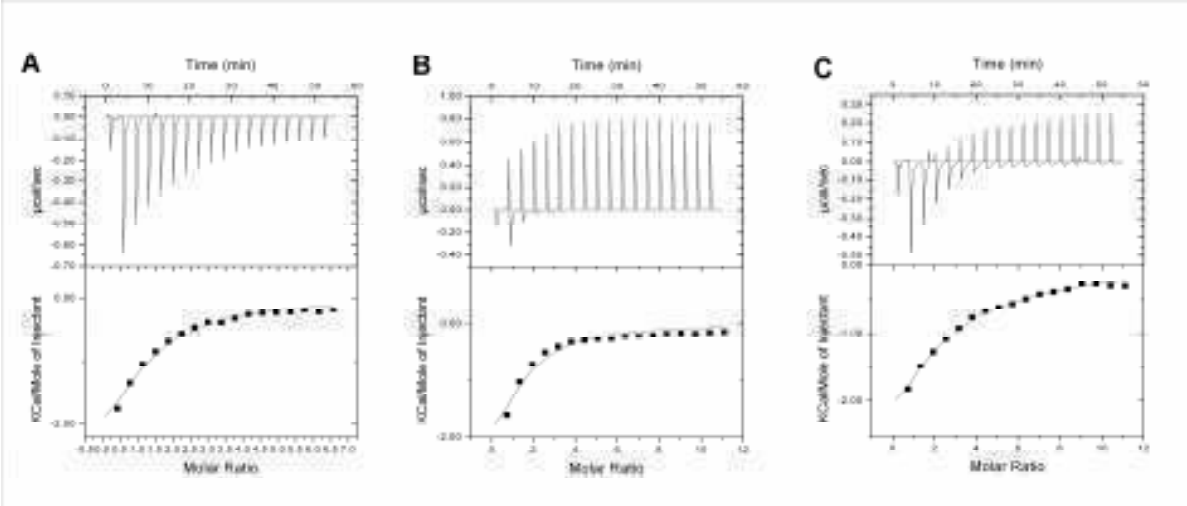

Figura 7. Analise por calorimetria de titulação isotérmica (ITC) referentes a ligação do SKH (**A**), Mg^{2+}ATP (**B**), ou Mg^{2+}ADP (**C**) na enzima livre *Mt*SK. Os gráficos superiores representam as isotermas geradas pela diferença de calor relativas a interação entre a enzima e o respectivo ligante. Os gráficos inferiores representam a variação de calor normalizada por mol de injetante em função da razão molar (ligante/concentração de *Mt*SK).

Tabela 2. Parâmetros termodinâmicos relativos à formação do complexo binário formado entre a enzima *Mt*SK e os substratos/produtos. O K_D representa a constante de dissociação em equilíbrio, ΔH é a entalpia de ligação, ΔS é a entropia de ligação, ΔG é a energia livre de Gibbs, e –TΔS é o negativo da temperatura (em Kelvin) multiplicando a entropia de ligação.

	K_D (μM)	ΔH (kcal/mol)	ΔS (cal/mol/deg)	ΔG (kcal/mol)	-TΔS (cal/mol)
SKH	181 (± 15)	-4.6 (± 0.2)	1.8 (± 0.2)	-5.1 (± 0.4)	-543 (± 47)
ATP	196 (± 29)	-5.1 (± 0.3)	-0.15 (± 0.02)	-5.1 (± 0.8)	44 (± 7)
ADP	562 (± 20)	-12.4 (± 0.2)	-27 (± 1)	-4.4 (± 0.2)	7930 (± 285)

Os resultados de ITC demonstraram diferenças de calor em relação aos ligantes (SKH, ATP, ou ADP) e a enzima *Mt*SK livre, fornecendo assinaturas termodinâmicas de interações não covalentes para cada processo de ligação. As entalpias observadas aumentam bastante como resultado de mudanças nas interações entre os átomos (por exemplo, ligações de hidrogênio e/ou interações de van der Waals), em que o sinal indica a formação de uma rede favorável (ΔH negativo) ou desfavorável (ΔH positivo) na redistribuição na rede de interações das espécies reativas (incluindo solvente), (O'Brien, 2004). As interações hidrofóbicas são relacionadas ao grau de desordem em sistemas livres e em sistemas acoplados, e estes efeitos se refletem nas mudanças entrópicas. A liberação de moléculas de água da superfície para o solvente é normalmente tido como um fator relevante em uma entropia favorável (ΔS positivo). Mudanças conformacionais tanto no ligante quanto na proteína, relativos à formação do complexo binário, são entropicamente desfavoráveis (ΔS negativo) (O'Brien, 2004).

Os resultados de ITC para a ligação entre Mg^{2+}ADP e a enzima *Mt*SK sugerem que esta formação de complexo é acompanhada por uma redistribuição nas ligações de hidrogênio e/ou interações de van der Waals, e uma grande contribuição entrópica desfavorável, resultando em um alto valor de constante de dissociação em equilíbrio (**Tabela 2**). Estes dados sugerem que esta grande mudança conformacional ocorre na estrutura da enzima durante a dissociação do Mg^{2+}ADP do complexo binário *Mt*SK:Mg^{2+}ADP. Concomitantemente, o alto valor de K_D para o ADP pode evitar a formação do complexo ternário abortivo *Mt*SK:Mg^{2+}ADP:SKH, que poderia desativar o sítio enzimático.

Os resultados de calorimetria obtidos na ligação entre o Mg^{2+}ATP e a enzima *Mt*SK indicam que este processo de reconhecimento molecular é acompanhado por uma pequena redistribuição nas interações entre átomos de hidrogênio e/ou interações de van

der Waals, e uma contribuição entrópica desfavorável (**Tabela 2**), podendo refletir em uma mudança conformacional. Como mencionado anteriormente, a enzima *Mt*SK pertence a família das NMP quinases, que são compostas dos domínios CORE, LID e ligação de NMP (ligação do SKH). O domínio LID fecha o sitio ativo e possui resíduos que são essenciais para a ligação do ATP (Pereira, 2004, Dias, 2007, Dhaliwal, 2004, Gan, 2006, Hatmann, 2006). Consequentemente, as NMP quinases sofrem uma grande mudança conformacional durante a catálise (Vonrhein, 1995). É importante salientar que um quarto domínio estrutural foi proposto na enzima *Mt*SK,, chamado, domínio RC (Hartmann, 2006). Interessantemente, o valor da constante de dissociação do ATP (196 μM) é menor do que a do ADP (562 μM). Esta diferença de valores pode ser devido à interação direta do fosfato γ- do ATP e também ao resíduo Arg117 observado na estrutura cristalográfica do complexo binário *Mt*SK:ATP ou ao resíduo de aminoácido Lys15 que faz parte do P-loop (Hartmann, 2006).

As contribuições desfavoráveis relacionadas à ligação do ATP/ADP à enzima livre podem ter ocorrido devido às mudanças conformacionais na estrutura da enzima. O domínio de ligação de NMP (ou SB) da enzima *Mt*SK possui função de reconhecer e se ligar ao SKH (Pereira, 2004, Dias, 2007, Dhaliwal, 2004, Gan, 2006, Hatmann, 2006). A interação entre o substrato SKH e a enzima livre é associada a interações entre átomos de hidrogênio e/ou interações de van der Waals favoráveis e uma contribuição entrópica positiva (**Tabela 2**). Este efeito pode ser reflexo da liberação de moléculas de água presas tanto ao sítio ativo da enzima quanto à estrutura do substrato. A constante de equilíbrio relacionada com a hidrólise intramolecular de ATP em ADP e do fosfato, ambos ligados ao sitio ativo, é considerada maior do que a constante de equilíbrio encontrada para a hidrólise do ATP em solução (Jencks, 1975). Os dados de calorimetria relacionados a ligação do SKH indicam a exclusão de moléculas de água do sítio ativo a

fim de minimizar a hidrólise do ATP, corroborando dados previamente descritos (Pereira, 2004).

Os dados de calorimetria indicam que mudanças conformacionais ocorrem na ligação entre a enzima e o ATP/ADP, e moléculas de agua são excluídas do sítio ativo no momento da ligação do SKH. Esta conclusão está de acordo com dados estruturais, que demonstraram um significativo movimento rotacional do domínio NB relacionado com a ligação do ATP/ADP, com aproximação do domínio ligador de SKH (Hartmann, 2006). Entretanto, os dados de ITC relacionados ao SKH não estão de acordo com o movimento rotacional do domínio ESB e fechamento causado pelo domínio LID no momento da ligação do substrato (Hartmann, 2006). Como podemos reconciliar estes dados de calorimetria e de cristalografia? Uma explicação para estes dados aparentemente contraditórios pode ser encontrada na idéia de que a contribuição entrópica desfavorável, devido às mudanças na conformação enzimática, foi sobreposta por uma contribuição entálpica favorável em decorrência da liberação de moléculas de água presas ao complexo proteína/substrato. Entretanto, a estrutura cristalográfica do complexo binário *Mt*DK:SKH indica que aparentemente ocorre uma diversa gama de conformações, e que a conformação mostrada não apresentou o fechamento do domínio LID sobre o SKH ligado (Hartmann, 2006), o que poderia ser consistente com a ausência de alteração conformação da enzima em decorrência da ligação do SKH, sendo esta ligação entropicamente desfavorável, onde a liberação das moléculas de água é o principal fator contribuinte para a entropia favorável.

Foi demonstrado que a enzima SK de *Erwinia chrysanthemi* (*Ec*SK), codificada pelo gene *aroL*, possui um K_M para o atp ATP (620 μM) aproximadamente quatro vezes menor que a sua constante de dissociação (2.6 mM) (Krell, 2001). Estes resultados corroboram a hipótese de ocorrência de mudanças conformacionais na enzima *Ec*SK

associadas a ligação do primeiro substrato, induzindo um aumento de afinidade pelo segundo substrato. Entretanto, baseado nos resultados relativos ao Mg^{2+}ATP, não se torna aparente que o mesmo se possa indicar para a *Mt*SK, posto que o valor de K_M (112 μM) está na mesma faixa de concentração do que os valores de K_D, determinados por espectroscopia de fluorescência (124 μM) e ITC(196 μM).

É descrito que o valor de K_M para um substrato em mecanismos de equilíbrio rápido e ordenado aleatório é igual à constante de dissociação do substrato do complexo ternário (Engel, 1977). O valor de K_M do substrato SKH (**Tabela 1**, 650 μM) é aproximadamente 3.6 vezes maior do que o valor de K_D (**Tabela 2**, 181 μM). Este resultado sugere uma energia livre positiva de acoplamento (ΔG_{coop} = 3.2 kJ mol^{-1}) relativo à ligação do SKH ao complexo *Mt*SK:Mg^{2+}ATP. A energia livre de acoplamento para o Mg^{2+}ATP é aparentemente negativa ($\Delta G_{coop} > 0$) (Weber, 1975). Este achado é intrigante, pois poderíamos esperar que a ligação do Mg^{2+}ATP na enzima *Mt*SK livre aumentaria a afinidade pelo SKH. Interessantemente, nenhuma interação entre o SKH e o domínio LID foi observada durante sua ligação como segundo componente de reação (Hartmann, 2006). Esta redução pode ser devido ao valor de K_M ser maior que o valor de K_D para o SKH.

Capítulo 06

Conclusão

6. CONCLUSÃO

Os estudos de cinética em estado estacionário, espectroscopia de fluorescência e calorimetria de titulação isotérmica demonstraram que a proteína *Mt*SK monomérica possui um mecanismo enzimático de equilíbrio rápido ordenado para adição dos substratos, e uma liberação ordenada dos produtos, liberando inicialmente o S3P, seguido pela liberação do ADP (**Figura 8**).

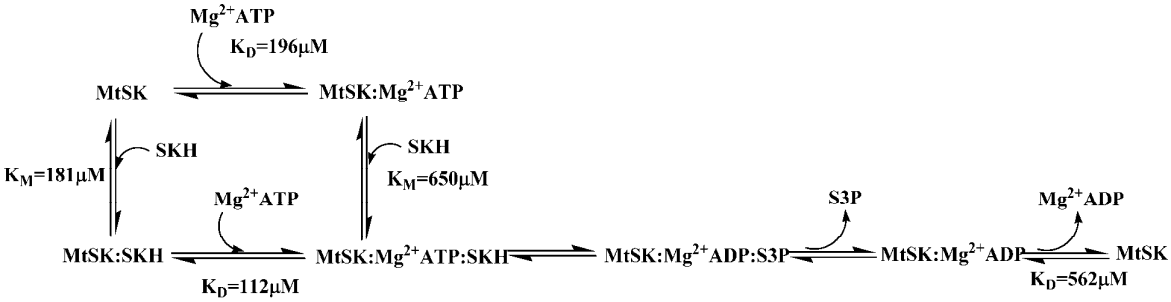

Figura 8. Mecanismo enzimático da proteína *Mt*SK e os valores das constantes de dissociação em equilíbrio do ligantes.

As assinaturas termodinâmicas de ligações não covalentes obtidas por ITC, relativas à ligação dos substratos/produtos na enzima livre, demonstraram que mudanças conformacionais ocorreram devido a ligação no domínio de associação de nucleotídeos e pela liberação de moléculas de água presas, no SKH e/ou ao sítio ativo da enzima.

O sequenciamento do genoma da cepa de *M. tuberculosis* H37Rv identificou a enzima *Mt*SK como uma enzima SK do tipo I codificada pelo gene *aroK* (SK I) (Cole, 1998), que possui um alto valor de K_{SKH} . Os experimentos para determinação dos parâmetros cinéticos verdadeiros em estado estacionário apresentados aqui e em outro trabalho (Gu, 2002) demonstraram que a enzima *Mt*SK deveria ser classificada como SK do tipo II codificada pelo gene *aroK* (SKII). Este resultado salienta a relevância do entendimento do modo de ação de uma enzima para determinação da sua função, além dos dados derivados de sua sequência primária e da resolução de sua estrutura,

fornecendo informações que de outro modo não seriam acessíveis e que permitem a determinação mais criteriosa de novas funções e o refinamento das definições atuais do EC (Almonacid, 2010).

O repertório atual de agentes anti-micobacterianos possui uma gama de alvos validados, tais como RNA polimerase, DNA girase, enoil-ACP redutase dependente de NADH e ATP sintase (Balganesh, 2008). O sequenciamento completo do genoma da cepa de *M. tuberculosis* H37Rv acelerou o estudo e a validação de alvos, auxiliando o desenvolvimento de novas drogas anti-TB (Cole, 2008). Consequentemente, análises de mecanismos de reação deveriam ser incluídas em programas que tem enzimas como alvos para o desenvolvimento racional de drogas. A metodologia de ITC vem sendo utilizada como uma importante ferramenta para a determinação direta de parâmetros termodinâmicos e cinéticos de reações enzimáticas (Bianconi, 2007). Recentemente, reconheceu-se que limitações inerentes à abordagem de *hight-throughtput screening* (triagem em larga escala) no processo de descoberta de novos candidatos a drogas promoveram a retomada do interesse da pesquisa farmacêutica nos métodos de desenvolvimento racional de drogas (Ladbury, 2010). A compreensão do modo de ação da *Mt*SK permitirá o planejamento de inibidores específicos para esta enzima com potencial aplicação na quimioterapia da TB. Os resultados aqui apresentados servirão como base para o planejamento racional de novos compostos anti-TB, podendo ainda contribuir para a maior compreensão da biologia do *M. tuberculosis*.

Referências

REFERÊNCIAS

A.J. Pittard, in: F.C. Neidhardt (Ed.), *Escherichia coli* and *Salmonella*: Cellular and Molecular Biology, ASM Press, Washington DC, 1996, pp.458-484.

B. Dhaliwal, C.E. Nichols, J. Ren, M. Lockyer, I. Charles, A.R. Hawkins, D.K. Stammers, FEBS Lett. 574 (2004) 49-54.

C. Vonrhein, G.J. Schlauderer, GE. Schulz, Structure, 3 (1995) 483-490.

C. W. Roberts., F. Roberts, R. E. Lyons, M. J. Kirisits, E. J. Mui, J. Finnerty,J. J. Johnson, D. J. Ferguson, J. R. Coggins, T. Krell, G. H. Coombs, W. K.Milhous, D. E. Kyle, S. Tzipori, J. Barnwell, J. B. Dame, J. Carlton, R.McLeod. (2002). J. Infect. Dis. 185(Suppl. 1):S25–S36

Cole ST, et al. Deciphering the biology of Mycobacterium tuberculosis from the complete genome sequence. Nature. 1998; 393: 537-544;

D.E. Almonacid, E.R. Yera, J.B.O. Mitchell, P.C. Babbitt, PLoS Comput. Biol. 6(3) 2010 e10000700.

F. Roberts, C. W. Roberts, J. J. Johnson, D. E. Kyle, T. Krell, J. R. Coggins,G. H. Coombs, W. K. Milhous, S. Tzipori, D. J. Ferguson, D. Chakrabarti, R. McLeod. (1998) Nature 393:801–805.

G. A. McConkey, (1999). Antimicrob. Agents Chemother. 43:175– 177.

G. A. McConkey., J. W. Pinney, D. R. Westhead, K. Plueckhahn, T. B. Fitzpatrick, P. Macheroux, B. Kappes. (2004). Trends Parasitol. 20:60–65.

G. Millar, A. Lewendon, M.G. Hunter, J.R. Coggins, Biochem. J. 237 (1986) 427–437.

G. Weber, Adv. Protein Chem. 29 (1975) 1-83.

Goodman & Gilman A, et al. As bases farmacológicas da terapêutica. Rio de Janeiro. Ed. McGraw-Hill, 2006: 1821p;

H. Chassaigne, R. Lobinski, Analyst 123 (1998) 2125–2130.

H. Fukada, K. Takahashi, Proteins. 33 (1998) 159-166.

H.Yan, M. D. Tsai. Adv. Enzymol. Relat. Areas Mol. Biol. (1999).73:103–134

Hargreaves S., WHO report highlights alarming rise of resistant tuberculosis. 2008; 8: 220;

I. Segel, Enzyme Kinetics, Behavior and Analysis of Rapid Equilibrium and Steady-state Enzyme Systems, John Wiley and Sons, New York, 1975.

J. Gan, Y. Gu, Y. Li, H. Yan, X. Ji, Biochemistry. 45 (2006) 8539-8545.

J.E. Ladbury, G.K. Klebe, E. Freire, Nat. Rev. Drug Discov. 9 (2010) 23-27.

J.H. Pereira, Oliveira J.S., F. Canduri, M.V. Dias, M.S. Palma, L.A. Basso, D.S. Santos, W.F.Jr. Azevedo, Acta Crystallogr. D Biol. Crystallogr. 60 (2004) 2310-2319.

J.S. Oliveira, C.A. Pinto, L.A. Basso, D.S. Santos, Protein Expr. Purif. 22 (2001) 430–435.

M.D. Hartmann, G.P. Bourenkov, A. Oberschall, N. Strizhov, H.D. Bartunik, J. Mol. Biol. 364 (2006) 411-423.

M.E. Maguire, J.A. Cowan, BioMetals. 15 (2002) 203-210.

M.J. Whipp, A.J. Pittard, J. Bacteriol. 177 (1995) 1627-1629.

M.L. Bianconi, Biophys. Chem. 126 (2007) 59-64.

M.M. Bradford, R.A. McRorie, W.L. Williams, Anal. Biochem. 72 (1976) 248–254).

M.V. Dias, L.M. Faím, I.B. Vasconcelos, J.S. Oliveira, L.A. Basso, D.S. Santos, W.F.Jr. Azevedo, Acta Crystallogr. Sect. F Struct. Biol. Cryst. Commun. 63 (2007) 63: 1-6.

Nikki M Parrish, James D Dick, William R Bishai, Mechanisms of latency in *Mycobacterium tuberculosis*, 1998, 6 , 107-112;
P. Edman, Arch. Biochem. 13 (1949) 283-286.

P. J. Keeling., J. D. Palmer, R. G. Donald, D. S. Roos, R. F. Waller, G. I. McFadden. (1999). Nature 397:219–220.

P.C. Engel, Enzyme Kinetics, John Wiley & Sons, Inc, New York, 1977.

P.F. Cook, W.W. Cleland, Enzyme Kinetics and Mechanism, Garland Science Publishing, New York, 2007.

P.H. Hirel, M.J. Schmitter, P. Dessen, G. Fayat, S. Blanquet, Proc. Natl. Acad. Sci. 86 (1989) 8247-8251.

R. Bentley, Crit. Rev. Biochem. Mol. Biol. 25 (1990) 307–384.

R. O'Brien, I. Haq, in J.E. Ladbury, M.L. Doyle (Eds.), Biocalorimetry 2: Applications of Calorimetry in the Biological Sciences, John Wiley & Sons, Ltd, West Sussex, London, 2004, pp.3-34.

R.G. Ducati, L.A. Basso, D.S. Santos Current drug targets, 3, (2007), 423-435.

S.A. Campbell., T. A. Richards, E. J. Mui, B. U. Samuel, J. R. Coggins, R. McLeod, C. W. Roberts. Int. J. Parasitol. (2004). 34:5–13.

S.T. Cole, R. Brosch, J. Parkhill, T. Garnier, C. Churcher, D. Harris, S.V. Gordon, K. Eiglmeier, S. Gas, C. E. 3rd Barry, F. Tekaia, K. Badcock, D. Basham, D. Brown, T. Chillingworth, R. Connor, R. Davies, K. Devlin, T. Feltwell, S. Gentles, N. Hamlin, S. Holroyd, T. Hornsby, K. Jagels, A. Krogh, J. McLean, S. Moule, L. Murphy, K. Oliver, J. Osborne, M. A. Quail, M. A. Rajandream, J. Rogers, S. Rutter, K. Seeger, J. Skelton, R. Squares, S. Squares, J. E. Sulston, K. Taylor, S. Whitehead, B.G. Barrell, Nature. 393 (1998) 537-544.

T. Krell, J. Maclean, D.J. Boam, A. Cooper, M. Resmini, K. Brocklehurst, S.M. Kelly, N.C. Price, A.J. Lapthorn, J.R. Coggins, Protein Sci. 10 (2001) 1137–1149.

T. Parish, N.G. Stoker, Microbiology, (2002), 148, 3069–3077

T.S. Balganesh, P.M. Alzari, S.T. Cole, Trends Pharmacol. Sci. 29 (2008) 576-581.

U.K. Laemmli, Cleavage of structural proteins during the assembly of the head of bacteriophage T4, Nature. 227 (1970) 680-685.

W.P. Jencks, Catalysis in Chemistry and Enzymology, Dover Publications, Inc., New York, 1975.

World Health Organization, Global Tuberculosis Control: a short update to the 2009 report, (2010).

Y Gu, L. Reshetnikova, Y. Li, Y. Wu, H. Yan, S. Singh, Ji X 319 (2002) 779-789.

Y. Zhang, P.S. Cremer, Curr. Opin. Chem. Biol. 10 (2006) 658-663.

Zahrt TC., 2003; 5: 159-167;

Anexos

Anexo A – The mode of action of recombinant Mycobacterium tuberculosis Shikimate Kinase: kinetics and thermodynamics analyses

Anexo B – Kinetic mechanism determination and analysis of metal requirement of dehydroquinate synthase from *Mycobacterium tuberculosis* H37Rv: an essential step in the function-based rational design of anti-TB drugs

Anexo C – UMP kinase from *Mycobacterium tuberculosis*: Mode of action and allosteric interactions, and their role in pyrimidine metabolism regulation

Anexo D – Recombinant *Escherichia coli* GMP reductase: Kinetic, catalytic and chemical mechanisms, and thermodynamics of enzyme-ligand binary complex formation

Anexo A

The mode of action of recombinant Mycobacterium tuberculosis Shikimate Kinase: kinetics and thermodynamics analyses

Leonardo Astolfi Rosado, Igor Bordin Vasconcelos, Mario Sérgio Palma, Diógenes Santiago Santos, Luiz Augusto Basso

Artigo submetido ao *Archives in Biochemistry and Biophysics*.

The mode of action of recombinant *Mycobacterium tuberculosis* Shikimate Kinase: kinetics and thermodynamics analyses

Leonardo A. Rosado[1,2], Igor B. Vasconcelos[1,3], Mario S. Palma[4], Diógenes S. Santos[1,2,3,*] and Luiz A. Basso[1,2,3,*]

[1]Centro de Pesquisas em Biologia Molecular e Funcional (CPBMF), Instituto Nacional de Ciência e Tecnologia em Tuberculose (INCT-TB), Pontifícia Universidade Católica do Rio Grande do Sul (PUCRS), Av. Ipiranga 6681, Porto Alegre, RS 90619-900, Brazil.
[2]Programa de Pós-Graduação em Medicina e Ciências da Saúde, PUCRS, Av. Ipiranga 6681, Porto Alegre, RS 90619-900, Brazil.
[3]Programa de Pós-Graduação em Biologia Celular e Molecular, PUCRS, Av. Ipiranga 6681, Porto Alegre, RS 90619-900, Brazil.
[4]Laboratório de Biologia Estrutural e Zooquímica, Centro de Estudos de Insetos Sociais, Departamento de Biologia, Instituto de Biociências de Rio Claro, Universidade Estadual Paulista (UNESP), Rio Claro, SP, Brazil.

[†]This work was supported by the National Institute of Science and Technology on Tuberculosis (DECIT/SCTIE/MS-MCT-CNPq-FNDCT-CAPES) and the Millennium Initiative Program (CNPq) to D.S.S. and L.A.B. D.S.S. (CNPq, 304051/1975-06), L.A.B. (CNPq, 520182/99-5), and M.S.P. (CNPq, 500079/90-0) are Research Career Awardees of the National Research Council of Brazil (CNPq). L.A.R. is recipient of an MSc student scholarships awarded by CAPES.

Running title: Mode of action of *M. tuberculosis* Shikimate Kinase

*Corresponding authors: Luiz A. Basso or Diógenes S. Santos

Av. Ipiranga 6681 – Tecnopuc – Prédio 92A, ZIP CODE 90619-900, Porto Alegre, RS, Brazil. Phone/Fax: +55 51 33203629; E-mail addresses: luiz.basso@pucrs.br or diogenes@pucrs.br

Abstract

Tuberculosis (TB) still remains as one of main cause of mortality worldwide due to a single infectious agent, *Mycobacterium tuberculosis*. The *aroK*-encoded *M. tuberculosis* Shikimate Kinase (*Mt*SK), the fifth enzyme of the shikimate pathway, catalyzes phosphate transfer from ATP to the carbon-3 hydroxyl group of shikimate, yielding shikimate 3-phosphate and ADP. Disruption of *aroK* gene has demonstrated that *Mt*SK is essential for the viability of *M. tuberculosis*. Here we present purification of *Mt*SK to homogeneity, mass spectrometry analysis, N-terminal amino acid sequencing, and oligomeric state determination of the recombinant protein. Steady-state kinetics, and studies on ligand binding by fluorescence spectroscopy and isothermal titration calorimetry (ITC) suggest that the chemical reaction catalyzed by monomeric *Mt*SK follows a rapid-equilibrium random order of substrate binding, and ordered product release in which shikimate-3-phosphate release is followed by ADP dissociation to yield free enzyme. ITC results showed significant heat changes upon ligand binding to free *Mt*SK enzyme, thereby providing thermodynamic signatures of non-covalent interactions to each binding process. These results provide a better understanding of the mode of action of *Mt*SK that should be useful to guide the rational (function-based) design of inhibitors of this enzyme that can be further be evaluated as anti-TB drugs.

Keywords: steady-state kinetics; isothermal titration calorimetry; fluorescence spectroscopy; enzyme mechanism; shikimate kinase; tuberculosis

1. **Introduction**[1]

Tuberculosis (TB), owing to *Mycobacterium tuberculosis* infection, still remains as a major global health problem. Approximately 9 million new cases of TB are detected each year, and close to 2 million people die from the disease [1]. In 2008, it has been estimated that 390 000–510 000 cases of multidrug-resistant tuberculosis (MDR-TB is defined as TB caused by strains of *M. tuberculosis* that are resistant to at least isoniazid and rifampicin) emerged globally [2]. In 2008, MDR-TB caused an estimated 150 000 deaths. It has also been reported that 5.4% of MDR-TB cases were found to have extensively drug-resistant tuberculosis (XDR-TB is defined as MDR-TB plus resistance to a fluoroquinolone and at least one second-line injectable agent: amikacin, kanamycin and/or capreomycin) [2]. In addition, TB cases due to infection with totally drug-resistant strains (TDR-TB) have been reported [3]. The emergence of drug-resistant strains of *M. tuberculosis* has thus highlighted the need for the development of new therapeutic strategies to combat TB.

Rational inhibitor design relies on mechanistic and structural information on the target enzyme. Enzymes offer unique opportunities for drug design that are not available to cell surface receptors, nuclear hormone receptors, ion channel, transporters, and DNA [4]. It has been pointed out that one of the lessons to be learned from marketed enzyme inhibitors is that the most potent and effective inhibitors take advantage of enzyme chemistry to achieve inhibition [5]. Moreover, the recognition of the limitations of high-

[1] *Abbreviations used:* ADP, adenosine 5'-diphosphate; ATP, adenosine 5'-triphosphate; *Ec*SK, *aroL*-encoded SK from *Erwinia chrysanthemi*; E4P, D-erythrose 4-phosphate; ESI-MS, electrospray ionization mass spectrometry; HEPES, *N*-2-hydroxyethylpiperazyne-*N'*-2-ethanesulfonic acid; ITC, isothermal titration calorimetry; LDH, L-lactate dehydrogenase; MDR-TB, human infection with to multi-drug resistant strains of *M. tuberculosis*; *Mt*SK, *Mycobacterium tuberculosis* Shikimate Kinase; NADH, nicotinamide adenine dinucleotide; NMP, nucleoside monophosphate; PEP, phosphoenolpyruvate; PK, pyruvate kinase; SDS-PAGE, sodium dodecyl sulfate-polyacrylamide gel eletrophoresis; SKH, shikimate, [3*R*-(3α,4α,5β)]3,4,5-trihydroxy-1-cyclohexene-1-carboxylic acid; S3P, shikimate 3-phosphate; TB, tuberculosis; TDR-TB, human infection with totally drug-resistant strains of *M. tuberculosis*; Tris, tris(hydroxymethyl)aminomethane; XDR-TB, human infection with to extensively drug-resistant strains of *M. tuberculosis*.

throughput screening approaches in the discovery of candidate drugs has rekindled interest in rational design methods [6]. Accordingly, mechanistic analysis should always be a top priority for enzyme-targeted drug programs aiming at the rational design of potent enzyme inhibitors. Moreover, targets that are both essential to survival of, and exclusive to, *M. tuberculosis* are particularly promising as their inhibition could lead to the development of non-toxic drugs to the human host and having effective killing effect on the pathogen [7].

The biosynthesis of aromatic rings from carbohydrate precursors involves a range of chemical transformations that together constitute the shikimate pathway; through seven enzymatic steps (**Fig. 1**), phosphoenolpyruvate (PEP) and D-erythrose 4-phosphate (E4P) are condensed to the branch point compound chorismate (endproduct), which leads to several additional terminal pathways [7,8]. The shikimate pathway is essential in algae, higher plants, fungi, bacteria, apicomplexan parasites and sea anemone, but absent from humans [7-16]. The mycobacterial shikimate pathway (the main trunk) leads to the biosynthesis of chorismic acid, which is converted by five distinct enzymes to prephenate (precursor of phenylalanine and tyrosine), anthranilate (precursor of tryptophan), aminodeoxychorismate (precursor of *para*-aminobenzoic acid -PABA – which, in turn, leads to tetrahydrofolate synthesis), *para*-hydroxybenzoic acid (precursor of ubiquinone or Coenzyme Q), and isochorismate (common precursor of naphtoquinones, menaquinones and mycobactins) [7].

The *aroK*-encoded *M. tuberculosis* Shikimate Kinase (*Mt*SK; EC 2.7.1.71), the fifth enzyme of the pathway, catalyzes a phosphate transfer from ATP to the carbon-3 hydroxyl group of shikimate (SKH) forming shikimate 3-phosphate (S3P) (**Fig. 2**). Disruption of *aroK* gene has demonstrated that *Mt*SK, and thus the common aromatic biosynthesis pathway, is essential for the viability of *M. tuberculosis* [17]. We have

previously reported cloning and expression in *Escherichia coli* of recombinant *Mt*SK in functional form [18], thereby confirming the correct *in silico* assignment to the structural gene encoding this protein. Our research group [19,20] and others [21-23] have reported crystal structure determinations of *Mt*SK. Three functional motifs of nucleotide-binding enzymes were recognizable in *Mt*SK, including a Walker A-motif (that forms the phosphate-binding loop; P-loop), a Walker B-motif, and an adenine-binding loop. *Mt*SK belongs to the family of nucleoside monophosphate (NMP) kinases, which are composed of three domains: (1) the CORE domain containing the five stranded parallel β-sheet and the P-loop (residues 9-17), which forms the binding site for nucleotides; (2) the LID domain (residues glycine-112 to aspartate-124), which closes over the active site and has residues that are essential for the binding of ATP; and (3) the NMP-binding domain (residues threonine-33 to glutamate-61; also known as SB domain in *Mt*SK), which functions to recognize and bind shikimate [19-22]. More recently, based on an analysis of global movements upon ligand binding, it has been proposed that *Mt*SK is comprised of four domains [23]: (1) the ESB domain (extended SB; residues 32-93); (2) the nucleotide-binding (NB) site that includes the P-loop (Walker A motif, residues 9-17), the AB-loop (residues 148-155), and the segment of 101-110; (3) the LID domain (residues 112-124); and (4) the Reduced Core (RC) domain. A characteristic feature of NMP kinases is that they undergo large conformational changes during catalysis [24].

Based on a series of high-resolution crystal structures of *Mt*SK in apo form and as binary and ternary complexes, it has been proposed that the enzyme mechanism is random sequential binding of SKH and ATP, and release of ADP product is followed by S3P to generate free enzyme [23]. However, no description of *Mt*SK enzyme mechanism in solution has, to the best of our knowledge, ever been described. Here we present purification of recombinant *Mt*SK to homogeneity, mass spectrometry analysis, N-terminal

amino acid sequencing, and oligomeric state determination of the recombinant protein. We also present true steady-state kinetic parameters determination, and ligand binding by fluorescence spectroscopy and isothermal titration calorimetry data. These data demonstrate that the chemical reaction catalyzed by monomeric *Mt*SK follows a random order mechanism of substrate binding, and that S3P product is released first followed by ADP dissociation to yield free enzyme. Understanding the mode of action of *Mt*SK will inform us on how to better design inhibitors targeting this enzyme with potential therapeutic application in TB chemotherapy. The results here presented may also help chemical biologists to design function-based chemical compounds to carry out either loss-of-function (inhibitors) or gain-of-function (activators) experiments to reveal the biological role of *Mt*SK in the context of whole *M. tuberculosis* cells. Accordingly, it is hoped that the results here described may be useful to the rational design of anti-TB agents and that they may contribute to our understanding of the biology of *M. tuberculosis*.

2. Material and methods

2.1 Purification of M. tuberculosis Shikimate Kinase (MtSK)

The recombinant enzyme was expressed in *Escherichia coli* BL21 (DE3) host cells as previously described [18]. Approximately 6 g of cells were suspended in 24 mL of Tris-HCl 50 mM pH 7.6, disrupted by sonication, and the cell debris removed by centrifugation (48,000*g* for 60 min). $MgCl_2$ was added to the supernatant to a final concentration of 10 mM followed by addition of 1 mg of DNAse, stirred for 30 min at 4 °C, and centrifuged (10,000*g* for 30 min). Interestingly, addition of $MgCl_2$ resulted in precipitation of *Mt*SK whereas a number of proteins remained in the supernatant. Accordingly, this step served two purposes in the purification protocol: lysis of DNA by DNAse, and *Mt*SK precipitation. The pellet was suspended in Tris-HCl 50 mM pH 7.6 containing KCl 500 mM, and centrifuged (10,000*g* for 15 min). This solution was concentrated down to approximately 20 mL, and 20 mL of Tris-HCl 50mM pH 7.6 containing KCl 500 mM and $(NH_4)_2SO_4$ 2M, resulting in a solution containing 1M $(NH_4)_2SO_4$. This solution was clarified by centrifugation. The supernatant was loaded on a Phenyl Sepharose 16/10 column (GE healthcare) previously equilibrated with buffer A (Tris-HCl 50mM, KCl 500mM, $(NH_4)_2SO_4$ 1M, pH 7.6) and the adsorbed material eluted with a linear gradient of buffer B (Tris-HCl 50mM, KCl 500mM, pH 7.6) at 1 mL min^{-1}. The protein fractions containing the *Mt*SK were pooled and loaded on a Sephacryl S-100 HR column (GE Healthcare) and isocratically eluted with buffer B at 0.25 mL min^{-1}. The fractions containing homogeneous recombinant *Mt*SK were pooled, and stored in 85 % $(NH_4)_2SO_4$. Expression and protein purification of recombinant *Mt*SK was confirmed by 12 % sodium dodecyl sulfate-

polyacrylamide gel eletrophoresis (SDS-PAGE) stained with Coomassie Brilliant Blue [25]. Protein concentration was determined by the method of Bradford *et al*. [26].

2.2 Electrospray ionization mass spectrometry (ESI-MS) analysis

The homogeneity of recombinant protein preparation was assessed by electrospray ionization mass spectrometry (ESI-MS), employing some adaptations made to the system described by Chassaigne and Lobinski [27]. Samples were analyzed on a triple quadrupole mass spectrometer (model QUATTRO II) equipped with a standard electrospray (ESI) probe (Micromass, Altrincham, United Kingdom), and adjusted to a flow rate of *ca*. 250 μL min^{-1}. The source temperature (80 °C) and needle voltage (3.6 kV) were maintained constant throughout the experimental data collection, applying a drying gas (nitrogen) flow of 200 L h^{-1} and a nebulizer gas flow of 20 L h^{-1}. The mass spectrometer was calibrated with intact horse heart myoglobin and its typical cone-voltage induced fragments. The subunit molecular mass of recombinant *Mt*SK protein was determined by ESI-MS, by adjusting the mass spectrometer to give a peak with at half-height of 1 mass unit, and the sampling cone-to-skimmer lens voltage controlling the transfer of ions to the mass analyzer was set to 38 V. About 50 pmol (10 μL) of each sample was injected into the electrospray transport solvent. The ESI spectrum was obtained in the multichannel acquisition mode, scanning from 500 to 1,800 *m*/*z* at a scan time of 7 s. The mass spectrometer is equipped with MassLynx and Transform software for data acquisition and spectrum handling.

2.3 N-terminal amino acid sequencing

The N-terminal amino acid residues of homogeneous recombinant MtSK were identified by automated Edman degradation sequencing method [28] using PPSQ 21A gas-phase sequencer (Shimadzu).

2.4 Oligomeric state determination

The oligomeric state of homogeneous *Mt*SK was determined by size exclusion liquid chromatography on Superdex 200 (HR 10/30) column (GE Healthcare). The column was pre-equilibrated with 50 mM Tris-HCl pH 7.5 containing 200 mM NaCl at a flow rate of 0.4 mL min^{-1} (4 °C), with UV detection at 280 nm. The calibration curve was constructed employing the following protein standards: ribonuclease A (13.7 kDa), quimotripsinogen (25 kDa), ovalbumine (43 kDa), albumine (67 kDa), aldolase (158 kDa), catalase (232 kDa), and ferritine (440 kDa). The elution volumes (V_e) of were used to calculate their corresponding partition coefficient (K_{av}, Eq. 1). Blue dextran was utilized for determination of the void volume (V_o). V_t is the total bead volume of the column. A volume of 100 µL of recombinant protein was loaded on the gel filtration column to obtain V_e *Mt*SK. The K_{av} value for each protein was plotted against their corresponding molecular mass.

$$K_{av} = \frac{V_e - V_o}{V_t - V_o} \qquad \text{Eq. 1}$$

2.5 Steady-state kinetics

Recombinant *Mt*SK enzyme activity was assayed in the the forward direction by coupling the ADP product to the pyruvate kinase (PK; EC 2.7.1.40) and lactate dehydrogenase (LDH; EC 1.1.1.27) reactions following the protocol described elsewhere [18,29]. Shikimate-dependent oxidation of NADH was continuously monitored at 340 nm ($\varepsilon = 6.22 \times 10^3$ M^{-1} cm^{-1}). All reactions were carried out at 25 °C and initiated with addition of recombinant *Mt*SK (1 μg mL^{-1}). The assay mixture contained 100 mM Tris–HCl buffer, pH 7.6, 100 mM KCl, 5 mM $MgCl_2$, 1.5 mM PEP, 0.2 mM NADH, 6 U mL^{-1} PK, and 5 U mL^{-1} LDH. Initial steady-state rates were calculated from the linear portion of the reaction curve under experimental conditions in which less than 5 % of substrate was consumed. True steady-state kinetics parameters were determined from initial velocity measurements at varying concentrations of SKH (37 - 4800 μM) at varied-fixed ATP concentrations (9 - 1200 μM).

Values of the steady-state kinetics parameters and their respective errors were obtained by fitting the data to the appropriate equations using the non-linear regression function of SigmaPlot 9.0 (SPSS, Inc). Hyperbolic saturation curves of initial rate data at single concentration of the fixed substrate and varying concentrations of the other were fitted to the Michaelis-Menten equation (Eq. 2) [30,31].

$$v = \frac{VA}{K + A} \qquad \text{Eq. 2}$$

The family of lines intersecting to the left of the *y*-axis in double-reciprocal plots was fitted to Eq. 3, which describes a mechanism involving ternary complex formation and a sequential substrate binding [30,31].

$$v = \frac{VAB}{K_{ia}K_b + K_aB + K_bA + AB}$$ Eq. 3

For Eq. 2 and Eq. 3, v is the initial velocity, V is the maximal initial velocity, A and B are the concentrations of the substrates, K_a and K_b are their respective Michaelis constants, and K_{ia} is the dissociation constant for enzyme-substrate A binary complex formation.

2.6 Equilibrium fluorescence spectroscopy

*Mt*SK intrinsic protein fluorescence measurements were carried out to both determine the order of substrate/product addition/dissociation on/from the catalytic site and distinguish the enzyme kinetic mechanism. As *Mt*SK has no tryptophan residues, changes in protein tyrosine fluorescence (the polypeptide chain of *Mt*SK has 3 Tyr residues) upon ligand binding were monitored. Fluorescence measurements were carried out in a RF-5301 PC Spectrofluorophotometer (Shimadzu) at 25 °C. Excitation and emission wavelengths were, respectively, 280 and 315 nm. Excitation and emission slits were 5 nm. As protein tyrosine typically has a low sensitivity (low maximum absorbance and low fluorescence quantum yield), *Mt*SK concentration for binding experiments was 10 μM. Fluorescence titrations of binary complex formation were carried out by making microliter additions of the following compounds to 2 mL solution containing 10 μM *Mt*SK in 100 mM Tris-HCl, 100 mM KCl, 5 mM $MgCl_2$, pH 7.6: 120 mM SKH stock solution (10 – 1100 μM final concentration); 120 mM S3P stock solution (59.97-952.3 μM final concentration). Control experiments were performed in the same experimental conditions except that no substrate was added, and these values were subtracted from those

obtained in the presence of substrate. However, owing to a large inner filter effect, ATP and ADP binding to free *Mt*SK could not be determined by fluorescence spectroscopy.

Equilibrium fluorescence spectroscopy data were fitted to Eq. 4, in which F is the observed fluorescence, F_0 is the initial fluorescence, ΔF is the change in fluorescence, and K_D represents the equilibrium dissociation constant for protein:ligand binary complex formation.

$$F = F_0 + \frac{\Delta F[LIGAND]}{K_D + [LIGAND]} \qquad \text{Eq. 4}$$

2.7 Isothermal titration calorimetry (ITC)

ITC experiments were carried out using an iTC_{200} Microcalorimeter (Microcal, Inc., Northampton, MA). The equipment's reference cell volume is 200 µL and syringe final volume is 39 µL. Calorimetric experiments were carried out with substrates (SKH and ATP), and with products (S3P and ADP) at 25 °C. The reference cell (200 µL) was loaded with water during all experiments and the sample cell (200 µL) was filled with *Mt*SK at a concentration of 100 µM for ATP and ADP binding experiments, and at 130 µM for SKH and S3P binding experiments. The injection syringe (39 µL) was filled with substrates or products at different concentrations: ATP and ADP at 6 mM, and SKH and S3P at 4.2 mM. Owing to the large enthalpy of ionization of Tris buffer used in steady-state kinetics and fluorescence spectroscopy [32], all ITC measurements were carried out in HEPES 50 mM, KCl 50 mM and $MgCl_2$ 5mM, pH 7.5. The binding reaction started with one injection of 0.5 µL of ligand followed by 17 injections of 2.26 µL at intervals of 180 s, reaching a final volume 39 µL with a stirring speed of 500 RPM. The heat variation was monitored inside the cell allowing to determine the binding enthalpy of the process (ΔH) and the

equilibrium association constant (K_a). All enthalpy values for binding reactions were exothermic. Control titrations were performed to subtract the heats of dilution and mixing for each experiment.

The Δ*G* (Gibbs free energy) of binding was calculated using the relationship described in Eq. 5, in which *R* is the gas constant (8.314 J K^{-1} mol^{-1}), *T* is the temperature in Kelvin (T = °C + 273.15), and K_a is the association constant at equilibrium. The entropy of binding (Δ*S*) can also be determined by this mathematical formula. Single set of sites model was utilized to determine the binding and thermodynamics constants. The initial value for *n* was fixed as 1 since *Mt*SK is monomeric in solution, and estimates for K_a, and Δ*H* parameters were refined by standard Marquardt nonlinear regression method provided in the Origin 7 SR4 software.

$$\Delta G^o = -RT \ln K_a = \Delta H^o - T\Delta S^o \qquad \text{Eq. 5}$$

3. Results and discussion

3.1 Recombinant MtSK protein purification

Recombinant *Mt*SK was purified to homogeneity using a three-step protein purification protocol comprising a crude extract precipitation, a hydrophobic chromatographic step (Phenyl Sepharose) followed by a gel filtration column (Sephacryl S-100). The protein precipitation of the crude extract with $MgCl_2$ at a final concentration of 10 mM was efficient at precipitating *Mt*SK whereas a number of contaminants remained in the supernatant (**Fig. 3**). It has been pointed out that direct ion-macromolecule interactions as well as interactions with water molecules in the first hydration shell of macromolecules appear to play a central role to Hofmeister effects [33]. The Hofmeister series ranks the relative influence of ions on the physical behavior of a wide variety of aqueous processes ranging from colloidal assembly to protein folding. Usually, the specific ion effects of the Hofmeister series are more pronounced for anions than for cations [33]. The Cl^- anion is situated in the borderline between kosmotropes ("water structure makers", strongly hydrated, stabilizing and salting-out effects on proteins) and chaotropes ("water structure breakers", destabilize folded proteins and have salting-in effects on proteins) species. The Mg^{2+} ion has chaotropic (salting-in) effect. It is thus somewhat puzzling the salting-out effect of 10 mM $MgCl_2$ on *Mt*SK. However, it has recently been pointed out that the transport number of Mg^{2+} cation is higher than that for the other common biological cations, and the solvent exchange rate is over 3 orders of magnitude less than that for other common cations [34]. It would thus imply that Mg^{2+} cation would have a significant but largely unstudied effect on ordering of solvent and molecules in solution [34]. Notwithstanding, it is not warranted to advance any

explanation as regards the $MgCl_2$ salting-out effect on *Mt*SK. This protein precipitation step was followed by two chromatographic steps, namely, a hydrophobic followed by a size-exclusion column, yielding approximately 20 mg of functional homogenous *Mt*SK per 1.5 L of cell culture. The homogeneous recombinant *Mt*SK was stored in 85 % $(NH_4)_2SO_4$ at 4°C with no loss of activity.

3.2 Electrospray ionization mass spectrometry (ESI-MS) analysis

A value of 18,451 Da for the subunit molecular mass of recombinant *Mt*SK protein was determined by ESI-MS. This result is consistent with post-translational removal of N-terminal methionine residue (131.2 Da) from the full-length gene product (predicted mass, 18,583 Da). The ESI-MS result also revealed no peak at the expected mass of both *aroK*-encoded Shikimate Kinase I (19,526 Da) and *aroL*-encoded Shikimate Kinase II (18,998 Da) from *E. coli* SK [35], thus providing support for the identity of purified recombinant protein.

3.3 N-terminal amino acid sequencing

The first 8 N-terminal amino acid residues of recombinant *Mt*SK were identified as APKAVLGL by the Edman degradation sequencing method. This result unambiguously identifies the purified protein as *Mt*SK, since the N-terminal amino acid sequence of *aroK*-encoded Shikimate Kinase I and *aroL*-encoded Shikimate Kinase II from *E. coli* are, respectively, MAEKRNIFLV and MTQPLFLIGP. The Edman degradation result also confirms removal of the N-terminal methionine residue, and is in agreement with no observation of N-terminal methionine in the crystal structure of *Mt*SK:MgADP:SKH ternary

complex [19]. The excision of N-terminal methionine is a common type of post-translational modification process that occurs in protein synthesized in the cytoplasm of prokaryotic cells. The cleavage of the initiator methionine is usually directed by the penultimate amino acid residues with the smallest side chain radii of gyration (Gly, Ala, Ser, Thr, Pro, Val, and Cys) [36]. Removal of N-terminal methionine from recombinant *Mt*SK polypeptide chain conforms to this rule since alanine is the penultimate amino acid residue.

3.4 Oligomeric state determination

A value of 20.72 ± 0.5 kDa for the molecular mass of homogeneous recombinant *Mt*SK was estimated by gel filtration chromatography (data not shown). This result demonstrates that *Mt*SK is a monomer in solution, since ESI-MS analysis suggested a value of 18,451 Da for the subunit molecular mass for the recombinant protein.

3.5 Steady-state kinetics

Hyperbolic initial velocity as a function of substrate concentration (either ATP or SKH) was plotted as a linear function of reciprocal of initial velocity against the reciprocal of substrate concentration (double-reciprocal or Lineweaver-Burk plot). These data allow both determination of true steady-state kinetic parameters and *Mt*SK enzyme mechanism. The double-reciprocal plots showed a family of lines intersecting to the left of the *y*-axis (**Fig. 4**), which is consistent with ternary complex formation and a sequential mechanism. This pattern of lines rules out ping-pong (parallel lines), steady-state random (that gives non-linear reciprocal plots), and rapid-equilibrium ordered (one of the family of lines

should cross at a single value on the *y*-axis) mechanisms. However, the double-reciprocal plots alone cannot distinguish between rapid-equilibrium random and steady-state compulsory ordered bi bi mechanisms. The double-reciprocal data were fitted to the equation for a sequential initial velocity pattern (Eq. 3), yielding the following values for the true steady-state kinetic parameters (Table 1): k_{cat} = 60 (± 8) s^{-1}, K_{MgATP} = 112 (± 4) µM, K_{SKH} = 650 (± 28) µM, k_{cat}/K_{MgATP} = 5.4 (± 0.7) x 10^5 $M^{-1}s^{-1}$, and k_{cat}/K_{SKH} = 0.9 (± 0.1) x 10^5 $M^{-1}s^{-1}$. *E. coli* has two Shikimate Kinase enzymes: *aroK*-encoded SK I and *aroL*-encoded SK II [38]. The K_{SKH} value for *E. coli* SK I (20 mM) is larger than the value for *E. coli* SK II (200 µM) (Table 1). Although the complete sequencing of *M. tuberculosis* H37Rv genome has identified by sequence homology the presence of *aroK*-encoded SK I [39], the kinetic data presented here and elsewhere [37] show that *Mt*SK would more appropriately be described as a *aroL*-encoded type II enzyme. In addition, although the steady-state kinetic parameters are in good agreement with ones previously reported [37], no description of *Mt*SK enzyme mechanism has been presented. To distinguish between random and compulsory ordered bi bi mechanisms, substrate(s) and product(s) binding experiments were carried out as described below.

3.6 Equilibrium fluorescence spectroscopy

In equilibrium binary complex formation experiments, there was a quench in the intrinsic *Mt*SK protein fluorescence upon binding of either SKH or S3P. Titration of *Mt*SK with SKH was hyperbolic (**Fig. 5**), and fitting the data to Eq. 4 yielded a value of 124 (± 7) µM for the equilibrium dissociation constant of SKH (K_D). No change in protein fluorescence could be observed for S3P binding to free *Mt*SK (data not shown). However, it cannot be assumed that no *Mt*SK:S3P binary complex was formed because S3P

binding to free enzyme may result in no change in protein fluorescence. In addition, as previously mentioned, ATP and ADP binding to *Mt*SK could not be assessed by fluorescence spectroscopy due to large inner filter effects. Accordingly, ITC experiments were carried out.

3.7 Isothermal titration calorimetry (ITC)

ITC measurements were carried out to both determine the order, if any, of addition of substrate and the order of product release to yield free enzyme. In agreement with fluorescence spectroscopy results, no binding of S3P to free enzyme could be detected by ITC measurements (data not shown). On the other hand, ITC measurements showed binding of SKH, Mg^{2+}ATP and Mg^{2+}ADP to free *Mt*SK enzyme (**Fig. 6**, Table 2). These results support a mechanism in which binding of substrates (SKH and ATP) to *Mt*SK is random, and S3P product release is followed by ADP dissociation yield free enzyme. The value for the SKH equilibrium dissociation constant determined by fluorescence spectroscopy (124 μM) is in good agreement with the value determined from ITC data (181 μM). As the double-reciprocal plots of initial velocity measurements could not distinguish between rapid-equilibrium random and steady-state compulsory ordered bi bi mechanisms, fluorescence spectroscopy and ITC results indicate that the bi bi mechanism of *Mt*SK is rapid-equilibrium random order of substrate addition. Based on a series of crystal structures, it has been proposed that substrate binding to *Mt*SK is random [23], in agreement with the results presented here. However, whether an enzyme mechanism is rapid equilibrium or steady state cannot be identified by crystal structure determinations. In addition, crystal structure analysis suggested that ADP product release is followed by S3P to generate free enzyme [23]. Here we clearly demonstrate that S3P

product is released first, followed by dissociation of ADP from *Mt*SK:ADP binary complex to generate free enzyme for the next round of catalysis.

The ITC results showed significant heat changes upon ligand (SKH, ATP, or ADP) binding to free *Mt*SK enzyme, thereby providing thermodynamic signatures of non-covalent interactions to each binding process. Observed enthalpies arise largely as a result of changes in interatomic interactions (e.g., hydrogen bonds and/or van der Waals interactions), in which the sign indicates whether there is a net favourable (negative ΔH) or unfavourable (positive ΔH) redistribution of the network of interactions between the reacting species (including solvent) [40]. Hydrophobic interactions are related to the relative degrees of disorder in the free and bound systems and thus these interactions are reflected in the entropy change. The release of "bound" water molecules from a surface to the bulk solvent is usually a source of favourable entropy (positive ΔS). Protein conformational changes in either ligand or protein upon binary complex formation are entropically unfavourable (negative ΔS) [40].

The ITC data for Mg^{2+}ADP binding to *Mt*SK suggest that it is accompanied by a favourable redistribution of H-bonds and/or van der Waals interactions, and a large entropically unfavorable contribution, resulting in a large value for the equilibrium dissociation constant (Table 2). It is thus tempting to suggest that large *Mt*SK protein conformational changes occurring upon dissociation of Mg^{2+}ADP from *Mt*SK:Mg^{2+}ADP binary complex would regenerate free enzyme in a conformation that allows binding of substrate(s) to start a new cycle of catalysis. In addition, the large K_D value for ADP may avoid *Mt*SK:Mg^{2+}ADP:SKH dead-end ternary complex formation, which would lock the enzyme active site in an inactive form. The ITC data for Mg^{2+}ATP binding to *Mt*SK indicate that the molecular recognition process is accompanied by small favourable redistribution of H-bonds and/or van der Waals interactions, and unfavourable entropic

contribution (Table 2). The latter may reflect protein conformational changes upon Mg^{2+}ATP binding. As pointed out above, *Mt*SK belongs to the family of NMP kinases, which are composed of CORE, LID and NMP-binding (SKH-binding) domains. The LID domain closes the active site and has residues that are essential for ATP binding [19-23]. Moreover, NMP kinases undergo large conformational changes during catalysis [24]. It should be pointed out that a fourth domain has been proposed to be present in *Mt*SK structure, namely, the RC domain [23]. Interestingly, the dissociation constant value for binding of ATP (196 μM) is smaller than for ADP (562 μM). It may be accounted for by the direct interaction between the γ-phosphate of ATP and either Arg117 residue observed in the crystal structure of *Mt*SK:ATP binary complex or Lys15 that is part of the P-loop [23]. The unfavourable entropic contributions upon ATP and ADP binding to free *Mt*SK enzyme can thus be accounted for by protein conformational changes. The NMP-binding (or SB) domain of *Mt*SK functions to recognize and bind SKH [19-23]. The SKH substrate binding to free *Mt*SK is associated with favourable H-bonds and/or van der Waals interactions and a positive entropic contribution (Table 2). The latter may reflect release of “bound” water molecules either from substrate or from *Mt*SK active site to solvent. The equilibrium constant for the intramolecular hydrolysis of bound ATP to bound ADP and phosphate at enzyme active sites is considerably larger than the equilibrium constant for ATP hydrolysis in solution [41]. The ITC data on SKH binding may indicate exclusion of water molecules from *Mt*SK active site to minimize ATP hydrolysis, in agreement with previous proposals [19]. Taken together, the ITC data may be reporting on protein conformational changes upon ATP or ADP binding, and on exclusion of water molecules from *Mt*SK active site upon SKH binding. These conclusions are in agreement with structural data on *Mt*SK that showed large rotational movement of the NB domain upon ADP and ATP binding, bringing it closer to the SKH binding domain [23]. However, the ITC data on SKH

are not in agreement with rotational movements of the ESB domain and LID closure upon substrate binding to *Mt*SK [23]. How to reconcile the ITC and crystal structure data on SKH binding to *Mt*SK? A conceivable explanation to these apparently conflicting data may be that the entropically unfavourable contribution due to protein conformational changes was off-set by a large entropically favourable contribution due to release of "bound" waters from protein/substrate to the bulk solvent. However, the crystal structure of *Mt*DK:SKH binary complex indicated that there appears to be a continuum of conformations, and that one of them showed no closure of the LID domain upon SKH binding [23], which would be consistent with no conformational changes upon SKH binding that would be entropically unfavourable and water release as the main contribution to the favourable entropy (positive ΔS).

It has been shown for *aroL*-encoded SK from *Erwinia chrysanthemi* (*Ec*SK) that the K_M for ATP (620 μM) is approximately four times lower than its K_D value (2.6 mM) [42]. These results prompted the proposal that the conformational changes in *Ec*SK associated with binding of the first substrate leads to an increase in the affinity for the second substrate. However, based on the results for Mg^{2+}ATP, it does not appear to hold for *Mt*SK since the K_M value (112 μM) is in the same concentration range of K_D values determined by both fluorescence spectroscopy (124 μM) and ITC (196 μM). It has been put forward that the K_M value for a substrate in rapid-equilibrium random-order mechanisms is equal to the dissociation constant for dissociation of the substrate from the ternary complex [43]. The K_M value for SKH (Table 1, 650 μM) is approximately 3.6-fold larger than its K_D value (Table 2, 181 μM). These results suggest a positive free energy coupling (ΔG_{coop} = 3.2 kJ mol^{-1}) for SKH binding to *Mt*SK:Mg^{2+}ATP. There thus appears to be a negative cooperativity ($\Delta G_{coop} > 0$) [44] in energy coupling of Mg^{2+}ATP binding to *Mt*SK on SKH binding to the binary complex and ensuing ternary complex formation. This

finding is somewhat puzzling because one would expect that Mg^{2+}ATP binding to *Mt*SK should result in increased affinity for SKH. Interestingly, no direct interaction between SKH and the LID domain of *Mt*SK was seen when SKH binds as the second ligand to the nucleotide-bound enzyme [23]. These reduced interactions may account for the larger K_M value as compared to K_D for SKH.

4. Summary

Steady-state kinetics, fluorescence spectroscopy and isothermal titration calorimetry data showed that the enzyme mechanism of monomeric *Mt*SK is rapid-equilibrium random order of substrate addition, and ordered product release with S3P being released first followed by ADP dissociation from the binary complex to regenerate free enzyme. The thermodynamic signatures of non-covalent interactions obtained from ITC data upon substrate(s)/product(s) binding to *Mt*SK demonstrated conformational changes following nucleotide binding and release of "bound" water molecules from SKH and/or *Mt*SK active site to bulk solvent. Interestingly, although the genome sequencing of *M. tuberculosis* H37Rv strain has identified *Mt*SK as an *aroK*-encoded enzyme (SK I) [39], which has a large value for K_{SKH}, the measurements of true steady-state kinetic parameters presented here and elsewhere [37] show that *Mt*SK would more appropriately be described as an *aroL*-encoded type II enzyme (SK II). Incidentally, it has recently been pointed out that understanding the mode of action of an enzyme can be used to inform functional annotation of newly determined sequences and structures, to select appropriate enzyme scaffolds for engineering new functions, and to refine definitions in the current EC classifications [45].

The currently available repertoire of antimycobacterial agents reveals only a handful of comprehensively validated targets, namely RNA polymerase, DNA gyrase, NADH-dependent enoyl-ACP reductase and ATP synthase [46]. The complete genome sequencing of *M. tuberculosis* H37Rv strain has accelerated the study and validation of molecular targets aiming at the rational design of anti-TB drugs [39]. The target-based rational design of new agents with anti-TB activity includes functional and structural efforts. Accordingly, mechanistic analysis should be included in enzyme-targeted drug programs aiming at the rational design of potent enzyme inhibitors. Moreover, ITC has been used as an important technique for the direct determination of thermodynamic and kinetic parameters of enzymatic reactions [47]. It has recently been pointed out that recognition of the limitations of high-throughput screening approaches in the discovery of candidate drugs has rekindled interest in rational design methods [48]. Moreover, understanding the mode of action of *Mt*SK will inform us on how to better design inhibitors targeting this enzyme with potential therapeutic application in TB chemotherapy. It is thus hoped that the results here described may be useful to the rational design of anti-TB agents and that they may contribute to our understanding of the biology of *M. tuberculosis*.

References

[1]. World Health Organization, Global Tuberculosis Control: a short update to the 2009 report, (2010).

[2]. World Health Organization, Multidrug and extensively drug-resistant TB (M/XDR-TB): 2010 global report on surveillance and response, (2010).

[3]. A.A. Velayati, P. Farnia, M.R. Masjedi, T.A. Ibrahim, P. Tabarsi, R.Z. Haroun, H.O. Kuan, J. Ghanavi, P. Farnia, M. Varahram, Totally drug-resistant tuberculosis strains: evidence of adaptation at the cellular level. Eur. Respir. J. 34 (2009) 1202-1203.

[4]. J.G. Robertson, Mechanistic basis of enzyme-targeted drugs, Biochemistry. 44 (2005) 5561-5571.

[5]. J.G. Robertson, Enzymes as a special class of therapeutic target: clinical drugs and modes of action. Curr. Opin. Struct. Biol. 17 (2007) 674-679.

[6]. J.E. Ladbury, G.K. Klebe, E. Freire, Adding calorimetric data to decision making in lead discovery: a hot tip. Nat. Rev. Drug Discov. 9 (2010) 23-27.

[7]. R.G. Ducati, L.A. Basso, D.S. Santos, Curr. Drug Targets. 8 (2007), 423-435.

[8]. R. Bentley, Crit. Rev. Biochem. Mol. Biol. 25 (1990) 307–384.

[9]. S.A. Campbell, T.A. Richards, E.J. Mui, B.U. Samuel, J.R. Coggins, R. McLeod, C.W. Roberts, Int. J. Parasitol. 34 (2004) 5–13.

[10]. C.W. Roberts, F. Roberts, R.E. Lyons, M.J. Kirisits, E.J. Mui, J. Finnerty, J.J. Johnson, D.J. Ferguson, J.R. Coggins, T. Krell, G.H. Coombs, W.K. Milhous, D.E. Kyle, S. Tzipori, J. Barnwell, J.B. Dame, J. Carlton, R.McLeod, J. Infect. Dis. 185, (2002) S25–S36.

[11]. F.Roberts, C.W. Roberts, J.J. Johnson, D.E. Kyle, T. Krell, J.R. Coggins, G.H. Coombs, W.K. Milhous, S. Tzipori, D.J. Ferguson, D. Chakrabarti, R. McLeod, Nature. 393 (1998) 801–805.

[12]. P.J. Keeling., J.D. Palmer, R.G. Donald, D.S. Roos, R.F. Waller, G.I. McFadden, Nature. 397 (1999) 219–220.

[13]. G.A. McConkey, Antimicrob. Agents Chemother. 43 (1999) 175–177.

[14]. G.A. McConkey, J.W. Pinney, D.R. Westhead, K. Plueckhahn, T.B. Fitzpatrick, P. Macheroux, B. Kappes, Trends Parasitol. 20 (2004) 60–65.

[15]. G.I. McFadden, M.E. Reith, J. Munholland, N. Lang-Unnasch, Nature. 381 (1996) 482.

[16]. A. Starcevic, S. Akthar, W.C. Dunlap, J.M. Shick, D. Hranueli, J. Cullum, P.F. Long, Proc. Natl. Acad. Sci. USA. 105 (2008) 2533-2537.

[17]. T. Parish, N.G. Stoker, Microbiology. 148 (2002) 3069–3077.

[18]. J.S. Oliveira, C.A. Pinto, L.A. Basso, D.S. Santos, Protein Expr. Purif. 22 (2001) 430–435.

[19]. J.H. Pereira, Oliveira J.S., F. Canduri, M.V. Dias, M.S. Palma, L.A. Basso, D.S. Santos, W.F.Jr. Azevedo, Acta Crystallogr. D Biol. Crystallogr. 60 (2004) 2310-2319.

[20]. M.V. Dias, L.M. Faím, I.B. Vasconcelos, J.S. Oliveira, L.A. Basso, D.S. Santos, W.F.Jr. Azevedo, Acta Crystallogr. Sect. F Struct. Biol. Cryst. Commun. 63 (2007) 63: 1-6.

[21]. B. Dhaliwal, C.E. Nichols, J. Ren, M. Lockyer, I. Charles, A.R. Hawkins, D.K. Stammers, FEBS Lett. 574 (2004) 49-54.

[22]. J. Gan, Y. Gu, Y. Li, H. Yan, X. Ji, Biochemistry. 45 (2006) 8539-8545.

[23]. M.D. Hartmann, G.P. Bourenkov, A. Oberschall, N. Strizhov, H.D. Bartunik, J. Mol. Biol. 364 (2006) 411-423.

[24]. C. Vonrhein, G.J. Schlauderer, GE. Schulz, Structure, 3 (1995) 483-490.

[25]. U.K. Laemmli, Cleavage of structural proteins during the assembly of the head of bacteriophage T4, Nature. 227 (1970) 680-685.

[26]. M.M. Bradford, R.A. McRorie, W.L. Williams, Anal. Biochem. 72 (1976) 248–254).

[27]. H. Chassaigne, R. Lobinski, Analyst 123 (1998) 2125–2130.

[28]. P. Edman, Arch. Biochem. 13 (1949) 283-286.

[29]. G. Millar, A. Lewendon, M.G. Hunter, J.R. Coggins, Biochem. J. 237 (1986) 427–437.

[30]. I. Segel, Enzyme Kinetics, Behavior and Analysis of Rapid Equilibrium and Steady-state Enzyme Systems, John Wiley and Sons, New York, 1975.

[31]. P.F. Cook, W.W. Cleland, Enzyme Kinetics and Mechanism, Garland Science Publishing, New York, 2007.

[32]. H. Fukada, K. Takahashi, Proteins. 33 (1998) 159-166.

[33]. Y. Zhang, P.S. Cremer, Curr. Opin. Chem. Biol. 10 (2006) 658-663.

[34]. M.E. Maguire, J.A. Cowan, BioMetals. 15 (2002) 203-210.

[35]. M.J. Whipp, A.J. Pittard, J. Bacteriol. 177 (1995) 1627-1629.

[36]. P.H. Hirel, M.J. Schmitter, P. Dessen, G. Fayat, S. Blanquet, Proc. Natl. Acad. Sci. 86 (1989) 8247-8251.

[37]. Y Gu, L. Reshetnikova, Y. Li, Y. Wu, H. Yan, S. Singh, Ji X 319 (2002) 779-789.

[38]. A.J. Pittard, in: F.C. Neidhardt (Ed.), *Escherichia coli* and *Salmonella*: Cellular and Molecular Biology, ASM Press, Washington DC, 1996, pp.458-484.

[39]. S.T. Cole, R. Brosch, J. Parkhill, T. Garnier, C. Churcher, D. Harris, S.V. Gordon, K. Eiglmeier, S. Gas, C. E. 3rd Barry, F. Tekaia, K. Badcock, D. Basham, D. Brown, T. Chillingworth, R. Connor, R. Davies, K. Devlin, T. Feltwell, S. Gentles, N. Hamlin, S. Holroyd, T. Hornsby, K. Jagels, A. Krogh, J. McLean, S. Moule, L. Murphy, K. Oliver, J. Osborne, M. A. Quail, M. A. Rajandream, J. Rogers, S. Rutter, K. Seeger, J. Skelton, R. Squares, S. Squares, J. E. Sulston, K. Taylor, S. Whitehead, B.G. Barrell, Nature. 393 (1998) 537-544.

[40]. R. O'Brien, I. Haq, in J.E. Ladbury, M.L. Doyle (Eds.), Biocalorimetry 2: Applications of Calorimetry in the Biological Sciences, John Wiley & Sons, Ltd, West Sussex, London, 2004, pp.3-34.

[41]. W.P. Jencks, Catalysis in Chemistry and Enzymology, Dover Publications, Inc., New York, 1975.

[42]. T. Krell, J. Maclean, D.J. Boam, A. Cooper, M. Resmini, K. Brocklehurst, S.M. Kelly, N.C. Price, A.J. Lapthorn, J.R. Coggins, Protein Sci. 10 (2001) 1137–1149.

[43]. P.C. Engel, Enzyme Kinetics, John Wiley & Sons, Inc, New York, 1977.

[44]. G. Weber, Adv. Protein Chem. 29 (1975) 1-83.

[45]. D.E. Almonacid, E.R. Yera, J.B.O. Mitchell, P.C. Babbitt, PLoS Comput. Biol. 6(3) 2010 e10000700.

[46]. T.S. Balganesh, P.M. Alzari, S.T. Cole, Trends Pharmacol. Sci. 29 (2008) 576-581.

[47]. M.L. Bianconi, Biophys. Chem. 126 (2007) 59-64.

[48]. J.E. Ladbury, G.K. Klebe, E. Freire, Nat. Rev. Drug Discov. 9 (2010) 23-27.

Figure legends

Fig.1. Shikimate pathway (adapted from [7]).

Fig. 2. Shikimate Kinase catalyzed phosphate transfer from ATP to C3 hydroxyl group of shikimate (SKH), yielding shikimate 3-phosphate (S3P) and ADP.

Fig. 3. 12% SDS-PAGE analysis of pooled fractions from *Mt*SK purification steps. Lane 1, Protein Molecular Weight Marker (Fermentas); lane 2, soluble *E. coli* BL21 (DE3) [pET-23a(+)::*aroK*] extract; lane 3, Soluble proteins after 10 mM $MgCl_2$ precipitation step; lane 4, Phenyl Sepharose 16/10 column elution; and lane 5, Sephacryl S-100 HR column elution.

Fig. 4. Double-reciprocal plots for steady-state kinetics of *Mt*SK using either ATP (**A**) or SKH (**B**) as the variable substrate. Each curve represents varied-fixed levels of the co-substrate, ranging from 37 to 4800 μM for SKH and from 9 to 1200 μM to ATP.

Fig. 5. Fluorescence spectroscopy of the equilibrium binding of SKH to *Mt*SK, measuring the quench in intrinsic protein fluorescence upon ligand binding andp plotting the relative fluorescence change as a function of SKH concentration.

Fig. 6. Isothermal titration calorimetry (ITC) analysis of either SKH (**A**), Mg^{2+}ATP (**B**), or Mg^{2+}ADP (**C**) binding to *Mt*SK. The top graphs show raw data of the heat pulses resulting from titration of *Mt*SK (100 μM for ATP and ADP, and 130 μM for SKH and S3P) in the calorimetric cell with one injection of 0.5 μL of ligand followed by 17 injections of 2.26 μL

injection. The injection syringe (39 µL) contained either ATP and ADP at 6mM or SKH and S3P at 4.2 mM. The bottom graphs show the integrated heat pulses, normalized per mol of injectant as a function of the molar ratio (ligand/*Mt*SK concentration). These binding curves were best fitted to a single set of sites model equation.

Fig. 7. Enzyme mechanism of *Mt*SK and values for the equilibrium dissociation constants of ligands

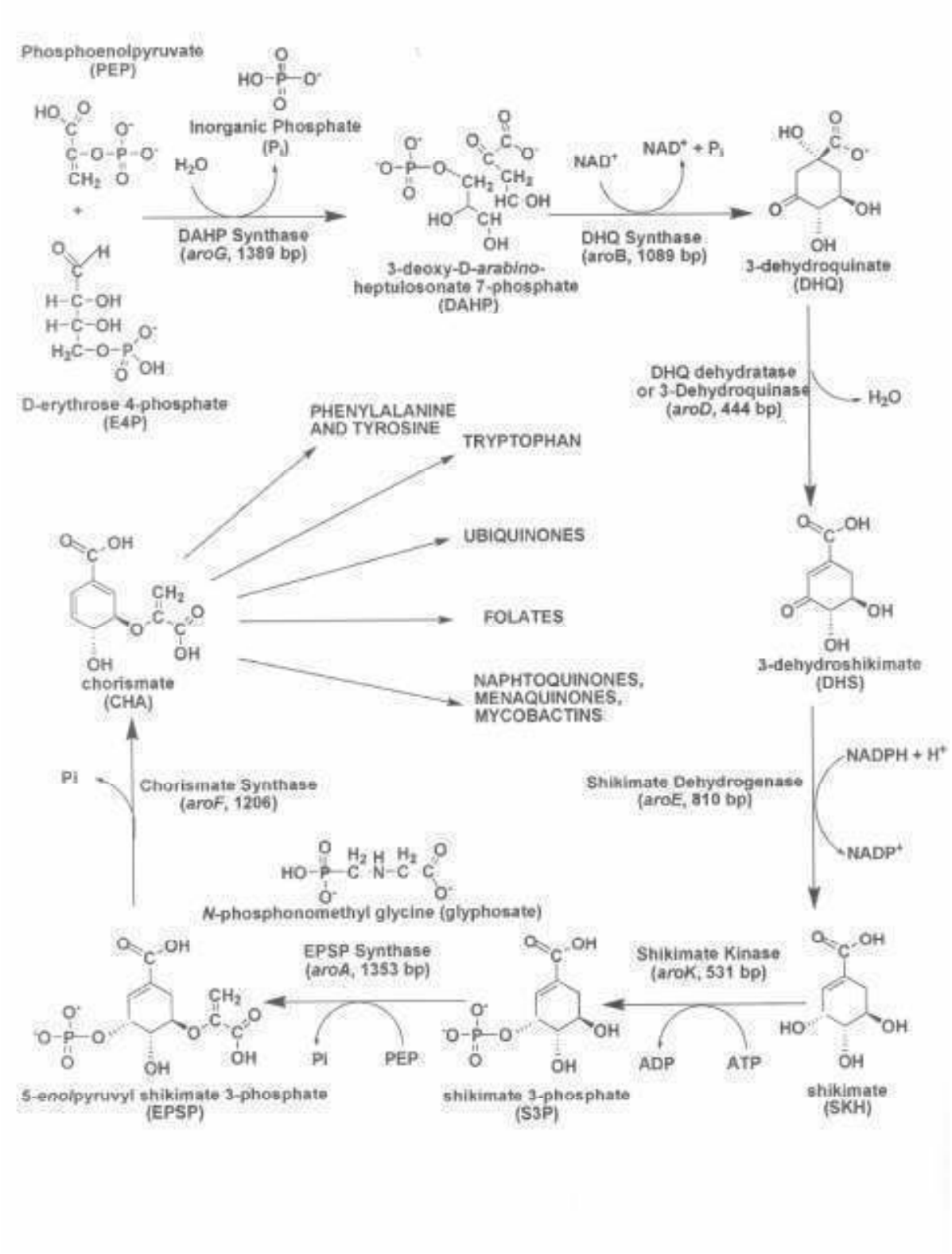
Phosphoenolpyruvate
(PEP)
Inorganic Phosphate
(Pi)
H2O
DAHP Synthase
(aroG, 1389 bp)
3-deoxy-D-arabino-
heptulosonate 7-phosphate
(DAHP)
NAD+
NAD+ + Pi
DHQ Synthase
(aroB, 1089 bp)
3-dehydroquinate
(DHQ)
D-erythrose 4-phosphate
(E4P)
DHQ dehydratase
or 3-Dehydroquinase
(aroD, 444 bp)
H2O
PHENYLALANINE
AND TYROSINE
TRYPTOPHAN
UBIQUINONES
FOLATES
NAPHTOQUINONES,
MENAQUINONES,
MYCOBACTINS
chorismate
(CHA)
3-dehydroshikimate
(DHS)
Pi
Chorismate Synthase
(aroF, 1206)
Shikimate Dehydrogenase
(aroE, 810 bp)
NADPH + H+
NADP+
N-phosphonomethyl glycine (glyphosate)
EPSP Synthase
(aroA, 1353 bp)
Shikimate Kinase
(aroK, 531 bp)
Pi
PEP
ADP
ATP
5-enolpyruvyl shikimate 3-phosphate
(EPSP)
shikimate 3-phosphate
(S3P)
shikimate
(SKH)

Figura 1.

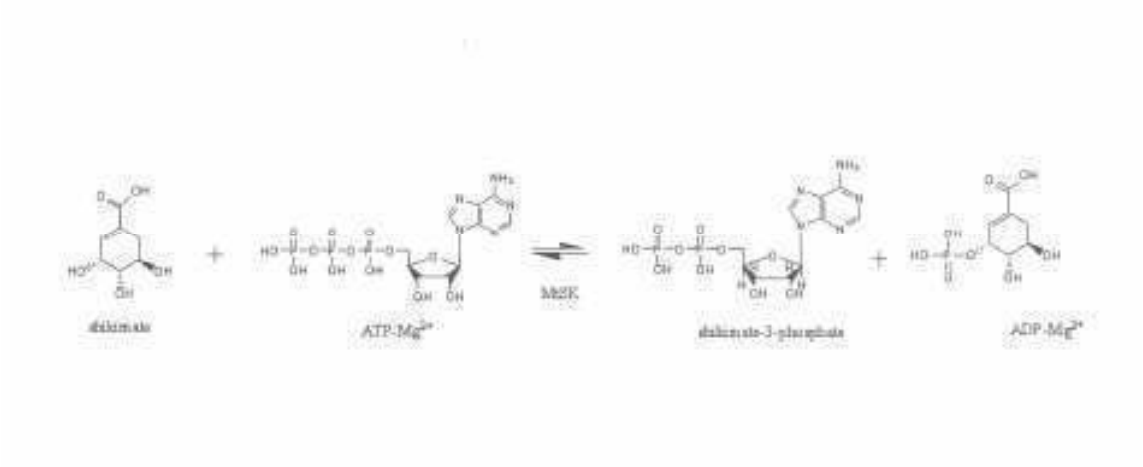

Figura 2

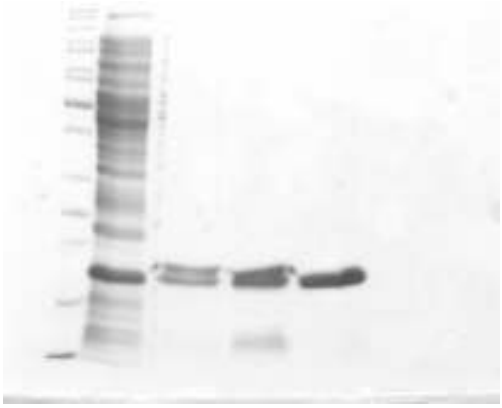

Figura 3

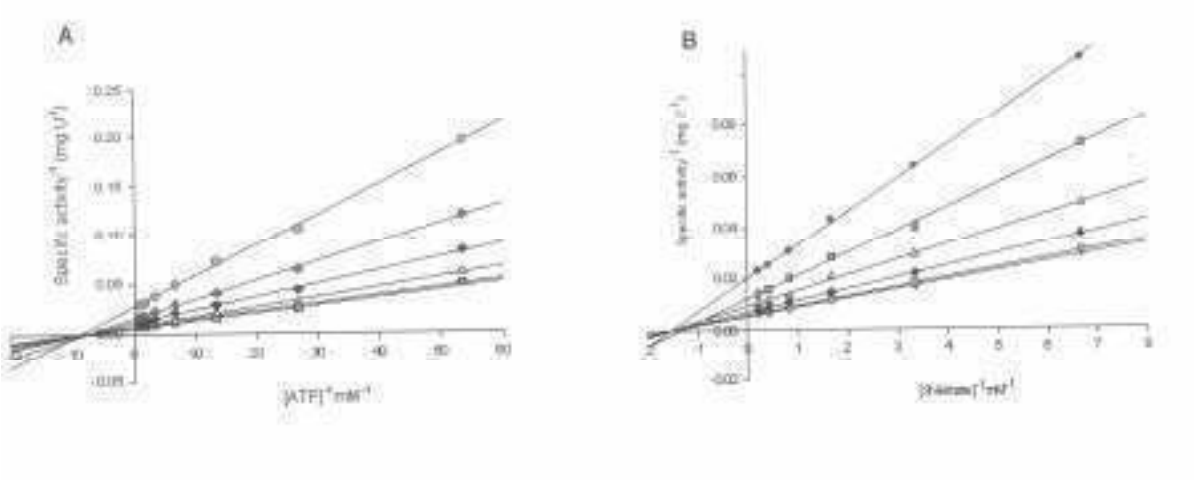

Figura 4

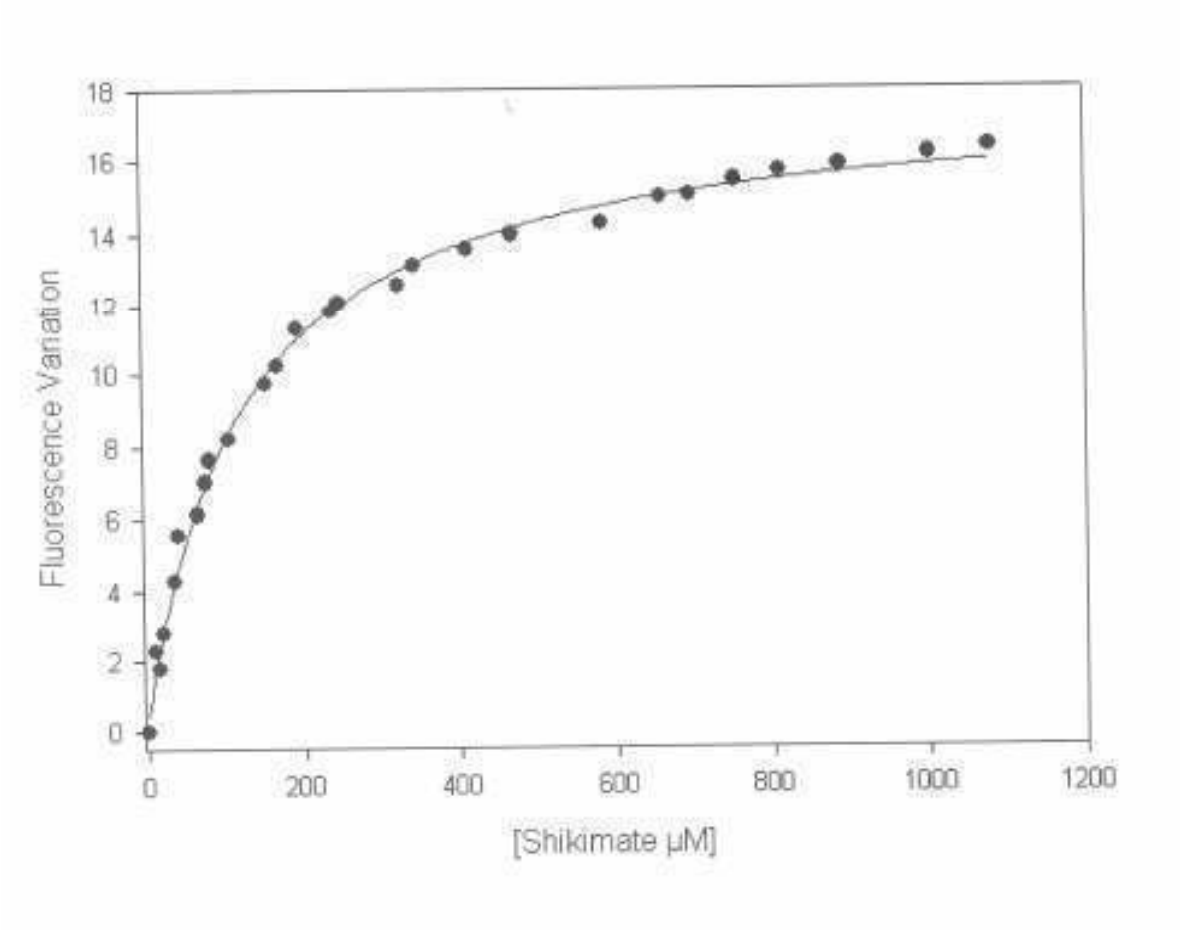
Fluorescence Variation
[Shikimate µM]
0
2
4
6
8
10
12
14
16
18
0
200
400
600
800
1000
1200

Figura 5

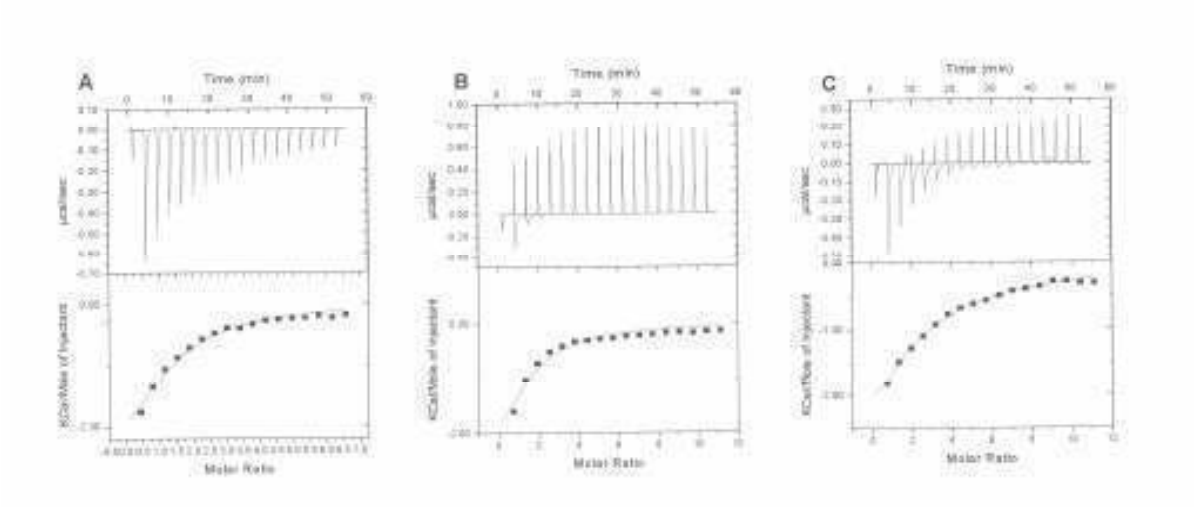

Figura 6

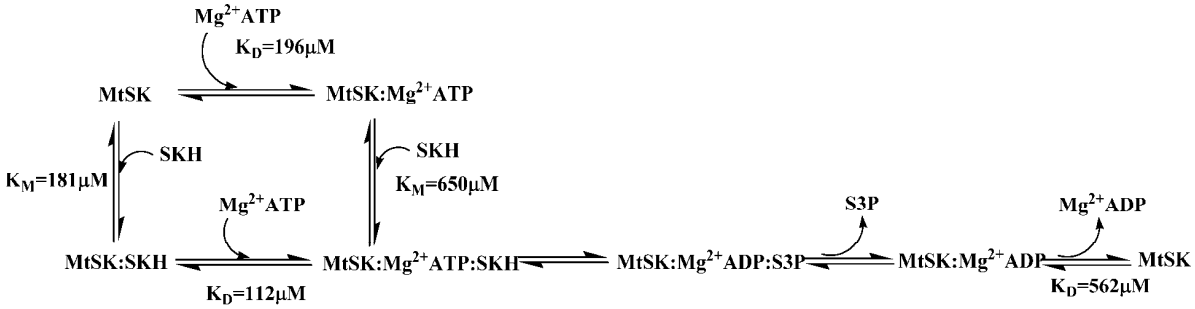
Mg2+ATP
KD=196μM
MtSK
MtSK:Mg2+ATP
SKH
KM=181μM
SKH
KM=650μM
Mg2+ATP
S3P
Mg2+ADP
MtSK:SKH
MtSK:Mg2+ATP:SKH
MtSK:Mg2+ADP:S3P
MtSK:Mg2+ADP
MtSK
KD=112μM
KD=562μM

Figura 7

Luiz Augusto Basso

From: ees.yabbi.0.db7e3.6f8082ab@eesmail.elsevier.com on behalf of ABB **Sent:** Thu 12/9/2010 6:48 PM
To: Luiz Augusto Basso
Cc:
Subject: ABBI-10-710: Final Decision
Attachments:

Ms. No.: ABBI-10-710
Title: The mode of action of recombinant Mycobacterium tuberculosis Shikimate Kinase: kinetics and thermodynamics analyses
Archives of Biochemistry and Biophysics

Dear Dr Basso,

Thank you for submitting the above manuscript to Archives of Biochemistry and Biophysics.

Your manuscript has been reviewed with the help of two reviewers. On the basis of these reviews, I am notifying the Editorial Office of Archives of Biochemistry and Biophysics that your manuscript is not recommended for publication.

The comments of the reviewers are enclosed for your interest and information. While you may be disappointed by this decision, I would like to urge to you to continue to consider ABB for publication of future manuscripts.

Sincerely,

Paul F. Fitzpatrick
Executive Editor
Archives of Biochemistry and Biophysics

Reviewers' comments:

Reviewer #1: This manuscript presents studies on E. coli-expressed shikimate kinase from M. tuberculosis. This enzyme is proposed to be a target for the future development of inhibitors that may have therapeutic potential as antimycobacterial agents.

The authors present the purification, MS, and N-terminal sequencing and also establish that the protein behaves as a monomer in gel filtration analysis. Some of this aspect of the manuscript may represent duplication of previous reports in particular related to citations from the author's own laboratory (#18,19, and 20) so this part of the manuscript is not really new.

The main work that is disclosed concerns the steady state kinetic analysis and ligand binding studies. For the kinetic analysis the authors use a coupled assay to enable spectroscopic analysis of ADP production. This assay is rather classical and it would have been preferable to develop a new, more direct assay. The authors note that the kinetic parameters are in good agreement with those reported previously (Table 1 and ref 37) note - the authors omitted the journal name in the citation (JMB). In this case it is not clear why if the values have been reported previously why they are again reported in this MS although there is some analysis of the description of the mechanism on p. 18 that may be new.
The authors also measure substrate and product binding through a combination of fluorescence spectroscopy (with intrinsic protein fluorescence) and ITC. The fluorescence studies are ambiguous for the reasons that the authors note (that no response does not mean "no binding" it just may be the the binding event does not perturb the fluorescence). With respect to the ITC studies - thermodynamic parameters are provided for ATP, ADP and shikimic acid and then there is a fairly lengthy analysis of these parameters with some speculation as to the significance of some of the observations.

I find that the current manuscript does not afford sufficient new and significant information to be suitable for publication in ABB at this time. Many of the results represent a recapitulation of information already

reported by these authors or others and the only really new information relates to the ITC studies, which really need to be supported in the framework of other new results to be appropriate for publication.

Reviewer #2: This manuscript describes the expression of recombinant M. tuberculosis shikimate kinase and some structural and kinetic characterization of the enzyme. Expression and purification of the enzyme has previously been described. The structure is known. The steady state kinetic parameters have been published. The new results are ITC analyses but they do not add significantly to our understanding of this enzyme.

Anexo B

Kinetic mechanism determination and analysis of metal requirement of dehydroquinate synthase from *Mycobacterium tuberculosis* H37Rv: an essential step in the function-based rational design of anti-TB drugs

Jordana Dutra de Mendonça, Osao Adachi, Leonardo Astolfi Rosado, Rodrigo Gay Ducati, Diogenes Santiago Santos, Luiz Augusto Basso

Artigo publicado – *Molecular Biosystems, 2011, 7:119-128*.

Molecular BioSystems

Cite this: *Mol. BioSyst.*, 2011, **7**, 119–128

www.rsc.org/molecularbiosystems

PAPER

Kinetic mechanism determination and analysis of metal requirement of dehydroquinate synthase from *Mycobacterium tuberculosis* H37Rv: an essential step in the function-based rational design of anti-TB drugs

Jordana Dutra de Mendonça,[ab] Osao Adachi,[c] Leonardo Astolfi Rosado,[ad] Rodrigo Gay Ducati,[a] Diogenes Santiago Santos*[a] and Luiz Augusto Basso*[a]

Received 7th July 2010, Accepted 13th August 2010
DOI: 10.1039/c0mb00085j

The number of new cases of tuberculosis (TB) arising each year is increasing globally. Migration, socio-economic deprivation, HIV co-infection and the emergence of drug-resistant strains of *Mycobacterium tuberculosis*, the main causative agent of TB in humans, have all contributed to the increasing number of TB cases worldwide. Proteins that are essential to the pathogen survival and absent in the host, such as enzymes of the shikimate pathway, are attractive targets to the development of new anti-TB drugs. Here we describe the metal requirement and kinetic mechanism determination of *M. tuberculosis* dehydroquinate synthase (*Mt*DHQS). True steady-state kinetic parameters determination and ligand binding data suggested that the *Mt*DHQS-catalyzed chemical reaction follows a rapid-equilibrium random mechanism. Treatment with EDTA abolished completely the activity of *Mt*DHQS, and addition of Co^{2+} and Zn^{2+} led to, respectively, full and partial recovery of the enzyme activity. Excess Zn^{2+} inhibited the *Mt*DHQS activity, and isotitration microcalorimetry data revealed two sequential binding sites, which is consistent with the existence of a secondary inhibitory site. We also report measurements of metal concentrations by inductively coupled plasma atomic emission spectrometry. The constants of the cyclic reduction and oxidation of NAD^+ and NADH, respectively, during the reaction of *Mt*DHQS was monitored by a stopped-flow instrument, under single-turnover experimental conditions. These results provide a better understanding of the mode of action of *Mt*DHQS that should be useful to guide the rational (function-based) design of inhibitors of this enzyme that can be further evaluated as anti-TB drugs.

Introduction

Although the estimated per capita tuberculosis (TB) incidence was stable in 2005, the number of new cases arising each year is still increasing globally.[1] Among the 15 countries with the highest estimated TB incidence rates, 13 are located in Africa, a phenomenon linked to high rates of *Mycobacterium tuberculosis*, the causative agent of TB in humans, and HIV co-infection, making TB the major cause of death in HIV-positive patients, which represent 23% of the estimated 2 million HIV deaths in 2007. According to the World Health Organization, there were an estimated 9.4 million new TB cases in 2008, from which 1.4 million were HIV-positive, with 1.8 million deaths total—equal to 4500 deaths a day.[2] Migration, socio-economic deprivation, HIV co-infection and the greater use of immunosuppressive agents in healthcare have all contributed to the increasing number of TB cases worldwide, mainly in countries where it was considered eradicated.[3] Furthermore, the recent report of the occurrence of at least one case of extensively-resistant drug TB—resistant to isoniazid and rifampicin plus resistance to any fluoroquinolone and at least one of three injectable second line drugs used in TB treatment—in 57 countries worldwide, has characterized a global spread and alarmed the public health authorities.[4] Even more recently, totally drug-resistant TB strains (TDR-TB) have been identified that are resistant to all first- and second-line drugs tested (*i.e.* aminoglycosides, cyclic polypeptides, fluoroquinolones, thioamides, serine analogues and salicylic acid derivatives).[5]

[a] *Centro de Pesquisas em Biologia Molecular e Funcional (CPBMF), Instituto Nacional de Ciência e Tecnologia em Tuberculose (INCT-TB), Pontifícia Universidade Católica do Rio Grande do Sul (PUCRS), 6681/92-A Av. Ipiranga, 90619-900, Porto Alegre, RS, Brazil. E-mail: luiz.basso@pucrs.br, diogenes@pucrs.br; Tel: +55-51-33203629*
[b] *Programa de Pós-Graduação em Ciências Biológicas: Bioquímica, Universidade Federal do Rio Grande do Sul (UFRGS), Porto Alegre, RS, Brazil*
[c] *Department of Biological Chemistry, Faculty of Agriculture, Yamaguchi University, Yamaguchi 753-8515, Japan*
[d] *Programa de Pós-Graduação em Medicina e Ciências da Saúde (PUCRS), Porto Alegre, RS, Brazil*

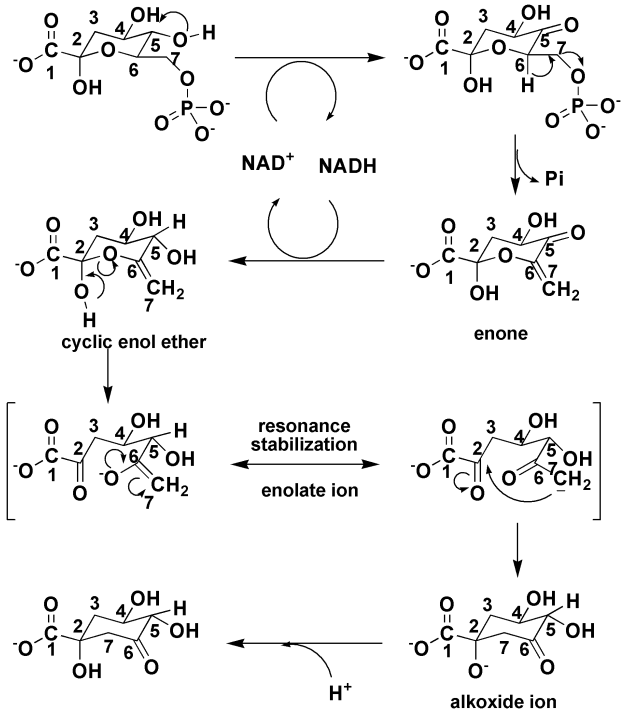

Fig. 1 Chemical reaction catalyzed by DHQS.

Although TB can be cured with the current short-course therapy, this six-month-long treatment and its host toxicity lead to patients' non adherence.[6] There is thus an urgent need for the development of both better vaccines and new and more efficient antimycobacterial agents with novel mechanisms of action. Future drugs should present selective toxicity, be active against drug-resistant and non-resistant strains, shorten the duration of TB treatment to improve patients' compliance and, ideally, do not have pharmacological interactions with antiretroviral drugs commonly used to treat HIV.[7,8]

The complete sequencing of the *M. tuberculosis* H37Rv genome has provided a better understanding of the biology of this pathogen and has also identified potential targets and biochemical pathways that may be used in prophylactic and therapeutic interventions.[9] Proteins that are essential to the pathogen survival and absent from the host, such as enzymes of the shikimate pathway, are attractive targets for the development of new antitubercular drugs. In 2002, Parish and Stoker showed that this pathway is essential to the viability of the bacilli, thereby validating the shikimate pathway enzymes as potential targets for the design of inhibitors with potential anti-TB activity.[10]

The *aroB*-encoded dehydroquinate synthase (DHQS, EC 4.6.1.3) catalyzes the conversion of 3-deoxy-D-*arabino*-heptulosonate 7-phosphate (DAHP) to dehydroquinate (DHQ) in the shikimate pathway (Fig. 1). This pathway leads to the biosynthesis of chorismate, the precursor of aromatic compounds such as phenylalanine, tyrosine and tryptophan, and a range of other metabolites.[11] DHQS has been characterized in other microorganisms (*E. coli*,[12] *B. circulans*,[13] *N. crassa*,[14] *A. nidulans*[15]) and higher plants (*P. mungo*[16] and *Sorghum*[17]) as a metalloenzyme with preference for Co^{2+} and Zn^{2+} that requires catalytic amounts of NAD^+. Pathogenic bacteria harboring mutations in the *aroB* gene sequence are attenuated for virulence.[18] The mechanism of the DHQS reaction appears to closely resemble that of 2-deoxy-*scyllo*-inosose synthase (DOIS) in the 2-deoxystreptamine biosynthesis, as well as the protein sequence.[19,20] The TDR targets database has ranked *M. tuberculosis* DHQS (*Mt*DHQS) as one of the top 50 druggable protein targets for anti-TB drug development,[21] and Target-TB identified *Mt*DHQS as a protein target belonging to intermediary metabolism and respiration class.[22]

The rational design of chemotherapeutic agents may be divided into function-based and structure-based design. Knowledge of the molecular structure of the active site and of the mode of action of an enzyme should thus aid the design of inhibitors that may be used as antimycobacterial agents. Here we describe the kinetic mechanism of the *Mt*DHQS-catalyzed chemical reaction assessed by steady-state and pre-steady-state kinetics, fluorescence spectroscopy, and isothermal titration calorimetry. We also present the metal requirements of this enzyme studied by enzyme activity measurements and atomic absorption analysis. These results represent an important step for the rational

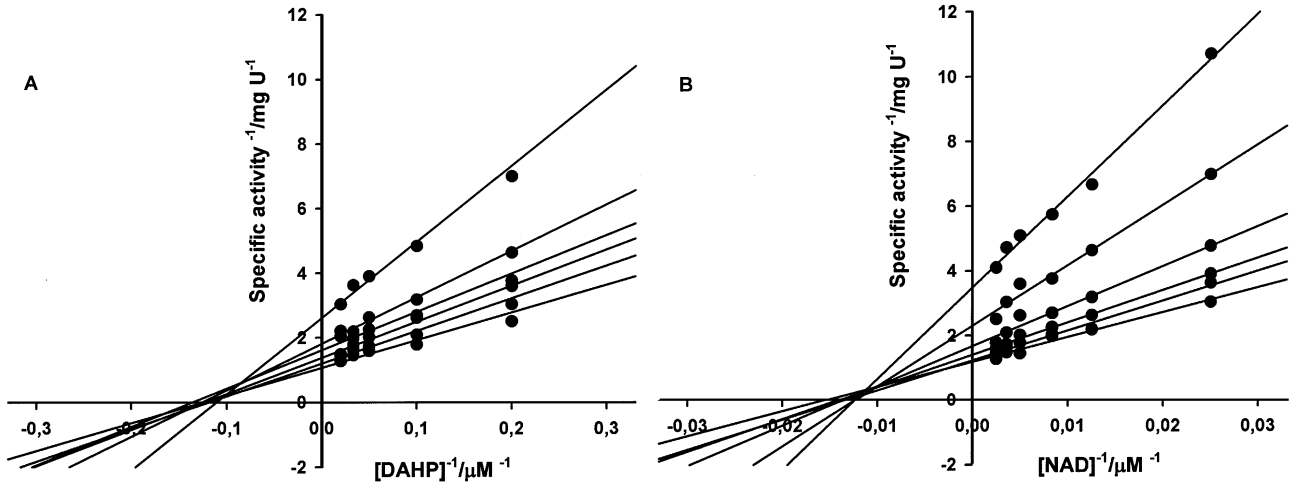

Fig. 2 Double-reciprocal plots for *Mt*DHQS with either DAHP (A) or NAD^+ (B) as the variable substrate. Each curve represents fixed-varying levels of the co-substrate, ranging from 40 to 400 μM for NAD^+ and 3 to 50 μM for DAHP.

design of potent *Mt*DHQS inhibitors that can further be used as anti-TB drugs.

Results

Steady-state kinetic parameters and enzyme mechanism

To determine the true steady-state kinetic parameters and the *Mt*DHQS enzyme mechanism, initial velocity as a function of substrate concentration was plotted as a linear function of reciprocal of initial velocity against the reciprocal of substrate concentration (double-reciprocal or Lineweaver–Burk plot). The double-reciprocal plots showed a family of lines intersecting to the left of the *y*-axis (Fig. 2), which is consistent with ternary complex formation and a sequential mechanism.[23] Data were plotted in reciprocal form and fitted to the equation for a sequential initial velocity pattern (eqn (1)), yielding the following values for the true steady-state kinetic parameters: k_{cat} = 0.63 (± 0.03) s^{-1}, K_{DAHP} = 6.3 (± 1.1) μM, K_{NAD^+} = 70 (± 12) μM, k_{cat}/K_{DAHP} = 1.0 (± 0.2) × 10^5 M^{-1} s^{-1}, and k_{cat}/K_{NAD^+} = 9.0 (± 1.6) × 10^3 M^{-1} s^{-1}, and $K_{D(DAHP)}$ = 9.9 (± 3.4) μM.

Metal requirement analysis

As divalent metal has been proposed as an important cofactor for DHQS catalysis, analysis of metal requirement for *Mt*DHQS enzyme activity was carried out. No increase in the maximum velocity of *Mt*DHQS was observed at saturating concentrations of DAHP and NAD^+ when the non-chelated enzyme was assayed in the presence of different divalent metals, thereby justifying the absence of these compounds in the assay mixture (data not shown).

Effect of metal ion removal by EDTA on *Mt*DHQS enzyme activity. Treatment of *Mt*DHQS with EDTA was carried out for metal ion removal from the enzyme active site to ascertain its need for catalysis. Addition of 100 μM of EDTA to the enzyme in the absence of substrates was capable of abolishing *Mt*DHQS activity after 10 min of incubation. DAHP and NAD^+ were tested separately for their ability to protect the *Mt*DHQS enzyme against inactivation by EDTA. In the presence of saturating levels, DAHP (120 μM/6.3 μM = 19 × K_{DAHP}) protected the enzyme from inactivation even at higher concentrations of EDTA (1 mM), whereas NAD^+ (600 μM/70 μM = 8.6 × K_{NAD^+}) was ineffective (data not show). These data show that the metal bound to the *Mt*DHQS active site is less accessible to EDTA in solution when DAHP is bound to the enzyme active site. It is thus tempting to propose that the metal ion binding site is precluded from solvent in *Mt*DHQS:DAHP:metal ion ternary complex, and that it is likely to be located in the neighbourhood of the DAHP binding site. On the other hand, the metal ion is exposed to the solvent and can thus be chelated by EDTA in solution when in the form of *Mt*DHQS:NAD^+:metal ion ternary complex. This proposal is in agreement with structural data on *Aspergillus nidulans* DHQS presented in the Discussion section.

Metal reactivation. The formation of dehydroquinate by *Mt*DHQS enzyme was abolished by chelating agents such as EDTA (0.1 mM) after 10 min of incubation and was completely restored by an excess of cobalt salt. Although *Mt*DHQS activity was partially restored by Zn^{2+}, this metal inhibited 70% of the enzyme activity at 5 mM final concentration (data not shown). Other divalent metals could also restore *Mt*DHQS activity to varying degrees (Table 1).

Table 1 Effect of divalent metal ions and EDTA on *Mt*DHQS enzyme activity. Purified enzyme was incubated with 0.1 mM EDTA for 10 min, with subsequent addition of 1 mM of the metal ions. The reaction was initiated by addition of DAHP and DHase

Non-chelated DHQS	100%	Cd^{2+}	24%
None[a]	<1%	Mg^{2+}	15%
Co^{2+}	94%	Mn^{2+}	11%
Zn^{2+}	43%	Ni^{2+}	4%
Ca^{2+}	38%	Ba^{2+}	4%

[a] Activities relative to the maximum activity of non-chelated *Mt*DHQS.

Atomic absorption analysis. Metal concentration analysis by inductively coupled plasma atomic emission spectrometry (ICP-AES) yielded the following results: Ca^{2+}, 0.78 mg L^{-1}; Cd^{2+}, <0.004 mg L^{-1}; Co^{2+}, <0.004 mg L^{-1}; Cu^{2+}, 0.42 mg L^{-1}; Mg^{2+}, <0.001 mg L^{-1}; Mn^{2+}, <0.32 mg L^{-1}; Ni^{2+}, <0.01 mg L^{-1}; and Zn^{2+}, 3.74 mg L^{-}. These results indicate the presence of approximately 0.2 mol of Zn^{2+} per mol of *Mt*DHQS (57.2 μM/347.4 μM).

Isothermal titration calorimetry

To determine the relative affinities of the metal binding site of the two divalent metals that showed the best effect on restoring *Mt*DHQS enzyme activity, Co^{2+} and Zn^{2+} were titrated to chelated enzyme (56 μM). Fig. 3 shows the isotherm generated by isothermal titration calorimetry (ITC) and the data after peak integration, subtraction of blank titration data (not shown), concentration normalization (heat normalized to the molar ratio), and analysis by Origin 7.0 suite programs.

Data from Co^{2+} titration analysis indicated the presence of two sequential binding sites (Fig. 3A, where the primary binding site has a K_D of 16 μM and the secondary site has a K_D of 781 μM (exothermic processes). The overall binding isotherm for the interaction of *Mt*DHQS with Zn^{2+} is biphasic (Fig. 3B) and it is best fitted to a model of two sequential binding sites. Binding to the first binding site is accompanied by a negative enthalpy change (K_D of 167 μM; exothermic process), whereas binding to the second site (K_D of 0.3 μM) is accompanied by a positive enthalpy change (endothermic process).

Equilibrium ligand binding to *Mt*DHQS

*Mt*DHQS intrinsic protein fluorescence measurements were carried out to both determine the order of substrate/product addition/dissociation on/from the catalytic site and distinguish the enzyme kinetic mechanism. DAHP binding to free *Mt*DHQS enzyme resulted in a decrease of intrinsic protein fluorescence. The quench in protein fluorescence upon *Mt*DHQS-DAHP binary complex formation plotted as a function of substrate concentration (Fig. 4A) was hyperbolic yielding an equilibrium dissociation constant value of 73 (± 7) μM.

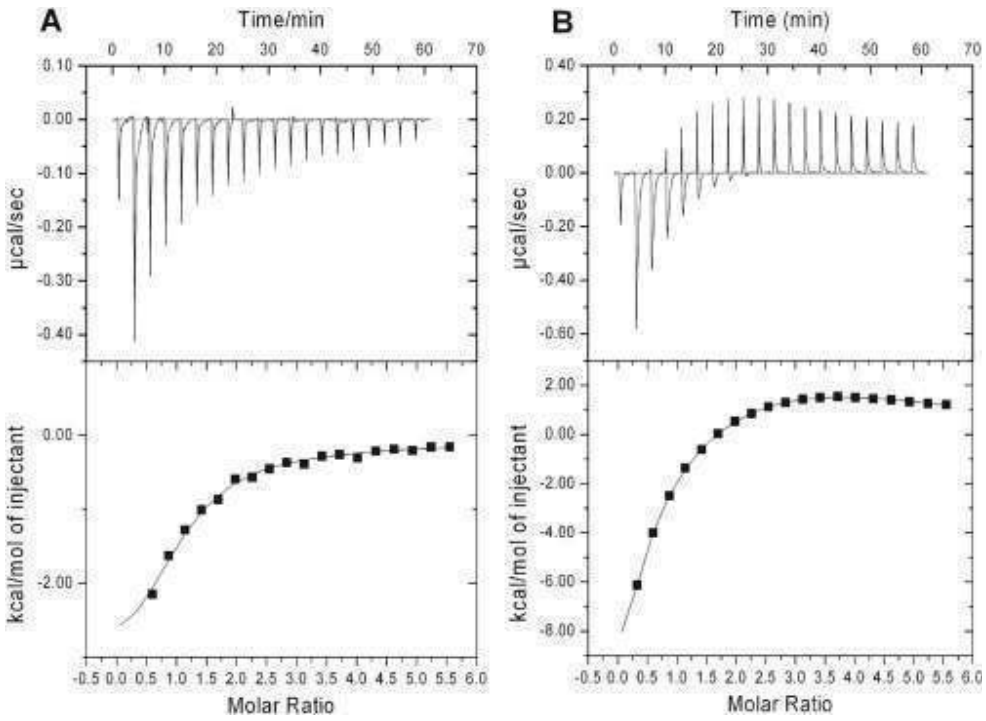

Fig. 3 ITC analysis of Co^{2+} (A) and Zn^{2+} (B) binding to *Mt*DHQS. The top graphs show raw data of the heat pulses resulting from a titration of metal-free *Mt*DHQS (56 µM) in the calorimetric cell with a 0.5 µL injection of 1.5 mM of each metal followed by 19 subsequent 2 µL injections. The bottom graphs show the integrated heat pulses, normalized per mol of injectant as a function of the molar ratio (metal concentration/*Mt*DHQS concentration). These binding curves were best fitted to a two-site sequential model equation.

No change in intrinsic protein fluorescence could be detected upon binding of NAD^+ to free *Mt*DHQS. However, the absence of protein fluorescence change upon NAD^+ binding to free enzyme cannot firmly be interpreted as absence of *Mt*DHQS-NAD^+ binary complex formation. Accordingly, a competitive assay with NADH (an inhibitor of DHQS) was performed.[14,24] The titration of NADH in *Mt*DHQS solution causes a hyperbolic increase in nucleotide fluorescence (460 nm) upon excitation of intrinsic protein fluorescence at 300 nm, indicating the binding of NADH to free *Mt*DHQS, with K_D = 215 (± 13) µM (Fig. 4B-inset). These results show that there is resonance energy transfer (RET) in which the energy of protein fluorescence (340 nm) is transferred to NADH resulting in nicotinamide fluorescence at 460 nm. In the presence of NADH at concentration near its K_D value, NAD^+ was added and the RET nicotinamide fluorescence was measured. Plots of NAD^+ concentration *versus* relative nicotinamide fluorescence variation were hyperbolic, and the data were fitted to an equation for competitive binding (eqn (2)). This analysis yielded a value of 895 (± 50) µM for the equilibrium dissociation constant of NAD^+ (Fig. 4B). Binding of both products resulted in intrinsic protein fluorescence changes, and the hyperbolic plots yielded equilibrium dissociation constant values of 3100 (± 135) µM for DHQ (Fig. 4C) and 920 (± 80) µM for Pi (Fig. 4D).

Pre-steady-state kinetic analysis

NADH transient formation in the oxidation of DAHP by NAD^+ was monitored by pre-steady-state kinetics in a stopped-flow instrument (Fig. 5). Single-turnover experimental conditions (20 µM *Mt*DHQS, 2.5 mM NAD^+ and 15 µM DAHP; mixing-chamber concentrations) were employed in which a large NAD^+ concentration was pre-incubated with *Mt*DHQS enzyme. These experimental conditions were chosen to try to both ensure that most of *Mt*DHQS is in the form of binary complex with NAD^+ and to simplify the reaction model with a substrate, an intermediate, and a product (Fig. 6A and B). A scheme has been proposed by Hirayama *et al.*[25] that involves a reversible binding step (Fig. 6A). In this scheme, k_1 is the rate of oxidation of NAD^+ and concomitant formation of the first intermediate (Fig. 1), k_{-1} is the rate constant for the back reaction, and k_2 is the rate constant containing the phosphate elimination step and the reduction step of the enone intermediate to form the cyclic enol ether intermediate and oxidation of NADH to NAD^+ (Fig. 1 and 6A). On the other hand, an even simpler case of two consecutive irreversible reactions (Fig. 6B) can be considered for analysis of pre-steady-state kinetics data under single turnover conditions.[26,27] In this scheme (Fig. 6B), k_1 is an apparent first-order rate constant comprising the reduction of NAD^+ to NADH, formation of the first intermediate, and the phosphate β-elimination step (including abstraction of a proton at C-5) with concomitant formation of the enone intermediate (Fig. 1), whereas k_2 is an apparent first-order rate constant containing the reduction of the enone intermediate by NADH to form the cyclic enol ether with concomitant NAD^+ formation (Fig. 1 and 6B). It should be pointed out that this analysis implies that the rate of DAHP binding to *Mt*DHQS is much faster than the remaining rate

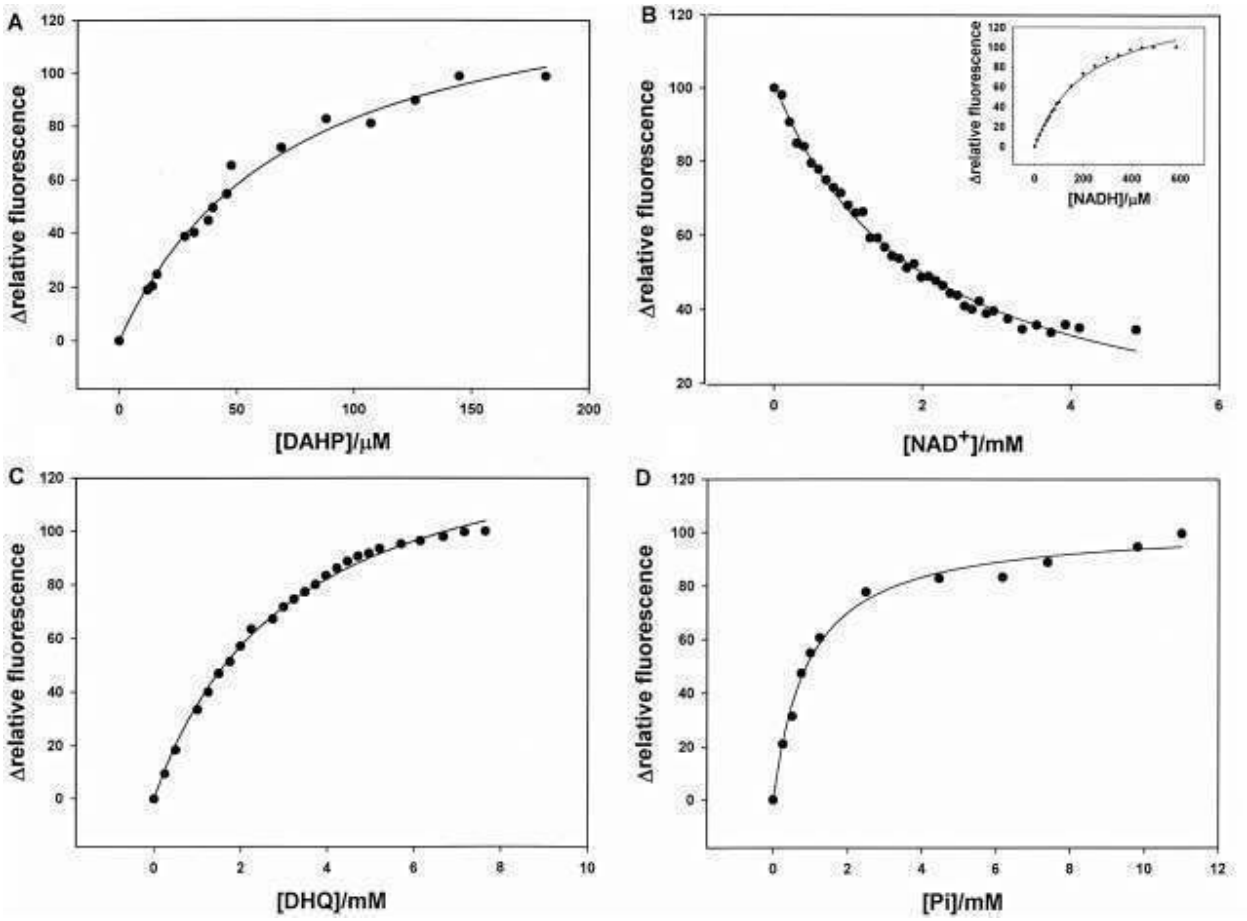

Fig. 4 Fluorescence spectroscopy of equilibrium ligand binding to *Mt*DHQS. Dependence of *Mt*DHQS relative protein fluorescence change upon binding of DAHP substrate (A), and the products DHQ (C) and P_i (D). The dependence of the change in *Mt*DHQS-NADH fluorescence in the competitive assay as a function of increasing NAD^+ concentration is presented in (B). The inset shows the dependence of the enhancement of nicotinamide fluorescence (460 nm) due to resonance energy transfer from the enhancement in protein fluorescence (350 nm) upon NADH binding to free enzyme.

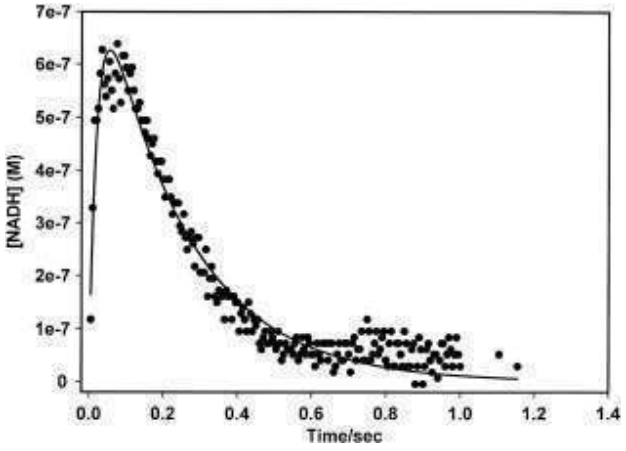

Fig. 5 Pre-steady-state kinetic analysis of *Mt*DHQS reaction. The NADH production (M) was monitored by a stopped-flow instrument under single turnover conditions (20 μM *Mt*DHQS was pre-incubated with 2.5 mM NAD^+ and mixed with 15 μM DAHP; mixing-chamber concentrations). Experimental data are presented by black-filled circles, and fitting the experimental data to eqn (3) yielded the predicted values plotted as a solid line.

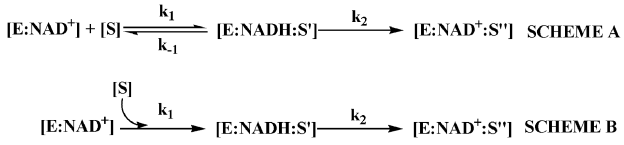

Fig. 6 Proposed pre-steady-state kinetic model of the *Mt*DHQS reaction. The rate constant k_1 is the substrate oxidation rate by NAD^+, and k_2 is the rate containing the elimination step of phosphate and reduction step by NADH. Absorbance at 340 nm for NADH formed in the enzyme reaction was monitored and fitted to eqn (3) Scheme A is for a mechanism that involves a reversible binding step followed by an irreversible reaction, whereas scheme B is for a mechanism of two consecutive irreversible reactions.

constants (not rate limiting). Moreover, assuming the two steps (Fig. 6B) as irreversible is justifiable because these reactions occur in the absence of products. Moreover, in this scheme it is implicit that measurements of absorbance at 340 nm detect the rate of formation of E:NADH:S′ intermediate (k_1) and the rate of decay of this intermediate to form $E:NAD^+:S''$. This simplified analysis allows fitting the results to eqn (3), yielding values of $k_1 = 47 (\pm 2)\ s^{-1}$ and $k_2 = 4.36 (\pm 0.06)\ s^{-1}$ (Fig. 5).

Discussion

The rational-based development of *Mt*DHQS inhibitors requires characterization of its catalytic mechanism. Because of the complex mechanism in which DHQS is involved, the enzyme has been speculated as a spectator of its own reaction and suggest its catalysis as a simple oxidoreductase with several reactions occurring spontaneously.[28] However, the arrangement of the active site of DHQS indicates that the enzyme is not just a spectator in catalysis but stabilizes intermediates and prevents side reactions through its entire reaction pathway.[29] The elimination of phosphate from DAHP to generate DHQ catalyzed by DHQS requires catalytic amounts of NAD^+ for activity, even though the enzyme-catalyzed chemical reaction is redox neutral. DHQS has attracted considerable mechanistic interest and has long been regarded as a catalytic marvel due to its ability to perform several consecutive chemical reactions in one active site during each catalyzed turnover of substrate into product. In this sequence (Fig. 1), which is mechanistically unusually diverse for a single enzyme, it appears to mediate five sequential transformations:[12] (i) the oxidation of the secondary alcohol at C-5; (ii) the β-elimination of inorganic phosphate across C-6 and C-7; (iii) the reduction of the resulting enone at C-5; (iv) the ring opening of the enol pyranose; and (v) the final intramolecular aldol-like reaction to yield DHQ (resonance stabilization of enolate ion, and nucleophilic addition of C-7—as a carbanion—to C-2 carbonyl, production of an alkoxide ion, and protonation of the latter). It has been shown that the β-elimination of Pi across C-6 and C-7 occurs in a *syn* fashion and the transition state for the subsequent intramolecular aldol reaction has a chairlike geometry.[30]

The mechanism of the DHQS reaction is similar to the mechanism described for DOIS in the 2-deoxystreptamine biosynthesis, including the divalent metal ion requirement for activity, and Co^{2+} as the most effective to enzyme activity, and the cyclic reduction and reoxidation of NAD^+ and NADH, respectively, during the enzyme-catalyzed reaction prior to release of DHQ from the active site.[19] The *Bacillus circulans btrC* gene shows significant sequence similarity to various DHQS and the catalytic domain, and the metal binding residues are conserved between DOIS and DHQSs.[20] However, it has been pointed out that there exist dissimilarities between *B. circulans* DOIS and DHQSs, particularly in the stereochemistry of overall reactions.[31] We have previously reported that amino acid sequence comparison between *Mt*DHQS and DHQSs from other organisms showed highly conserved residues,[32] which are likely involved in protein function and activity. Multiple sequence alignment between *Mt*DHQS (Gene bank access code: NP_217054.1), DHQS domain of *Aspergillus nidulans* AROM protein (*An*DHQS, for which there is structural data; PDB access code: 1DQS), and *Bacillus circulans* DOIS (*Bc*DOIS; PDB access code: 2GRU) amino acid sequences show conservation of key residues (Fig. 8).[33] Note that the numbering given here is for the actual position of a particular amino acid in the polypeptide chain of each enzyme, and the numbering given in Fig. 8 is to show sequence comparison results after introduction of gaps. The similarity of the mode of action of *Mt*DHQS and *Bc*DOIS is borne out by the conservation of key amino acid residues (Fig. 8). However, as there is structural data on *An*DHQS, emphasis of the likely roles played by *Mt*DHQS side chains will be placed on conservation of amino acid residues in *An*DHQS and in *Mt*DHQS polypeptide sequences. The crystal structure of *An*DHQS has been solved at 1.8 Å resolution[29] with Zn^{2+}, NAD^+ and carbaphosphonate. The latter is a sub-nanomolar slow-binding inhibitor of *E. coli* DHQS.[34] The active site is located in a cleft between two domains of homodimeric *An*DHQS.[29] The pentacoordinated Zn^{2+} interacts with Glu194, His271 and His287 and two carbaphosphonate inhibitor hydroxyls in *An*DHQS.[29] The corresponding amino acid residues in *Mt*DHQS are Glu186, His249 and His265 (Fig. 8), which are all conserved. In concert with hydride transfer of C5 of DAHP to C4 of the NAD^+ nicotinamide moiety, a proton from C5 hydroxyl group is transferred to a water molecule and relayed (proton-shuffling system) to His275 of *An*DHQS. A similar role may be played by the conserved His253 in *Mt*DHQS (Fig. 8). It has been suggested that a possible role for Zn^{2+} is to facilitate hydride transfer and proton loss by polarizing the C5 hydroxyl group of DAHP.[29] The β-elimination step appears to involve interactions between the oxygens of the phosphate group with Lys152, Asn162, Asn268 and Lys356 of one subunit, and Arg130 from the other monomer. The corresponding conserved residues in *Mt*DHQS are Lys144, Asn154, Asn246 and Lys323 of one subunit, and Arg122 from the other monomer. NADH hydride transfer to C5 ketone of the enone intermediate (Fig. 1) may be followed by proton transfer to C5 hydroxyl group from *Mt*DHQS His253 conserved side chain involved in the proton-shuffling system. After ring opening, there is a rotation about the C5–C6 bond that is followed by aldol condensation and protonation of the alkoxide intermediate (Fig. 1). To prevent epimerization at C2 in DHQS-catalyzed chemical reaction, the carboxylic acid

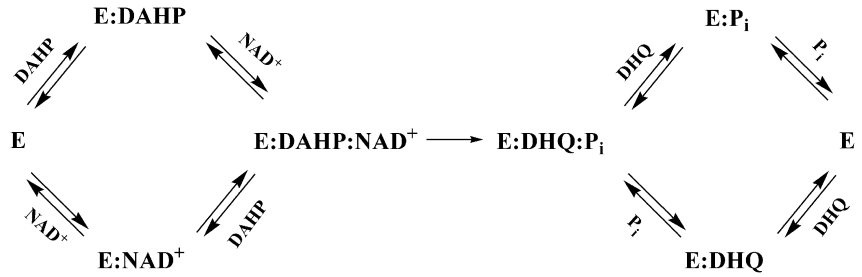

Fig. 7 Proposed kinetic mechanism for *Mt*DHQS.

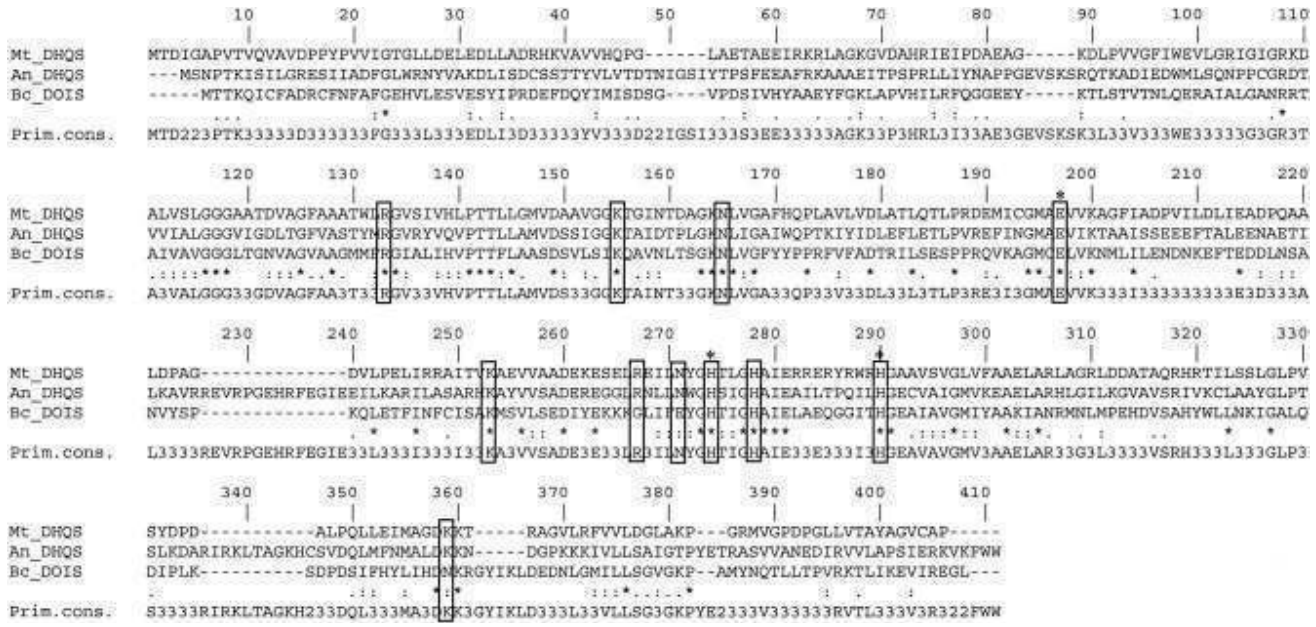

Fig. 8 Comparison of amino acid sequences. Shown are DHQS sequences for *M. tuberculosis* (Mt_DHQS; 362 amino acids; Gene bank access code: NP_217054.1), *Aspergillus nidulans* DHQS (An_DHQS; 402 amino acids; Gene bank access code: NT_107015.1), and *Bacillus circulans* DOIS (Bc_DOIS; 368 amino acids; Gene bank access code: BAE07067.1). Multiple amino acid sequence alignment was performed by ClustalW,[33] using the Gonnet matrix for amino acids substitutions and considering gap penalties.

group on C2 of the cyclic enol ether (Fig. 1) is held in place by interactions with a Lys152, Lys250 and Arg264 in *An*DHQS.[29] The corresponding residues in *Mt*DHQS are Lys144, Lys228 and Arg242, which are all conserved (Fig. 8).

The divalent metal cofactor has been proposed as an important factor during the catalysis of DHQSs. To elucidate this role, analysis of the metal requirement of *Mt*DHQS was performed. The need for no addition of divalent metal in the standard assay with non-chelated enzyme can be explained by the general conditions of the expression system that provided appropriate amounts of metal for *Mt*DHQS enzyme activity. The treatment with EDTA results in rapid formation of inactive apoenzyme, and DAHP binding prevents the removal of the metal from the active site, which suggests that the metal is less accessible to EDTA when DAHP is bound to the enzyme active site. Conversely, NAD^+ has no protective effect. This protective behavior of DAHP was previously described for *E. coli*[12] and *N. crassa*[14] enzymes. As discussed above, the pentacoordinated Zn^{2+} interacts with one glutamate and two histidine amino acid side chains and two hydroxyl groups of carbaphosphonate inhibitor,[29] which would account for the protective effect of DAHP. On the other hand, the lack of protective effect by NAD^+ suggests that there is no interaction between this cofactor and Zn^{2+} ion.

In the reactivation studies, the addition of Co^{2+} in the reaction mixture containing the chelating agent restored completely the *Mt*DHQS activity, similar to *B. subtilis*[13] and *E. coli*[12] enzymes, but differing from *N. crassa* that rapidly recovered the enzyme's activity with Zn^{2+} rather than Co^{2+}.[14] In contrast, the presence of excess of Zn^{2+} leads to decreased rates for *Mt*DHQS at concentration values larger than 200 μM (data not shown), which suggests that zinc may also bind to a second inhibitory site. This is similar to DHQS from *E. coli*[12] and *A. nidulans*[35] and was confirmed by the ITC assays of metal binding to the mycobacterial enzyme, where the titration of Co^{2+} and Zn^{2+} of *Mt*DHQS in solution indicated the existence of two sequential binding sites. There appears to be positive cooperativity between the two *Mt*DHQS binding sites since there is a decrease in the equilibrium dissociation constant for binding to the second site (0.3 μM) as compared to binding to the first site (167 μM). We have recently been able to obtain crystal of the *Mt*DHQS enzyme, and, hopefully, these structural efforts will shed further light on the role of a metal in catalysis and/or binding (ongoing experiments).

The atomic absorption analysis showed the absence of any significant quantity of cobalt and the presence of a small, but significant, amount of zinc. The zinc content of the final preparation is 0.2 mol of Zn^{2+} per mol of *Mt*DHQS, indicating that the metal sites of the enzyme were only partially saturated in crude extract. This substoichiometric value obtained may represent the loss of the metal during the purification process, similar to that described for other enzymes, like DAHP(Phe) synthase from *E. coli*.[36] It is interesting to note that the purified recombinant *Mt*DHQS enzyme did not contain significant amount of cobalt associated, even though the metal reactivation assays here described demonstrated preference for Co^{2+} However, based on the higher bioavailability of Zn^{2+}, it seems likely that DHQS is naturally a zinc-dependent metalloenzyme.[14] Taken together, these results demonstrate a central role for the metal ion in the catalytic mechanism, since each chemical transformation mediated by dehydroquinate synthase has, in simpler enzymatic systems, been shown to involve metal cofactors.[12]

The pattern of the double-reciprocal plots was consistent with ternary complex formation and a sequential mechanism. The mechanisms of ping-pong and rapid equilibrium ordered

could be discarded, since these mechanisms display parallel lines and intersecting lines at the *y*-axis, respectively.[23] The initial velocity data and equilibrium binding analysis are consistent with either a steady-state or a rapid-equilibrium random kinetic mechanism, in which both DAHP and NAD^+ bind to the free enzyme, and there is no preferential order for dissociation of the products, DHQ and Pi, from the active site (Fig. 7). However, steady-state random order mechanisms usually display non-linear Lineweaver–Burk plots due to squared terms in its rate equation.[23,37] Accordingly, the results here presented suggest that the *Mt*DHQS enzyme mechanism is rapid-equilibrium random order. The true kinetic parameters showed that *Mt*DHQS has a lower catalytic efficiency when compared to others DHQSs. The turnover numbers of 24 s^{-1} for *E. coli*,[38] 19 s^{-1} for *N. crassa*[14] and 6.8 s^{-1} for *A. nidulans*,[35] are significantly higher when compared with 0.63 s^{-1} for *Mt*DHQS. The K_{DAHP} values are, however, similar as compared to *E. coli* (5.5 μM),[12] *N. crassa* (1.4 μM),[14] and somewhat lower than the value for *A. nidulans* monofunctional DHQS domain (21 μM).[35] Notwithstanding, the DAHP substrate specificity constant value of 1.0×10^5 M^{-1} s^{-1} (k_{cat}/K_{DAHP} = apparent second-order rate constant) for *Mt*DHQS is more than 250-fold lower than the *E. coli* enzyme value (2.5×10^7 M^{-1} s^{-1}).[12] On the other hand, the NAD^+ Michaelis–Menten constant value for *Mt*DHQS (K_{NAD^+} = 70 μM) is approximately 900-fold larger than for *E. coli* (K_{NAD^+} = 80 nM),[12] 350-fold larger than *N. crassa* ($K_{NAD^+} < 0.2$ μM)[14] and 37-fold larger than *A. nidulans* monofunctional DHQS domain (K_{NAD^+} = 1.9 μM).[35]

DHQS is mechanistically distinguished by its catalytic use of NAD^+. The reduction of NAD^+ to NADH during the first step of the enzyme-catalyzed reaction is followed by reoxidation of NADH to NAD^+ at a later enzyme-catalyzed step prior to release of DHQ from the enzyme active site. Pre-steady-state kinetics assay of a single enzyme turnover was thus carried out to determine the rate constants of the conversion $NAD^+ \rightarrow NADH \rightarrow NAD^+$ (Fig. 5). Experimental conditions were chosen so that only a single turnover of *Mt*DHQS-catalyzed chemical reaction is possible and the transient changes in absorbance at 340 nm were measured. The single turnover data were analysed using a simple case for two consecutive reactions as described by Fersht[26] and Hiromi,[27] and fitting the data to eqn (3) yielded apparent rate constant values of 47 s^{-1} for k_1 and 4.36 s^{-1} for k_2 (Fig. 5). It is noteworthy that detection of part of the pre-steady-state absorbance signal due to NAD^+ to NADH conversion was not possible because it occurred in the dead time of the apparatus ($\leq$1.5 ms) (Fig. 5). It should be pointed out that we do not wish to imply that NADH to NAD^+ conversion may be associated with product release (P_i) and/or conversion of the first intermediate to the enone intermediate (Fig. 1). Importantly, the pre-steady-state kinetic data demonstrate that there is a transient increase in absorbance at 340 nm associated with NADH formation followed by its oxidation back to NAD^+ that occurs only in the presence of *Mt*DAHP-catalyzed conversion of DAHP to DHQ. In addition, the rates of $NAD^+ \rightarrow NADH \rightarrow NAD^+$ conversions are not rate limiting because they are larger than the k_{cat} value (0.63 s^{-1}).

Conclusions

Rational inhibitor design relies on mechanistic and structural information on the target enzyme. Enzyme inhibitors make up roughly 25% of the drugs marketed in the United States.[39] Enzymes catalyze multistep chemical reactions to achieve rate accelerations by stabilization of transition state structure(s).[40] Accordingly, mechanistic analysis should always be a top priority for enzyme-targeted drug programs aiming at the rational design of potent enzyme inhibitors. Moreover, ITC has been used as an important technique for the direct determination of thermodynamic and kinetic parameters of enzymatic reactions.[41] It has recently been pointed out that recognition of the limitations of high-throughput screening approaches in the discovery of candidate drugs has rekindled interest in rational design methods.[42] Understanding the mode of action of *Mt*DHQS will inform us on how to better design inhibitors targeting this enzyme with potential therapeutic application in TB chemotherapy. Accordingly, it is hoped that the results here described may be useful to the rational design of anti-TB agents and that they may contribute to our understanding of the biology of *M. tuberculosis*.

Experimental

Homogeneous *Mt*DHQS production

The homogeneous solution of recombinant *Mt*DHQS was obtained as we have previously described.[32] Protein concentration was determined by the Bradford Protein Assay Kit (Bio-Rad Laboratories), using bovine serum albumin as standard.[43]

Enzyme assay and initial velocity

*Mt*DHQS activity was measured by coupling the conversion of 3-*deoxy*-D-*arabino*-heptulosonate 7-phosphate (DAHP) into dehydroquinate (DHQ), and monitoring the dehydroquinate dehydratase-catalyzed conversion of DHQ to dehydroshikimate at 234 nm (ε_{234nm} = 12 000 M^{-1} cm^{-1}) in an UV-2550 UV/Visible spectrophotometer (Shimadzu).[38,44] The standard assay was performed in 5-mm pathlength quartz cuvettes at 25 °C in a total volume of 1.5 mL containing 50 mM Tris-HCl pH 7.5, 120 μM DAHP (Toronto Chemical Research), 600 μM NAD^+ (Sigma), and 1 unit of dehydroquinate dehydratase (DHase) from *M. tuberculosis*. The true steady-state kinetic parameters were determined by varying concentrations of DAHP (3–50 μM) against varied-fixed concentrations of NAD^+ (40–400 μM). One unit of enzyme activity was defined as the amount of protein that catalyzes the consumption of 1 μmol of DAHP/min at 25 °C. The family of lines intersecting to the left of the *y*-axis in double-reciprocal plots were fitted to eqn (1) for a mechanism involving ternary complex formation and a sequential substrate binding:

$$v = \frac{VAB}{K_{ia}K_b + K_aB + K_bA + AB} \quad (1)$$

in which V is the maximum steady-state velocity, A and B are substrate concentrations, K_a and K_b are Michaelis constants for substrates A and B, respectively, and K_{ia} is the dissociation constant for enzyme-substrate A binary complex formation.

Metal requirement analysis

Divalent metal ions were removed from all solutions by stirring with Chelex resin (BioRad), followed by filtration through a Milipore 0.22 μM sterilizing membrane.

Determination of the rate of metal ion loss in the presence of EDTA. In an assay at 25 °C, *Mt*DHQS (30 μL of a 35 μM solution) was added to 50 mM Tris-HCl buffer, pH 7.5, containing NAD^+ (600 μM) and EDTA (100 μM), in a final volume of 1.46 mL. The reaction was initiated by addition of DAHP (120 μM) and DHase (1 unit), and the initial rate determined at different reaction times.

Metal reactivation. To study the requirement of divalent metal ion to *Mt*DHQS enzyme activity, each metal chloride salt, including $ZnCl_2$, $MgCl_2{\cdot}6H_2O$, $3CdSO_4{\cdot}8H_2O$, $BaCl_2{\cdot}2H_2O$, $CaCl_2{\cdot}2H_2O$, $CoCl_2{\cdot}6H_2O$, $MnCl_2{\cdot}4H_2O$ and $NiCl_2{\cdot}6H_2O$ (Sigma-Aldrich), was added to a final concentration of 1 mM. Metal-free conditions were made by adding EDTA (0.1 mM final concentration) to enzyme and NAD^+ (600 μM final concentration) and incubating this mixture for 10 min. Metal chloride salts were added and incubated for further 1 min. The enzyme-catalyzed chemical reaction was started by adding *Mt*DAHP (120 μM) and DHase (1 unit).

Atomic absorption analysis. Analyses of Ca^{2+}, Cd^{2+}, Co^{2+}, Cu^{2+}, Mg^{2+}, Mn^{2+}, Ni^{2+}, and Zn^{2+} concentrations in *Mt*DHQS homogeneous protein solution were carried out by ICP-AES (Spectro Ciros CCD). All measurements were in duplicate. *Mt*DHQS was in Tris-HCl 50 mM pH 7.6 at 13.25 mg mL^{-1} final protein concentration (subunit molecular mass = 38 135.70 Da).

Isothermal titration calorimetry (ITC)

The protein binding constants of protein-divalent metal binary complex formation were determined by ITC using a MicroCal ITC-200 microcalorimeter (Thermo). ITC measurements were carried out at 25 °C, and titrations were carried out using a 40 μL-syringe and with stirring at 500 rpm. Each titration consisted of a preliminary injection of 0.5 μL, followed by 19 injections of 2 μL into a cell containing 200 μL of protein sample of 56 μM. To correct for dilution and mixture effects, a series of baselines were performed, in which injections of metal were carried out into buffer, and subtracted from data to obtain accurate heat exchanges. The integrated heat changes (area under each peak in μcal) were plotted as kcal/mole of injectant *versus* the molar ratio ligand/macromolecule (Fig. 3, lower panels). The binding curve data were best fitted to standard equations using a model for two-site sequential model as implemented in Microcal ORIGIN 7.0 software package (Thermo-MicroCal Software).

Equilibrium ligand binding to *Mt*DHQS

Fluorescence measurements were carried out in a RF-5301 PC Spectrofluorophotometer (Shimadzu) at 25 °C. Measurements of intrinsic *Mt*DHQS protein fluorescence were carried out using excitation wavelength at 300 nm in each binding experiment, and the emission wavelength ranged from 320 to 450 nm (maximum emission wavelength at 340 nm). For competitive assays of NADH and NAD^+, the nicotinamide fluorescence was monitored, with excitation wavelength at 300 nm and the emission wavelength ranging from 320 to 500 nm (with maximum emission wavelength at 460 nm due to RET). The slits for excitation and emission were 1.5 and 15 nm, respectively. Fluorescence titrations of binary complex formation were carried out by making microlitre additions of the following compounds to 2 mL containing 2 μM *Mt*DHQS: 4 mM DAHP stock solution (1.999–181.34 μM final concentration); 200 mM NAD^+ stock solution (0.0989–4.877 mM final concentration); 500 mM DHQ solution (0.249–7.634 mM final concentration); 500 mM Pi stock solution (0.249–11.00 mM final concentration); 20 mM NADH stock solution (9.995–582.52 μM final concentration). Control experiments were employed to both determine the maximum ligand concentrations to be used with no significant inner filter effect and to account for any dilution effect on fluorescence. Data were fitted to a hyperbolic equation for DAHP, NADH, DHQ, and Pi. For competitive binding to determine the equilibrium dissociation constant of NAD^+, the data of relative fluorescence (f) as a function of NAD^+ concentration were fitted to eqn (2), in which F represents the maximum relative fluorescence change upon ligand binding, A the NAD^+ concentration, K_a the equilibrium dissociation constant for NAD^+, K_i is the equilibrium dissociation constant for NADH (215 μM), and I the fixed NADH concentration (215 μM).

$$f = \frac{FA}{K_a\left(1 + \frac{I}{K_i}\right) + A} \qquad (2)$$

Pre-steady-state kinetic analysis

Absorption of NADH (340 nm) produced in the catalytic cycle was analyzed in an Applied-Photophysics SX-18MV-R (Leatherhead, UK) stopped-flow instrument. Data acquisition was carried out using a split time base (0.2 and 1 s), and a 1-cm pathlength mixing chamber. After pre-incubation of 20 μM *Mt*DHQS with 2.5 mM NAD^+ at 25 °C for 10 min, 15 μM DAHP was mixed to start the single-turnover enzyme reaction (mixed-chamber or final concentration). A large NAD^+ concentration was employed to ascertain that most of *Mt*DHQS is in the form of binary complex and to simplify the reaction model (Fig. 6A and B). Considering the simplest case for two consecutive reactions of pre-steady-state data under single turnover conditions,[26,27] eqn (3) can be employed to yield estimates for k_1 and k_2. Accordingly, pre-steady-state kinetics data were fitted to eqn (3) by regression analysis using SigmaPlot 9.1 package software (Systat Software, Inc.).

$$[ENADHS'] = \frac{[ENAD^+]k_1}{k_2 - k_1}\left[e^{-k_1 t} - e^{-k_2 t}\right] \qquad (3)$$

Acknowledgements

This work was supported by funds of Millennium Initiative Program and National Institute of Science and Technology on Tuberculosis (INCT-TB), MCT-CNPq, Ministry of Health - Department of Science and Technology (DECIT) - Secretary of Health Policy (Brazil) to L.A.B. and D.S.S. L.A.B. (CNPq, 520182/99-5) and D.S.S. (CNPq, 304051/1975-06)

are Research Career Awardees of the National Research Council of Brazil (CNPq). J.D.M. acknowledges an MSc scholarship awarded by CNPq.

References

1 WHO, 2010 http://www.who.int/mediacentre/factsheets/fs104/en/index.html. Accessed on 01-15-2010.
2 WHO, 2009 Global tuberculosis control: a short update to the 2009 report. WHO/HTM/TB/2009.426.
3 A. Goodman and M. Lipman, *Clin. Med.*, 2008, **8**, 531–534.
4 Centers for Disease Control and Prevention, *MMWR.*, 2006, **55**, 301–305; WHO, 2010. http://www.who.int/tb/challenges/xdr/xdr_map_sep09.pdf. Accessed on 01-21-2010.
5 A. A. Velayati, P. Farnia, M. R. Masjedi, T. A. Ibrahim, P. Tabarsi, R. Z. Haroun, H. O. Kuan, J. Ghanavi, P. Farnia and M. Varahram, *Eur. Respir. J.*, 2009, **34**, 1202–1203.
6 Y. Zhang, *Annu. Rev. Pharmacol. Toxicol.*, 2005, **45**, 529–564.
7 R. Ducati, L. A. Basso and D. S. Santos, *Curr. Drug Targets*, 2007, **8**, 423–435.
8 M. Jassal and W. R. Bishai, *Lancet Infect. Dis.*, 2009, **9**, 19–30.
9 S. T. Cole, R. Brosch, J. Parkhill, T. Garnier, C. Churcher, D. Harris, S. V. Gordon, K. Eiglmeier, S. Gas, C. E. Barry, 3rd, F. Tekaia, K. Badcock, D. Basham, D. Brown, T. Chillingworth, R. Connor, R. Davies, K. Devlin, T. Feltwell, S. Gentles, N. Hamlin, S. Holroyd, T. Hornsby, K. Jagels, A. Krogh, J. McLean, S. Moule, L. Murphy, K. Oliver, J. Osborne, M. A. Quail, M. A. Rajandream, J. Rogers, S. Rutter, K. Seeger, J. Skelton, R. Squares, S. Squares, J. E. Sulston, K. Taylor, S. Whitehead and B. G. Barrell, *Nature*, 1998, **393**, 537–544.
10 T. Parish and N. G. Stoker, *Microbiology*, 2002, **148**, 3069–3077.
11 R. Bentley, *Crit. Rev. Biochem. Mol. Biol.*, 1990, **25**, 307–384.
12 S. L. Bender, S. Mehdi and J. R. Knowles, *Biochemistry*, 1989, **28**, 7555–7560.
13 N. Hasan and E. W. Nester, *J. Biol. Chem.*, 1978, **253**, 4999–5004.
14 J. M. Lambert, M. R. Boocock and J. R. Coggins, *Biochem. J.*, 1985, **226**, 817–829.
15 J. D. Moore, J. R. Coggins, R. Virden and A. R. Hawkins, *Biochem J.*, 1994, **301**, 297–304.
16 E. Yamamoto, *Phytochemistry*, 1980, **19**, 779–781.
17 R. Saijo and T. Kosuge, *Phytochemistry*, 1978, **17**, 223–225.
18 A. Gunel-Ozcan, K. A. Brown, A. G. Allen and D. J. Maskel, *Microb. Pathog.*, 1997, **23**, 311–316.
19 F. Kudo, Y. Hosomi, H. Tamegai and K. Kakinuma, *J. Antibiot.*, 1999, **52**, 81–88.
20 F. Kudo, H. Tamegai, T. Fujiwara, U. Tagami, K. Hirayama and K. Kakinuma, *J. Antibiot.*, 1999, **52**, 559–571.
21 F. Agüero, B. Al-Lazikani, M. Aslett, M. Berriman, F. S. Buckner, R. K. Campbell, S. Carmona, I. M. Carruthers, A. W. Chan, F. Chen, G. J. Crowther, M. A. Doyle, C. Hertz-Fowler, A. L. Hopkins, G. McAllister, S. Nwaka, J. P. Overington, A. Pain, G. V. Paolini, U. Pieper, S. A. Ralph, A. Riechers, D. S. Roos, A. Sali, D. Shanmugam, T. Suzuki, W. C. Van Voorhis and C. L. Verlinde, *Nat. Rev. Drug Discovery*, 2008, **7**, 900–907.
22 K. Raman, K. Yeturu and N. Chandra, *BMC Syst. Biol.*, 2008, **2**, 10.
23 I. H. Segel, in *Enzyme Kinetics, Behavior and Analysis of Rapid Equilibrium and Steady-state Enzyme Systems*, John Wiley & Sons, Inc., New York, 1975, 957 pp.
24 P. R. Srinivasan, J. Rothschild and B. D. Sprinson, *J. Biol. Chem.*, 1963, **238**, 3176–3182.
25 T. Hirayama, F. Kudo, Z. Huang and T. Egushi, *Bioorg. Med. Chem.*, 2007, **15**, 418–423.
26 A. Fersht, in *Enzyme Structure and Mechanism*, W. H. Freeman and Company, 2nd edn, 1985, ch. 4, pp. 121–154.
27 K. Hiromi, in *Kinetics of Fast Enzyme Reactions: Theory and Practice*, Kodansha Scientific Books, Tokyo, 1979, ch. 4, pp. 188–253.
28 P. A. Barlett and K. Satake, *J. Am. Chem. Soc.*, 1988, **110**, 1628–1630.
29 E. P. Carpenter, A. R. Hawkins, J. W Frost and K. A. Brown, *Nature*, 1998, **394**, 299–302.
30 T. Widlanski, S. L. Bender and J. R. Knowles, *Biochemistry*, 1989, **28**, 7572–7582.
31 E. Nango, T. Eguchi and K. Kakinuma, *J. Org. Chem.*, 2004, **69**, 593–600.
32 J. D. Mendonça, F. Ely, M. S. Palma, J. Frazzon, L. A. Basso and D. S. Santos, *J. Bacteriol.*, 2007, **189**, 6246–6252.
33 J. D. Thompson, D. G. Higgins and T. J. Gibson, *Nucleic Acids Res.*, 1994, **22**, 4673–4680.
34 S. L. Bender, T. Widlanski and J. R. Knowles, *Biochemistry*, 1989, **28**, 7560–7572.
35 A. Park, H. K. Lamb, C. Nichols, J. D. Moore, K. A. Brown, A. Cooper, I. G. Charles, D. K. Stammers and A. R. Hawkins, *Protein Sci.*, 2006, **13**, 2108–2119.
36 C. M. Stephens and R. Bauerle, *J. Biol. Chem.*, 1991, **266**, 20810–20817.
37 P. C. Engel, in *Enzyme Kinetics: The Steady-state Approach*, John Wiley & Sons, Inc., New York, 1977, ch. 5, pp. 45–73.
38 U. S. Maitra and D. B. Sprinson, *J. Biol. Chem.*, 1978, **253**, 5426–30.
39 J. G. Robertson, *Biochemistry*, 2005, **44**, 5561–5571.
40 J. G. Robertson, *Curr. Opin. Struct. Biol.*, 2007, **17**, 674–679.
41 M. L. Bianconi, *Biophys. Chem.*, 2007, **126**, 59–64.
42 J. E. Ladbury, G. K. Klebe and E. Freire, *Nat. Rev. Drug Discovery*, 2010, **9**, 23–27.
43 M. M. Bradford, *Anal. Biochem.*, 1976, **72**, 248–254.
44 S. Mituhashi and B. D. Davis, *Biochim. Biophys. Acta*, 1954, **15**, 54–61.

Anexo C

UMP kinase from *Mycobacterium tuberculosis*: Mode of action and allosteric interactions, and their role in pyrimidine metabolism regulation

Diana Rostirolla, Ardala Breda, Leonardo Astolfi Rosado, Mário Sérgio Palma, Luiz Augusto Basso, Diogenes Santiago Santos

Artigo *in press – Archives of Biochemistry and Biophysics*.

Archives of Biochemistry and Biophysics xxx (2010) xxx–xxx

Contents lists available at ScienceDirect

Archives of Biochemistry and Biophysics

journal homepage: www.elsevier.com/locate/yabbi

UMP kinase from *Mycobacterium tuberculosis*: Mode of action and allosteric interactions, and their likely role in pyrimidine metabolism regulation ☆

Diana C. Rostirolla [a,b], Ardala Breda [a,b], Leonardo A. Rosado [a,c], Mario S. Palma [d], Luiz A. Basso [a,b,*], Diógenes S. Santos [a,b,*]

[a] *Centro de Pesquisas em Biologia Molecular e Funcional (CPBMF), Instituto Nacional de Ciência e Tecnologia em Tuberculose (INCT-TB), Pontifícia Universidade Católica do Rio Grande do Sul (PUCRS), Av. Ipiranga 6681 – Tecnopuc – Prédio 92-A, Porto Alegre 90619-900, RS, Brazil*
[b] *Programa de Pós-Graduação em Biologia Celular e Molecular, Pontifícia Universidade Católica do Rio Grande do Sul (PUCRS), Porto Alegre, RS, Brazil*
[c] *Programa de Pós-Graduação em Medicina e Ciências da Saúde, PUCRS, Av. Ipiranga 6681, Porto Alegre 90619-900, RS, Brazil*
[d] *Laboratório de Biologia Estrutural e Zooquímica, Centro de Estudos de Insetos Sociais, Departamento de Biologia, Instituto de Biociências de Rio Claro, Universidade Estadual Paulista (UNESP), Rio Claro, SP, Brazil*

ARTICLE INFO

Article history:
Received 25 July 2010
and in revised form 21 October 2010
Available online xxxx

Keywords:
UMPK
Cooperative kinetics
Allosteric regulation
Pyrimidine metabolism
Thermodynamic binding parameters
Antitubercular drug target

ABSTRACT

The *pyrH*-encoded uridine 5′-monophosphate kinase (UMPK) is involved in both *de novo* and salvage synthesis of DNA and RNA precursors. Here we describe *Mycobacterium tuberculosis* UMPK (*Mt*UMPK) cloning and expression in *Escherichia coli*. N-terminal amino acid sequencing and electrospray ionization mass spectrometry analyses confirmed the identity of homogeneous *Mt*UMPK. *Mt*UMPK catalyzed the phosphorylation of UMP to UDP, using ATP–Mg^{2+} as phosphate donor. Size exclusion chromatography showed that the protein is a homotetramer. Kinetic studies revealed that *Mt*UMPK exhibits cooperative kinetics towards ATP and undergoes allosteric regulation. GTP and UTP are, respectively, positive and negative effectors, maintaining the balance of purine versus pyrimidine synthesis. Initial velocity studies and substrate(s) binding measured by isothermal titration calorimetry suggested that catalysis proceeds by a sequential ordered mechanism, in which ATP binds first followed by UMP binding, and release of products is random. As *Mt*UMPK does not resemble its eukaryotic counterparts, specific inhibitors could be designed to be tested as antitubercular agents.

Introduction

Human tuberculosis (TB),[1] mainly caused by *Mycobacterium tuberculosis*, is a major cause of illness and death worldwide. *M. tuberculosis* is a remarkably successful pathogen that latently infects one third of the world population [1] and, despite the availability of effective chemotherapy and moderately protective vaccine, the tubercle bacillus continues to claim more lives than any other single infectious agent [2]. Increasing HIV–TB co-infections [2], the emergence of multidrug-resistant (MDR), extensively drug-resistant (XDR) [3], and, more recently, of totally drug-resistant strains (TDR) [4] have highlighted the need for the development of new therapeutic strategies to combat TB. Strategies based on the discovery of new targets for antimycobacterial agent development include elucidation of

☆ This work was supported by the National Institute of Science and Technology on Tuberculosis (DECIT/SCTIE/MS-MCT-CNPq-FNDCT-CAPES) and the Millennium Initiative Program (CNPq) to D.S.S. and L.A.B. D.S.S. (CNPq, 304051/1975-06), L.A.B. (CNPq, 520182/99-5), and M.S.P. (CNPq, 500079/90-0) are Research Career Awardees of the National Research Council of Brazil (CNPq). A.B. is recipient of a Ph.D. student scholarship awarded by BNDES. L.A.R. and D.C.R. are recipients of M.Sc. student scholarships awarded by, respectively, CAPES and CNPq.

* Corresponding authors at: Centro de Pesquisas em Biologia Molecular e Funcional (CPBMF), Instituto Nacional de Ciência e Tecnologia em Tuberculose (INCT-TB), Pontifícia Universidade Católica do Rio Grande do Sul (PUCRS), Av. Ipiranga 6681 – Tecnopuc – Prédio 92-A, Porto Alegre 90619-900, RS, Brazil. Fax: +55 51 33203629.

E-mail addresses: luiz.basso@pucrs.br (L.A. Basso), diogenes@pucrs.br (D.S. Santos).

[1] *Abbreviations used:* ADP, adenosine 5′-diphosphate; ATP, adenosine 5′-triphosphate; CMP, cytosine 5′-monophosphate; CTP, cytosine 5′-triphosphate; dCMP, deoxycytosine 5′-monophosphate; DMSO, dimethyl sulfoxide; DNA, deoxyribonucleic acid; dTMP, deoxythymidine 5′-monophosphate; ESI-MS, electrospray ionization mass spectrometry; FDA, Food and Drug Administration; GTP, guanosine 5′-triphosphate; Hepes, *N*-2-hydroxyethylpiperazyne-*N*′-2-ethanesulfonic acid; HIV, human immunodeficiency virus; IPTG, isopropyl-β-D-thiogalactopyranoside; ITC, isothermal titration calorimetry; LB, Luria–Bertani; MDR, multidrug-resistant; *Mt*UMPK, uridine 5′-monophosphate kinase from *Mycobacterium tuberculosis*; NADH, nicotinamide adenine dinucleotide; NDP, nucleoside diphosphate; NMP, nucleoside monophosphate; NTP, nucleoside triphosphate; PCR, polymerase chain reaction; PDB, Protein Data Bank; RNA, ribonucleic acid; SDS–PAGE, sodium dodecyl sulfate–polyacrylamide gel electrophoresis; TB, Terrific Broth; TB, tuberculosis; Tris, tris(hydroxymethyl)aminomethane; UDP, uridine 5′-diphosphate; UMP, uridine 5′-monophosphate; UMPK, uridine 5′-monophosphate kinase; UTP, uridine 5′-triphosphate; XDR, extensively drug-resistant.

0003-9861/$ - see front matter © 2010 Elsevier Inc. All rights reserved.
doi:10.1016/j.abb.2010.10.019

the role played by proteins of essential and, preferentially, exclusive biochemical pathways for mycobacterial growth [5].

Rational inhibitor design relies on mechanistic and structural information on the target enzyme. Enzyme inhibitors make up roughly 25% of the drugs marketed in United States [6]. Enzymes offer unique opportunities for drug design that are not available to cell surface receptors, nuclear hormone receptors, ion channel, transporters, and DNA [6]. It has been pointed out that one of the lessons to be learned from marketed enzyme inhibitors is that the most potent and effective inhibitors take advantage of enzyme chemistry to achieve inhibition [7]. Moreover, the recognition of the limitations of high-throughput screening approaches in the discovery of candidate drugs has rekindled interest in rational design methods [8]. Accordingly, mechanistic analysis should always be a top priority for enzyme-targeted drug programs aiming at the rational design of potent enzyme inhibitors.

Nucleotides are important molecules present in all living organisms as they constitute the building blocks for nucleic acids and also serve as energy sources for many biochemical reactions [9]. Pyrimidine nucleotides can be synthesized by *de novo* and salvage pathways resulting in a common product, the nucleotide uridine 5′-monophosphate (UMP) [10]. Subsequent phosphorylation of UMP yields UDP that leads to the synthesis of all other pyrimidine nucleotides [11]. Nucleoside monophosphate (NMP) kinases play an important role in the biosynthesis of nucleotides and represent a homogeneous family of catalysts related to adenylate kinase (EC 2.7.4.3). They catalyze the synthesis of nucleoside diphosphates (NDPs), which will be converted to nucleoside triphosphates (NTPs) by a non-specific nucleoside diphosphate kinase [12]. UMP kinases (UMPKs) catalyze the reversible transfer of the γ-phosphoryl group from ATP to UMP in the presence of a divalent cation, usually Mg^{2+} (Fig. 1) [13]. In general, eukaryotic UMP/CMP kinases (EC 2.7.4.14) are monomers, phosphorylate with comparable efficiency both UMP and CMP, and are structurally similar to other NMP kinases (such as adenylate kinase) [12,14–16]. In contrast, bacterial UMPKs (EC 2.7.4.22) are specific for UMP, exist in solution as stable homohexamers, and do not resemble either UMP/CMP kinases or NMP kinases from other organisms based on sequence comparisons [17,18]. Kinetic studies have shown that bacterial UMPKs can be activated by GTP and/or be subject to feedback inhibition by UTP, the major product of the reaction they catalyze [17–21], regulating the balance of purine versus pyrimidine nucleoside triphosphates synthesis [13].

As pyrimidine biosynthesis is an essential step in the progression of TB, enzymes of this pathway are attractive antitubercular drug targets [22]. Homologs to enzymes in the pyrimidine pathway have been identified in the genome sequence of *M. tuberculosis* [23]. A rapid recombination method for screening and confirmation of gene essentiality has recently been proposed to allow identification of which of the approximately 4000 genes of *M. tuberculosis* are worthy of further study as drug targets [24]. The product of *pyrH* (Rv2883) gene has been shown to be essential for *M. tuberculosis* growth by the rapid screening method [24].

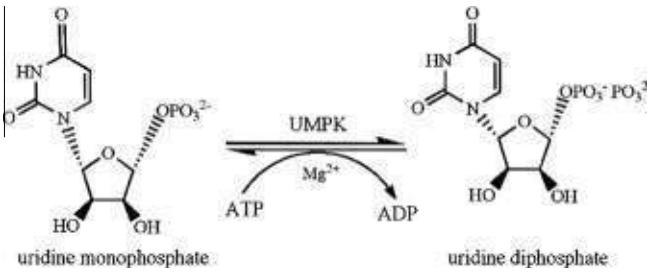

Fig. 1. Chemical reaction catalyzed by UMPK.

Genetic studies have provided evidence that UMPK is essential for growth in both Gram-negative (*Escherichia coli*) [25,26] and Gram-positive bacteria (*Streptococcus pneumoniae*) [19]. Although the *pyrH* gene has been proposed by sequence homology to encode a UMPK protein [23], there has been no formal biochemical proof as to ascertain the correct assignment to the open reading frame of *pyrH* gene in *M. tuberculosis*.

In the present work, the *pyrH* gene from *M. tuberculosis* strain H37Rv was PCR amplified, cloned, and recombinant UMPK (*Mt*UMPK) was purified to homogeneity. N-terminal amino acid sequencing and electrospray ionization mass spectrometry (ESI-MS) analyses were carried out to confirm the identity of the recombinant *Mt*UMPK protein. Initial velocity studies were performed to evaluate the kinetic parameters of the recombinant *Mt*UMPK. In addition, isothermal titration calorimetry study of substrates binding was carried out to demonstrate the order of substrate addition in the kinetic mechanism of *Mt*UMPK. Protein allosteric regulation by ATP, GTP, and UTP have also been demonstrated. These results represent an important step for the rational design of *Mt*UMPK inhibitors that can further be tested as anti-TB drugs.

Materials and methods

Amplification, cloning and DNA sequencing of the pyrH gene

The full-length *pyrH* (Rv2883c) coding region [23] was PCR amplified using the genomic DNA from *M. tuberculosis* H37Rv as template and a high fidelity proof-reading thermostable DNA polymerase (*Pfu*® DNA polymerase, Stratagene). The synthetic oligonucleotides used (forward primer, 5′-GTC ATA TGA CAG AGC CCG ATG TCG CCG GC-3′; and reverse primer, 5′-TAA AGC TTT CAG GTG GTG ACC AGC GTT CCG A-3′) were designed to contain, respectively, NdeI and HindIII (New England Biolabs) restriction sites (underlined). Dimethyl sulfoxide (DMSO) was added to a final concentration of 10%. The 786-bp amplicon was detected on 1% agarose gel and purified utilizing the Quick Gel Extraction kit (Invitrogen). The PCR fragment was cloned into pCR-Blunt® vector (Invitrogen) and, following transformation of *E. coli* strain DH10B (Novagen), the resulting plasmid was isolated utilizing the Qiaprep Spin Miniprep kit (Qiagen). Subsequently, the fragment was cleaved with NdeI and HindIII endonucleases and inserted into the pET-23a(+) expression vector (Novagen), previously digested with the same restriction enzymes. The complete *pyrH* nucleotide sequence was determined by automated DNA sequencing to corroborate sequence identity, integrity and to check the absence of mutations in the cloned fragment.

Expression and purification of recombinant MtUMPK

The recombinant plasmid pET-23a(+)::*pyrH* was transformed into BL21(DE3) *E. coli* electrocompetent cells (Novagen), and cells carrying the recombinant vector were selected on Luria–Bertani (LB) agar plates containing 50 μg mL^{-1} ampicillin [27]. A single colony was used to inoculate 50 mL of Terrific Broth (TB) medium containing the same antibiotic and grown overnight at 37 °C. Aliquots of this culture (2.5 mL) were used to inoculate 250 mL of TB medium in 5 × 1 L flasks supplemented with ampicillin (50 μg mL^{-1}) and grown at 37 °C and 180 rpm to an optical density (OD_{600nm}) of 0.4–0.6. When this OD_{600} value was reached, the temperature was lowered to 30 °C and protein expression was carried out without isopropyl-β-D-thiogalactopyranoside (IPTG) induction. After 24 h, the cells (12 g) were collected by centrifugation at 11,800*g* for 30 min at 4 °C and stored at −20 °C. The same protocol was employed for BL21 (DE3) *E. coli* cell transformed with pET-23a(+) as control. The expression of the recombinant protein was confirmed by 12% sodium

dodecyl sulfate–polyacrylamide gel electrophoresis (SDS–PAGE) stained with Coomassie Brilliant Blue [28].

Escherichia coli (2 g) cells overproducing the *Mt*UMPK were resuspended in 20 mL of 50 mM Tris–HCl, pH 7.5 (buffer A), stirred for 30 min at 4 °C in the presence of lysozyme (0.2 mg mL^{-1}, Sigma–Aldrich), and disrupted by sonication (eight pulses of 10 s, at an amplitude value of 60%). The lysate was centrifuged at 38,900*g* for 30 min to remove cell debris and the supernatant was treated with 1% (wt/vol) streptomycin sulfate (Sigma–Aldrich), stirred for 30 min, and the mixture was centrifuged at 38,900*g* for 30 min. The supernatant containing soluble *Mt*UMPK was dialyzed against 2 L of buffer A for 3 h.

All purification steps were carried out on an ÄKTA system (GE Healthcare) at 4 °C with UV detection at 215, 254, and 280 nm, and fractions were analyzed by SDS–PAGE. The crude extract was loaded on a HiPrep 16/10 Q XL (GE Healthcare) anion-exchange column pre-equilibrated with buffer A. Proteins were eluted using a 0–300 mM NaCl linear gradient at a flow rate of 1 mL min^{-1}. Fractions containing *Mt*UMPK in NaCl (ca. 280 mM) were pooled and $(NH_4)_2SO_4$ was added to a final concentration of 1 M, stirred for 30 min, and clarified by centrifugation at 38,900*g* for 30 min. The supernatant was loaded on a Butyl Sepharose High Performance (GE Healthcare) hydrophobic interaction column pre-equilibrated with 50 mM Tris–HCl, pH 7.5, containing 1 M $(NH_4)_2SO_4$. Proteins were eluted using a 0–100% linear gradient of buffer A at a flow rate of 1 mL min^{-1}. Pooled fractions containing *Mt*UMPK was dialyzed against buffer A to remove salt and loaded on a Mono Q 16/10 (GE Healthcare) anion-exchange column. *Mt*UMPK was eluted in a salt gradient (0–240 mM NaCl) at a flow rate of 1 mL min^{-1}. The pooled sample was dialyzed against 50 mM Tris–HCl, pH 7.5, containing 200 mM NaCl, concentrated using an AMICON (Millipore Corporation, Bedford, MA) ultra filtration membrane (MWCO = 10 kDa), and stored at −80 °C. Total protein concentration was determined by the method of Bradford [29], using the Bio-Rad protein assay kit (Bio-Rad Laboratories) and bovine serum albumin as standard.

Amino acid sequence and mass spectrometry analysis

The N-terminal amino acid residues of homogenous recombinant *Mt*UMPK were determined by automated Edman degradation sequencing using a PPSQ-21A gas-phase sequencer (Shimadzu) [30]. Recombinant *Mt*UMPK was analyzed by electrospray ionization mass spectrometry (ESI-MS) employing some adaptations made to the system described by Chassaigne and Lobinski [31]. Samples were analyzed on a Quattro-II triple-quadrupole mass spectrometer (Micromass; Altrincham, UK), using MassLynx and Transform softwares for data acquisition and spectrum handling.

Determination of MtUMPK molecular mass

Gel-filtration chromatography was performed on a Superdex 200 (HR 10/30) column (GE Healthcare) pre-equilibrated with 50 mM Tris HCl pH 7.5 containing 200 mM NaCl at a flow rate of 0.4 mL min^{-1}, with UV detection at 215, 254 and 280 nm. The LMW and HMW Gel Filtration Calibration Kits (GE Healthcare) were used to prepare a calibration curve. The elution volumes (V_e) of standard proteins (ferritin, catalase, aldolase, coalbumin, ovalbumin, ribonuclease A) were used to calculate their corresponding partition coefficient (K_{av}, Eq. (1)). Blue dextran 2000 (GE Healthcare) was used to determine the void volume (V_o). V_t is the total bead volume of the column. The K_{av} value for each protein was plotted against their corresponding molecular mass.

$$K_{av} = \frac{V_e - V_o}{V_t - V_o} \quad (1)$$

Multiple sequence alignment

The amino acid sequences of the following UMPK proteins, whose three-dimensional structures were solved, were included in the alignment: *E. coli* (NP_414713.1), *Ureaplasma parvum* (YP_001752598.1), *Pyrococcus furiosus* (NP_579136.1), *Sulfolobus solfataricus* (NP_342460.1), and *Bacillus anthracis* (NC_012659.1). The UMPK amino acid sequences of *S. pneumoniae* (YP_816317.1) and *B. subtilis* (NP_389533.2) [32] were also included in the alignment and compared with *M. tuberculosis* UMPK (NP_217399.1). Multiple amino acid sequence alignment was performed by ClustalW [33], using the Gonnet matrix for amino acids substitutions and considering gap penalties, to identify essential residues for nucleotide substrate(s) binding, as well as to infer possible similarities in their mechanism of catalysis. For alignment improvement, 8, 23, 11, 5, 5, and 29 amino acids residues were removed from the *E. coli*, *U. parvum*, *B. anthracis*, *S. pneumoniae*, *B. subtilis*, and *M. tuberculosis*, respectively.

Functional characterization of MtUMPK

*Mt*UMPK catalytic activity was measured for all purification steps in the forward direction at 25 °C, using a coupled spectrophotometric assay (0.5 mL final volume) as described elsewhere [34], on an UV-2550 UV/vis spectrophotometer (Shimadzu). In short, the reaction mixture contained 50 mM Tris–HCl, pH 7.5, 50 mM KCl, 5 mM $MgCl_2$ buffer; 1 mM phosphoenolpyruvate, 0.2 mM β-NADH, fixed concentrations of both ATP (3000 μM) and UMP (600 μM) substrates, 3 U of pyruvate kinase (EC 2.7.1.40) and 2.5 U of L-lactate dehydrogenase (EC 1.1.1.27). The reaction was started by the addition of *Mt*UMPK. The decrease in absorbance at 340 nm ($\varepsilon_{\beta\text{-NADH}} = 6.22 \times 10^{+3}\ M^{-1}\ cm^{-1}$) was continuously monitored and corrected for non-catalyzed chemical reactions in the absence of UMP. One unit of *Mt*UMPK is defined as the amount of enzyme necessary to convert 1 μmol of UMP in UDP per min in an optical path of 1 cm.

Steady-state kinetics

Determination of the apparent steady-state kinetic parameters were evaluated at varying concentrations of UMP (0–150 μM) and a fixed-saturating concentration of ATP (3000 μM), and at varying concentrations of ATP (0–3000 μM) and a fixed-saturating level of UMP (600 μM). Initial velocity data were analyzed by SigmaPlot (Systat Software, Inc.).

In order to evaluate the specificity for phosphate acceptor, UMP was replaced with other nucleoside monophosphates (CMP, dCMP or dTMP) at different concentrations. The specificity of the enzyme as regards the phosphoryl donors was tested by replacing ATP with 3 mM GTP, CTP, and UTP in the standard assay.

Inhibition studies were carried out in the presence of fixed non-saturating levels of ATP (1300 μM) and fixed-varied UTP concentration (0, 30, 50, and 70 μM) when UMP was the variable substrate. Inhibition studies were also carried out in the presence of fixed non-saturating concentration of UMP (40 μM) and fixed-varied UTP concentration (0, 20, 50, and 100 μM) when ATP was the variable substrate. In addition, saturation curves for UTP (0–400 μM) were carried out at three different sets of experiments: fixed-non-saturating ATP concentration (1300 μM) corresponding to its $K_{0.5}$, and saturating UMP concentration (600 μM = 19 × K_m); fixed-non-saturating ATP concentration (1300 μM) corresponding to its $K_{0.5}$, and non-saturating UMP concentration (30 μM ≅ K_m); and fixed-saturating ATP concentration (3000 μM = 2.3 × $K_{0.5}$) and non-saturating UMP concentration (30 μM ≅ K_m). The maximal rate for each reaction condition was determined in the absence of inhibitor. Initial velocity parameters were also analyzed as a

function of ATP concentrations at fixed-saturating UMP concentration (600 μM) either in the absence or presence of a fixed concentration of GTP (500 μM) to verify whether this substrate has any effect on the kinetic properties of *Mt*UMPK (70 nM). Initial velocity measurements were also carried out as a function of UMP concentration at fixed-saturating ATP concentration (3000 μM) in either absence or presence of GTP (500 μM).

Hyperbolic saturation curves were fitted by non-linear regression analysis to the Michaelis–Menten equation (Eq. (2)), in which v is the steady-state velocity, V_{max} is the maximal rate, [S] is the substrate concentration, and K_m is the Michaelis–Menten constant [35,36]. Sigmoidal curves were fitted to the Hill equation (Eq. (3)), where $K_{0.5}$ is the value of the substrate concentration where $v = 0.5\ V_{max}$, and n is the Hill coefficient (indicating the cooperative index) [35,36].

$$v = \frac{V_{max}[S]}{K_m + [S]} \tag{2}$$

$$v = \frac{V_{max}[S]^n}{K_{0.5}^n + [S]^n} \tag{3}$$

The K_i value for UTP towards UMP was calculated using the uncompetitive equation (Eq. (4)), in which [I] is the inhibitor concentration and K_i is the inhibition constant [35,36].

$$v = \frac{V_{max}[S]}{[S]\left(1 + \frac{[I]}{K_i}\right) + K_m} \tag{4}$$

The IC_{50} value, which defines the concentration of inhibitor required to half-saturate the enzyme population, was determined by fitting the data to Eq. (5), in which v_i and v_o are, respectively, the reaction velocity in the presence and in the absence of inhibitor, v_i/v_o represents the fractional activity remaining at a given inhibitor concentration (fraction of free enzyme), and n is the Hill coefficient [36].

$$\frac{v_i}{v_o} = \frac{1}{1 + \left(\frac{[I]}{IC_{50}}\right)^n} \tag{5}$$

Isothermal titration calorimetry (ITC)

ITC experiments were carried out using an iTC_{200} Microcalorimeter (MicroCal, Inc., Northampton, MA). The reference cell (200 μL) was loaded with Milli Q water during all experiments and the sample cell (200 μL) was filled with *Mt*UMPK at a concentration of 100 μM. The injection syringe (39.7 μL) contained substrates or effectors at different concentrations: ATP, ADP, GTP, and UTP at 1.5 mM, UMP at 3 mM, and UDP at 1.8 mM. In addition, titration was performed with the non-hydrolyzable ATP analog, adenosine 5′-(β,γ-imido)triphosphate tetralithium salt hydrate (AMP-PNP) at 1.2 mM to determine the ligand concentration necessary to saturate the enzyme active sites. Subsequently, UMP at 800 μM was titrated into the sample cell containing *Mt*UMPK (100 μM) and AMP-PNP at saturating concentration (250 μM). The latter permits evaluation of any effect that this ATP analog may have on UMP binding to *Mt*UMPK:AMP-PNP binary complex. The ligand binding isotherms were measured by direct titration (ligand into macromolecule). The enzyme was prepared for ITC analysis by dialysis against 50 mM Hepes at pH 7.5 containing 50 mM KCl, 5 mM $MgCl_2$, 200 mM NaCl. The same buffer was used to prepare all ligand solutions and Tris, used at the kinetic assays, was replaced with Hepes due to the high enthalpy of ionization of Tris [37,38]. The stirring speed was 500 rpm at a temperature of 25 °C for all ITC experiments. The first titration injection (0.5 μL), which was discarded in the data analysis, was followed by 17 injections of 2.2 μL each at 180 s intervals. Control titrations (ligand into buffer) were performed to subtract the heats of dilution and mixing for each experiment prior to data analysis. The data after peak integration of the isotherm generated by ITC, subtraction of control titration data and concentration normalization (heat normalized to the molar ratio), were analyzed by Origin 7 SR4 software (Microcal, Inc.).

The ΔG (Gibbs free energy) of binding was calculated using the relationship described in Eq. (6), in which R is the gas constant (8.314 J K^{-1} mol^{-1}), T is the temperature in K (T = °C + 273.15), and K_a is the association constant at equilibrium. The entropy of binding (ΔS) can also be determined by this mathematical formula. The initial estimates for n, K_a, and ΔH parameters were refined by standard Marquardt non-linear regression method provided in the Origin 7 SR4 software.

$$\Delta G^o = -RT \ln K_a = \Delta H^o - T\Delta S^o \tag{6}$$

Results and discussion

Amplification, cloning and sequencing of the pyrH gene

The 786-bp PCR amplicon was consistent with the *M. tuberculosis* H37Rv *pyrH* coding region (data not shown). The product was purified and ligated into pET-23a(+) expression vector as described in Section 'Amplification, cloning and DNA sequencing of the pyrH gene'. Automated DNA sequencing confirmed the identity and the absence of mutations in the cloned fragment.

Expression and purification of the recombinant MtUMPK

The resulting pET-23a(+)::*pyrH* recombinant plasmid was electroporated into BL21(DE3) *E. coli* cells and cultures were grown in TB medium for 24 h. Analysis by SDS–PAGE indicated that the supernatant of cell extract (Fig. 2A, lane 3), which was sonicated and centrifuged, contained a significant amount of protein with subunit molecular mass (ca. 27 kDa) in agreement with the predicted MW for *Mt*UMPK (27.4 kDa).

The overexpressed protein was purified by a three-step protocol consisting of an anion-exchange column (HiPrep Q XL), a hydrophobic interaction column (Butyl Sepharose HP) and a strong anion-exchange column (Mono Q). The target protein eluted at approximately 180 mM of NaCl from the Mono Q column, and

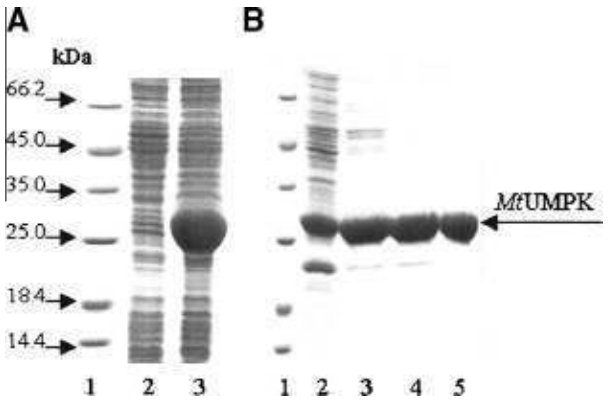

Fig. 2. (A) Twelve percent SDS–PAGE analysis of total soluble proteins. Expression of *Mt*UMPK of 24-h cell growth after reaching an $OD_{600\ nm}$ of 0.4–0.6 in TB medium without addition of IPTG. Lane 1, Protein Molecular Weight Marker (Fermentas); lane 2, soluble *E. coli* BL21 (DE3) [pET-23a(+) (control)] extract; lane 3, soluble *E. coli* BL21 (DE3) [pET-23a(+)::*pyrH*] extract. (B) Twelve percent SDS–PAGE analysis of pooled fractions from *Mt*UMPK purification steps. Lane 1, Protein Molecular Weight Marker (Fermentas); lane 2, crude extract; lane 3, HiPrep Q XL 16/10 elution; lane 4, Butyl Sepharose HP elution and Mono Q 16/10 elution.

Table 1
Purification of *Mt*UMPK from *E. coli* BL21 (DE3). Typical purification protocol from 2 g wet cell paste.

Purification step	Total protein (mg)	Total enzyme activity (U)	Specific activity (U mg^{-1})	Purification fold	Yield (%)
Crude extract	158	722	4.6	1.0	100
HiPrep Q XL	55	977	17.8	3.9	135
Butyl Sepharose	27	863	32	6.9	120
Mono Q	20	154	7.7	1.7	21

SDS–PAGE analysis showed that recombinant *Mt*UMPK was homogenous (Fig. 2B, lane 5). This 1.7-fold purification protocol yielded 20 mg of recombinant protein from 2 g of cells, indicating a 21% protein yield (Table 1). Enzyme kinetic measurements by NADH-coupled spectrophotometric assay showed that recombinant *Mt*UMPK indeed catalyzes the phosphorylation of UMP. Nevertheless, increase in the specific activity could be observed in the presence of high salt concentrations and a pronounced decrease after salt removal. This difference in activity may be attributed to ionic strength which, such as pH variations, is recognized to affect enzyme conformation, stability and activity [39,40]. Gagyi et al. [18] have also reported the addition of 100 mM NaCl as an approach to keep the *B. subtilis* UMPK stability. Accordingly, the homogenous protein was stored at −80 °C 50 mM Tris–HCl, pH 7.5, buffer containing 200 mM NaCl, which resulted in an apparent maximum velocity of 7.7 U mg^{-1} and allowed the kinetic assays to be carried out without affecting the coupled enzymes.

Mass spectrometry and N-terminal amino acid sequencing

The subunit molecular mass value was determined to be 27264.08 ± 13 Da by ESI-MS, which is lower than expected from the predicted amino acid sequence (27395.00 Da), indicating that the N-terminal methionine (130.92 Da) was removed.

The first 22 N-terminal amino acid residues identified by the Edman degradation method correspond to those predicted for the *pyrH* gene protein product and corroborate the N-terminal methionine removal. These results unambiguously identify the homogenous recombinant protein as the putative *Mt*UMPK.

MtUMPK molecular mass determination

The molecular mass of the native enzyme was determined by gel-filtration chromatography and yielded a single peak with elution volume corresponding to approximately 106 kDa, suggesting that *Mt*UMPK is a tetramer in solution (106,000 Da/27264.08 Da ≅ 3.9), differing from other bacterial homohexameric UMPKs [17–19].

Multiple sequence alignment

The currently available three-dimensional structures of UMPKs from several prokaryotic organisms deposited in the Protein Data Bank, such as *E. coli* (PDB code: 2BNE, 2BND, 2BNF, and 2V4Y) [13,41], *U. parvum* (PDB code: 2VA1) [21], *P. furiosus* (PDB code: 2BRI and 2BMU) [11], *S. solfataricus* (PDB code: 2J4J, 2J4K and 2J4L) [20] and *B. anthracis* (PDB code: 2JJX) [9], allow drug design based on a detailed model of the target binding site. The experimentally solved structures of *E. coli* UMPK [13,41] in complex with its substrates and the allosteric effector permit to propose the amino acid side chains in *M. tuberculosis* that are involved in ATP, UMP, and UDP binding as well as residues that participate in GTP-binding. To this end, multiple sequence alignment was carried out and

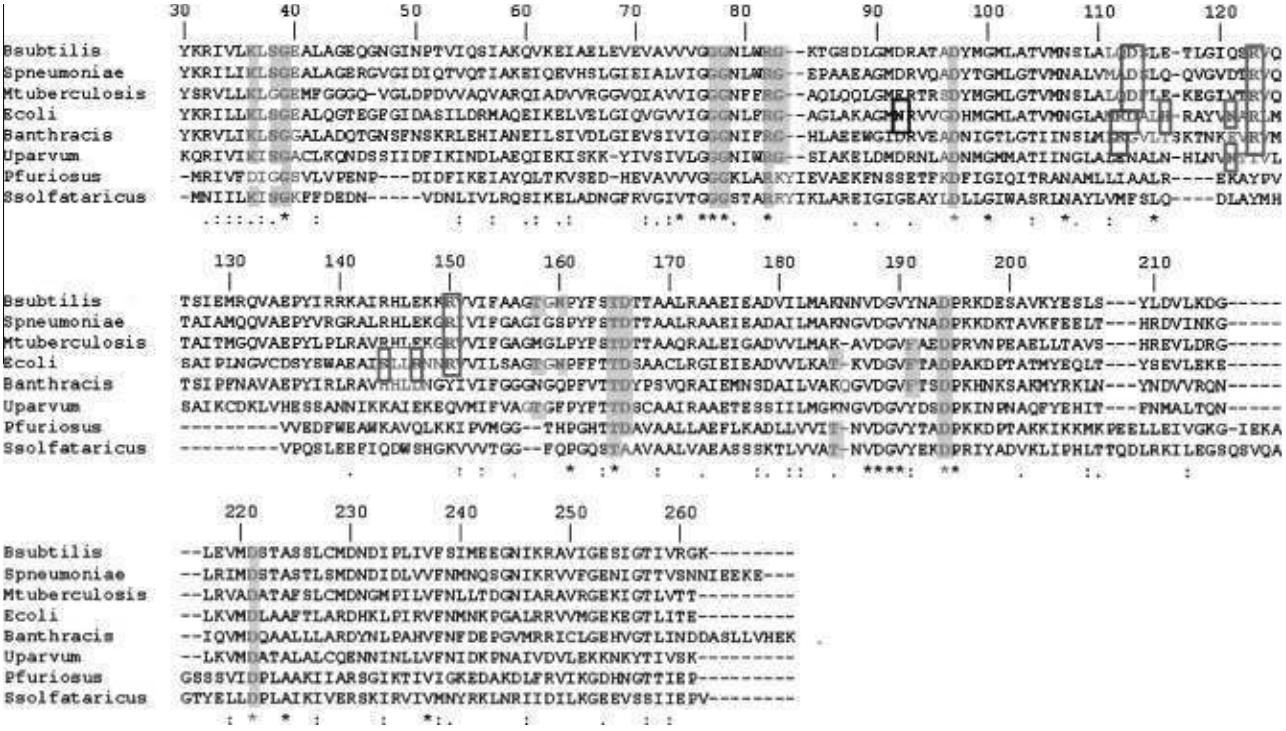

Fig. 3. Amino acids sequence alignment of UMPKs from eight prokaryotes. The residues inferred in *E. coli* as interacting with ATP, UMP or UDP are shaded in gray and the residues involved in GTP-binding are boxed [13,41]. (∗), (:), (.) and (−) indicate identity, strong similarity, weak similarity and gat inclusion among the residues, respectively. Amino acid residues were numbered after removing 29 N-terminal amino acids from the polypeptide sequence of *Mt*UMPK.

Please cite this article in press as: D.C. Rostirolla et al., Arch. Biochem. Biophys. (2010), doi:10.1016/j.abb.2010.10.019

the results suggest that the conserved *Mt*UMPK Gly83 and Asp97 (*M. tuberculosis* numbering) amino acid residues are equivalent to residues in *E. coli* UMPK [13] that interact with the 2′-OH ribose ring of UMP (Fig. 3). The amino acids Gly77, Gly78, Arg82, and Thr165, which are involved in UMP α-phosphate interactions, are conserved among all sequences aligned. The main differences among UMP binding residues are those associated with uracil binding. The interactions between *E. coli* UMPK and the uracil moiety of UMP are between the hydrophilic Thr138 and Asn140 amino acids, whereas in *Mt*UMPK these interactions are made by the hydrophobic Met158 and Leu160 residues. As no structural data for *Mt*UMPK have been available to date, it is tempting to suggest that these differences may be related to the distinct quaternary structures of *Mt*UMPK (tetramer) and *E. coli* UMPK (hexamer), since site-directed mutagenesis of Thr138 and Asn140 residues suggested their involvement in subunit contacts in the quaternary structure of the latter [13]. The interactions between the enzyme and uracil, ribose, or the UDP α-phosphate moiety are very similar to those with UMP, although UDP binding involves three additional amino acid residues [13]. The Lys36 and Gly39 residues (*M. tuberculosis* numbering) are conserved, whereas Gly39 in *Mt*UMPK sequence replaces a serine residue present in *E. coli* UMPK.

The amino acids Lys36, Asp166, Phe191, Asp194, and Asp221 in *Mt*UMPK are likely involved in ATP interaction since they are conserved in the *E. coli* UMPK and *Mt*UMPK polypeptide sequences. On the other hand, Lys185 in *Mt*UMPK replaces a threonine residue present in ATP binding site of *E. coli* UMPK. It is interesting to note that the Lys residue involved in ATP binding replaces Thr in five UMPK sequences [43] as in *Mt*UMPK. In *E. coli* UMPK, the GTP-binding site is between two dimers of the hexamer and GTP promotes a rearrangement of its quaternary structure, resulting in a tighter dimer–dimer interaction [41]. Asp113, which interacts with the GTP purine moiety, Arg123 and Arg150, both interacting with the phosphate group, are the most conserved amino acid residues (Fig. 3). These residues are absent in *U. parvum* and *S. solfataricus* UMPKs and may explain the lack of GTP stimulation of these enzymes [20,21].

MtUMPK kinetic parameters

The dependence of velocity with UMP as variable substrate at fixed-saturating ATP concentration (3000 μM) followed hyperbolic Michaelis–Menten kinetics (Fig. 4A), and the apparent constant values were thus calculated fitting the data to Eq. (2), yielding the following values: $V_{max} = 7.5$ (±0.3) U mg^{-1} and $K_m = 31$ (±3) μM. These results permit estimate a value of 3.4 (±0.1) s^{-1} for the UMP catalytic constant (k_{cat}) and of 11 (±1) × 10^4 M^{-1}s^{-1} for the UMP specificity constant (k_{cat}/K_m). The Michaelis–Menten constant values are similar to those reported for *B. subtilis* (K_m^{UMP} = 30 μM) and *E. coli* (K_m^{UMP} = 43 μM at pH 7.4) UMPKs [18,41].

The saturation curve for ATP at fixed-saturating UMP concentration (600 μM) was sigmoidal (Fig. 4B), suggesting cooperative kinetics. Accordingly, the data were fitted to the Hill equation (Eq. (3)), yielding the following values: $V_{max} = 8.8$ (±0.2) U mg^{-1}, $K_{0.5} = 1299$ (±32) μM and $n = 3.9$ (±0.3). The k_{cat} for ATP is 4.0 (±0.1) s^{-1}. The limiting value for the Hill coefficient (n) is four since we showed that *Mt*UMPK is a homotetramer in solution. The n value of 3.9 thus indicates strong positive cooperativity for ATP.

As demonstrated for others UMPKs [17,20,21], *Mt*UMPK was specific for UMP as the phosphoryl group acceptor as no enzyme activity was detected with CMP, dCMP or dTMP. The specificity for the phosphoryl group donor was tested with GTP, CTP and UTP, and UMP as the acceptor substrate. No activity was detected with GTP and CTP. UTP acted as phosphoryl donor at a velocity value of 0.5 U mg^{-1}. This value is 18-fold lower than for ATP (8.8 U mg^{-1}), suggesting that ATP is the more likely physiological phosphate donor for *Mt*UMPK.

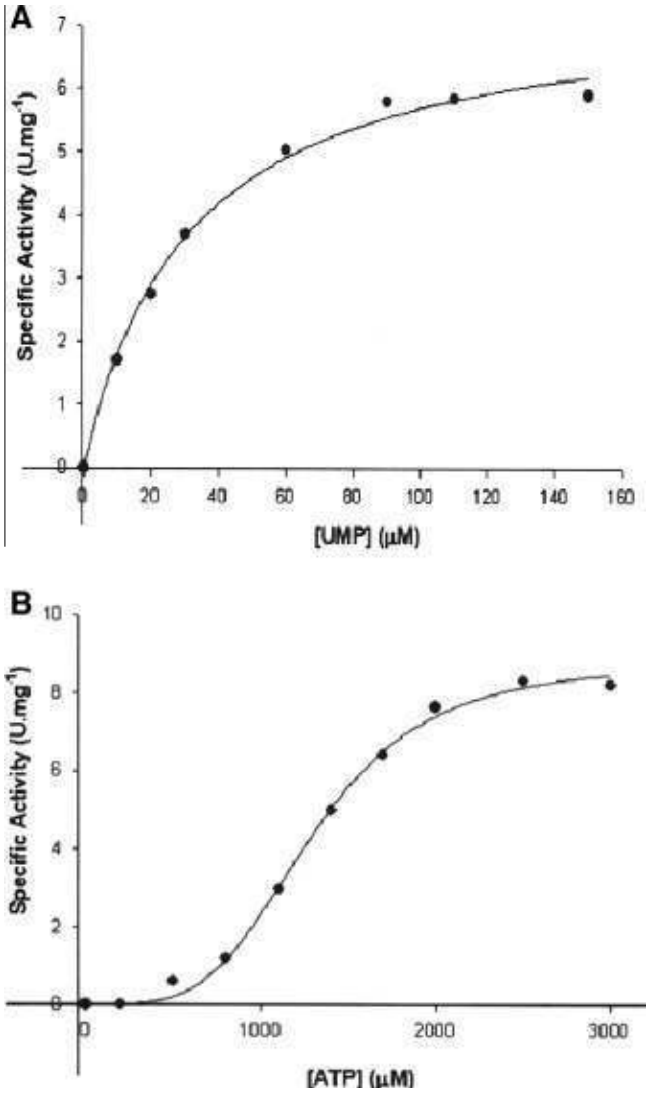

Fig. 4. Apparent steady-state kinetic parameters. (A) Specific activity (U mg^{-1}) versus [UMP] (μM) at fixed concentration of ATP (3000 μM). (B) Specific activity (U mg^{-1}) versus [ATP] (μM) at fixed concentration of UMP (600 μM). The *Mt*UMPK concentration was 70 nM on both assays.

UTP has been reported as a common negative regulator of UMPKs from Gram-negative bacteria, Gram-positive bacteria and archae [20,42,43]. To evaluate the inhibitory effect of UTP on *Mt*UMPK enzyme velocity, measurements of steady-state rates were carried out as described in Section 'Materials and methods'. Double-reciprocal plots at different UTP concentrations displayed a pattern of parallel lines, suggesting that UTP acts as an uncompetitive inhibitor towards UMP in which V_{max} and K_m values were simultaneously reduced (Fig. 5) at fixed non-saturating ATP concentration (1300 μM) and varying UMP concentration. Data fitting to Eq. (4) for uncompetitive inhibition yielded a K_i value of 87 (±5) μM for UTP. On the other hand, the plots of *Mt*UMPK activity versus ATP concentration in the presence of both non-saturating UMP (40 μM) and fixed-varied UTP concentrations (0, 30, 50, and 70 μM) were all sigmoidal. Although inhibition by UTP did not modify the sigmoidal shape of the curve, data fitting to Eq. (3) yielded increasing, though modest, values for apparent $K_{0.5}$, whereas V_{max} and the Hill coefficient values remained approximately constant (Table 2). These features appear to be a common

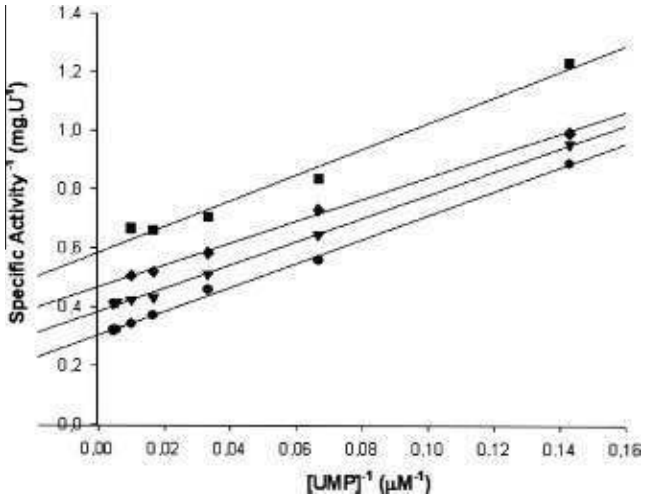

Fig. 5. Double-reciprocal plot of specific activity^{-1} (mg U^{-1}) versus [UMP]$^{-1}$ (μM^{-1}) at 0, 30, 50 and 70 μM UTP. The *Mt*UMPK concentration was 80 nM.

theme for UMPKs from Gram-positive and archae microorganisms [19,20,43].

The saturation curves for UTP inhibition in the presence of fixed-non-saturating ATP concentration and saturating UMP concentration, fixed-non-saturating ATP concentration and non-saturating UMP concentration, and fixed-saturating ATP concentration and non-saturating UMP concentration were all sigmoidal (data not shown). These data were thus fitted to Eq. (5), yielding estimates for IC_{50} values and the Hill coefficient (Table 3). The rates decreased with increasing UTP concentration, reaching a plateau of low enzyme activity (below 0.5 U mg^{-1}) at high UTP concentrations. The IC_{50} values of 80 μM (saturating UMP concentration) and 97 μM (non-saturating UMP concentration) were within experimental error. These results are in agreement with UTP acting as an uncompetitive inhibitor towards UMP (Fig. 5), thereby suggesting that UTP preferentially binds to a complex formed between *Mt*UMPK and UMP (it would have to be a ternary complex because we showed that ATP binding is followed by UMP binding). Stated otherwise, as the *Mt*UMPK enzyme mechanism is ordered (ATP binds first), the concentration of *Mt*UMPK:ATP binary complex, to which UMP binds, is unchanged as ATP concentration in both experiments were the same (1300 μM). It could be argued that increasing UMP fixed concentration (from 30 to 600 μM) would result in increasing concentration of *Mt*UMPK:ATP:UMP ternary complex, to which UTP binds, resulting in lower IC_{50} values for larger UMP concentrations. However, it should be kept in mind that the enzyme activity measurements here presented provide a value for the apparent K_m value of UMP and that this value represents an apparent dissociation constant that may be treated as the overall dissociation constant of all enzyme-bound species. In short, the true equilibrium dissociation constant of UMP from *Mt*UMPK:ATP:UMP ternary complex is not known, thereby precluding a proposal that increasing UMP concentration would result in increasing ternary complex concentration because the true dissociation constant value for UMP may be considerably larger than the concentrations employed here. In any case, the uncompetitive inhibition cannot be overcome by high UMP substrate concentrations, suggesting that UTP binds to an allosteric (regulatory) site. In addition, there was a decrease in the Hill coefficient (n) from 2.8 at non-saturating UMP concentration to 1.5 at saturating UMP concentration (Table 3). It thus appears that increasing UMP concentration results in decreasing degree of cooperativity. In the presence of saturating ATP concentration (3000 μM), there was a 2-fold increase in IC_{50} value for UTP, suggesting that UTP acts as a competitive inhibitor towards ATP. These data are consistent with ATP kinetics in which increasing fixed-varied concentrations of UTP in the presence of fixed-non-saturating UMP concentration yielded increasing values for apparent $K_{0.5}$ (Table 2). Moreover, since we have shown that UTP can act as a poor phosphoryl donor, it is thus likely that UTP can also bind to ATP binding site of *Mt*UMPK. These data suggest that UTP either binds to the ATP binding site with low affinity or to an allosteric site that results in uncompetitive inhibition towards UMP. Incidentally, it has been proposed that each subunit of bacterial UMPKs has three distinct nucleotide-binding sites [43].

Table 2
ATP kinetic parameters in the presence of fixed concentrations of UTP.

UTP concentration (μM)	V_{max}[a]	n[b]	$K_{0.5}$[c] (μM)
0	3.8 ± 0.3	2.4 ± 0.4	1.2 (±0.1) × 10^3
20	3.5 ± 0.3	2.1 ± 0.3	1.3 (±0.2) × 10^3
50	3.9 ± 0.4	2.5 ± 0.5	1.4 (±0.2) × 10^3
100	4 ± 1	2.3 ± 0.9	1.7 (±0.5) × 10^3

[a] V_{max} = maximal rate.
[b] n = the Hill coefficient.
[c] $K_{0.5}$ = value of the substrate concentration in which $v = 0.5\ V_{max}$.

Table 3
IC_{50} and n values for UTP in the presence of different fixed substrate concentrations.

Substrate concentrations	IC_{50}[a] (μM)	n[b]
ATP 1300 μM + UMP 600 μM	80 ± 4	1.5 ± 0.1
ATP 1300 μM + UMP 30 μM	97 ± 7	2.8 ± 0.4
ATP 3000 μM + UMP 30 μM	210 ± 6	3.6 ± 0.3

[a] IC_{50} = concentration of inhibitor required to half-saturate the enzyme population.
[b] n = the Hill coefficient.

GTP has been shown to be a positive effector for bacterial UMPKs [41,43]. The crystal structure of *E. coli* UMPK bound to GTP has recently been solved at 2.3 Å [41]. The presence of GTP (500 μM) resulted in both increased V_{max} values (from 2 to 3.2 U mg^{-1}) and affinity ($K_{0.5}$) of ATP for *Mt*UMPK (from 1335 to 545 μM) (Fig. 6). In addition, the Hill coefficient value of 4.4 in the absence of GTP decreased to 1.6 in the presence of GTP (500 μM), suggesting that this nucleotide decreased the degree of cooperativity of ATP upon *Mt*UMPK enzyme activity (Fig. 6). These results are in agreement with previously published results on UMPKs from Gram-positive bacteria [19,43]. On the other hand, the effect of GTP on UMP kinetics displayed a slight increase in the V_{max} values (from 1.63 ± 0.03 U mg^{-1} in the absence to 2.07 ± 0.05 U mg^{-1} in the presence of GTP), and no change of K_m values for UMP (data not shown).

Equilibrium binding of ligands assessed by ITC

To further elucidate the *Mt*UMPK kinetic mechanism, titration microcalorimetry of ligand binding to the recombinant enzyme was carried out. Equilibrium binding values of ligands were measured directly by ITC, determining the heat generated or consumed upon ligand–macromolecule binary complex formation at constant temperature and pressure. The measured of the heat released upon binding of the ligands allowed us to derive the binding enthalpy (ΔH) of the process, to estimate the stoichiometry of the interaction (n) and the association constant at equilibrium (K_a). The dissociation constant at equilibrium (K_d) could be calculated as the inverse of K_a ($K_d = 1/K_a$). Moreover, the Gibbs free energy (ΔG) and entropy (ΔS) of binding were determined from the association constant values at equilibrium as described in Eq. (6). The ITC data for binding of ligands to *Mt*UMPK (Fig. 7) are summarized in Table 4. The overall binding isotherms for ATP, ADP, UDP or

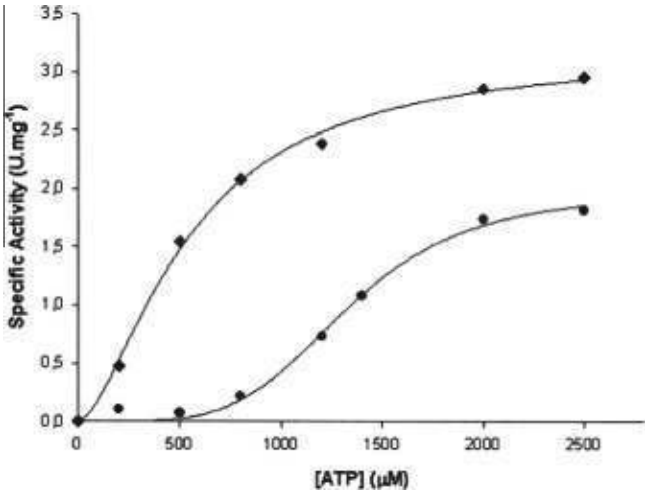

Fig. 6. Effect of GTP (500 μM) on ATP saturation curves. In the absence of effector (•), the curve is sigmoidal. In the presence of effector (♦), the sigmoidicity is reduced though still present. The *Mt*UMPK concentration was 70 nM.

GTP-binding to *Mt*UMPK were best fitted to a model of one set of sites (Table 4). The UTP binding isotherm was not well defined to obtain an adequate fit of the data to any model, probable because this substrate may exert different and simultaneous effects on *Mt*UMPK.

The mechanism of phosphoryl transfer of NMP kinases has been reported to follow a sequential random bi bi kinetic mechanism [12]. The *Mt*UMPK appears to deviate from this type of mechanism, since no significant heat changes were obtained for UMP binding, suggesting that it cannot bind to free enzyme. In contrast, all other ligands tested do bind to the free enzyme and exhibit exothermic reactions, as seen by negative changes in the binding enthalpy (Fig. 7). Interestingly, the binding isotherm of an ATP molecule does not appear to influence the affinity for the subsequent one, as the thermodynamic parameters for ATP binding provide single ΔH and K_a values. How can one reconcile these data with positive cooperativity displayed by the saturation curve (Fig. 4B) of steady-state kinetics for ATP in the presence of UMP? These data suggest that ATP binding has a positive heterotropic effect upon UMP binding to *Mt*UMPK:ATP binary complex, since UMP does not bind to the free enzyme. The *n* value of 0.57 sites for the ATP binding refers to the event of two subunits of *Mt*UMPK in the cell associating with each ATP molecule injected. In summary, we propose that ATP binding triggers a conformational change of *Mt*UMPK that results in increased affinity for UMP. To provide further experimental evidence for the proposed positive heterotropic effect of ATP, titration of UMP into a solution containing *Mt*UMPK:AMP-PNP binary complex (a non-hydrolyzable ATP analog) was carried out. The ligand binding isotherms showed no ITC signal upon UMP binding to free *Mt*UMPK enzyme (Fig. 7, panel E). On the other hand, the ITC signal for titration of *Mt*UMPK:AMP-PNP with UMP showed changes in the degree of heat response upon *Mt*UMPK:AMP-PNP:UMP ternary complex formation, displaying exothermic and endothermic responses (Fig. 7, panel F). The ITC data were analyzed with a model assuming a cooperative ligand binding interaction for a tetrameric protein. The UMP binding exhibited biphasic behavior (Fig. 7, panel F), which could be assessed by the endothermic and exothermic profile of the heat response. The ITC data showed a cooperative pattern and demonstrated that UMP binds to *Mt*UMPK:AMP-PNP binary complex (Table 4), even though it could not be demonstrated an obvious positive cooperative effect with increasing affinity for UMP as the binding sites are sequentially occupied. However, positive cooperativity is generally more difficult to distinguish from ITC studies alone, since the tendency is for the binding sites on any single molecule to saturate together unless the difference in affinity values between the sites were large. Notwithstanding, the ITC data are in agreement with the steady-state kinetics results showing that UMP binds to *Mt*UMPK:ATP binary complex and that ATP has a cooperative effect on tetrameric *Mt*UMPK enzyme.

The UDP product binds to free *Mt*UMPK enzyme with higher affinity than ADP product (Table 4), and both ligands displayed a stoichiometry of one ligand binding to each monomer of the tetrameric enzyme. The larger association constant of UDP as compared to ADP appears to be enthalpy driven (Table 4). These ITC results suggest that product release is random. The GTP-binding affinity is in the same range of UDP (Table 4). These ITC results demonstrate that GTP is capable of binding to free *Mt*UMPK enzyme with a stoichiometry close to unity. It is interesting to note that ATP (substrate) as compared to ADP (product) binding display approximately the same association constant at equilibrium (or Gibbs free energy), which is a result of the ubiquitous phenomenon of enthalpy–entropy compensation meaning that entropy losses often negate enthalpy gains [8]. In short, ITC and steady-state kinetic results provide evidence *Mt*UMPK follows an sequential ordered mechanism, in which ATP binds first to free enzyme followed by UMP binding to the *Mt*UMPK:ATP binary complex (Fig. 8). Release of products is, however, random. The mechanism for *S. solfataricus* UMPK has been shown to be random order for either addition of substrates or release of products [20].

Summary

Bacterial UMPKs have been proposed to be attractive drug targets because their primary amino acid sequence and three-dimensional structures are divergent from their eukaryotic counterparts. They are unique members of the NMP kinases family of enzymes and several research groups have demonstrate its essentiality for different organisms [17,19,25,26,44], and to *M. tuberculosis* in particular [24]. Moreover, they are oligomers with an exclusive and complex control of activity by GTP and UTP, representing an interesting model of allosteric regulation [43]. The elucidation of the mode of action of *Mt*UMPK is thus warranted. Although the *pyrH* gene has been proposed by *in silico* analysis to encode a UMPK enzyme [23], formal biochemical proof was still lacking as regards the correct assignment to its open reading frame in *M. tuberculosis*. Accordingly, here we describe PCR amplification of the *pyrH* coding region, cloning, heterologous expression, and purification of recombinant protein to homogeneity. N-terminal amino acid sequence and ESI-MS confirmed the identity of the homogeneous recombinant protein. Steady-state kinetic measurements confirmed that the *pyrH* gene encodes a UMPK enzyme in *M. tuberculosis*. Size exclusion chromatography showed that *Mt*UMPK is a tetramer in solution. Multiple sequence alignment analysis allowed identification of residues involved in substrate binding and/or catalysis.

Steady-state kinetic measurements showed that *Mt*UMPK is specific for both ATP and UMP substrates. This specificity for UMP is not surprising since it has been shown that the Rv1712 locus in *M. tuberculosis* codes for a functional cytosine monophosphate kinase that preferentially phosphorylates CMP and dCMP, and that UMP is a poor substrate [45]. In agreement with these results, *E. coli* has two distinct enzymes that display substrate specificity for UMP (UMPK) or CMP (CMP kinase) [46]. Steady-state kinetics and ITC data suggest a sequential ordered mechanism for substrate addition to *Mt*UMPK, in which ATP binds first to free enzyme followed by UMP binding; and a random order for release of products.

Please cite this article in press as: D.C. Rostirolla et al., Arch. Biochem. Biophys. (2010), doi:10.1016/j.abb.2010.10.019

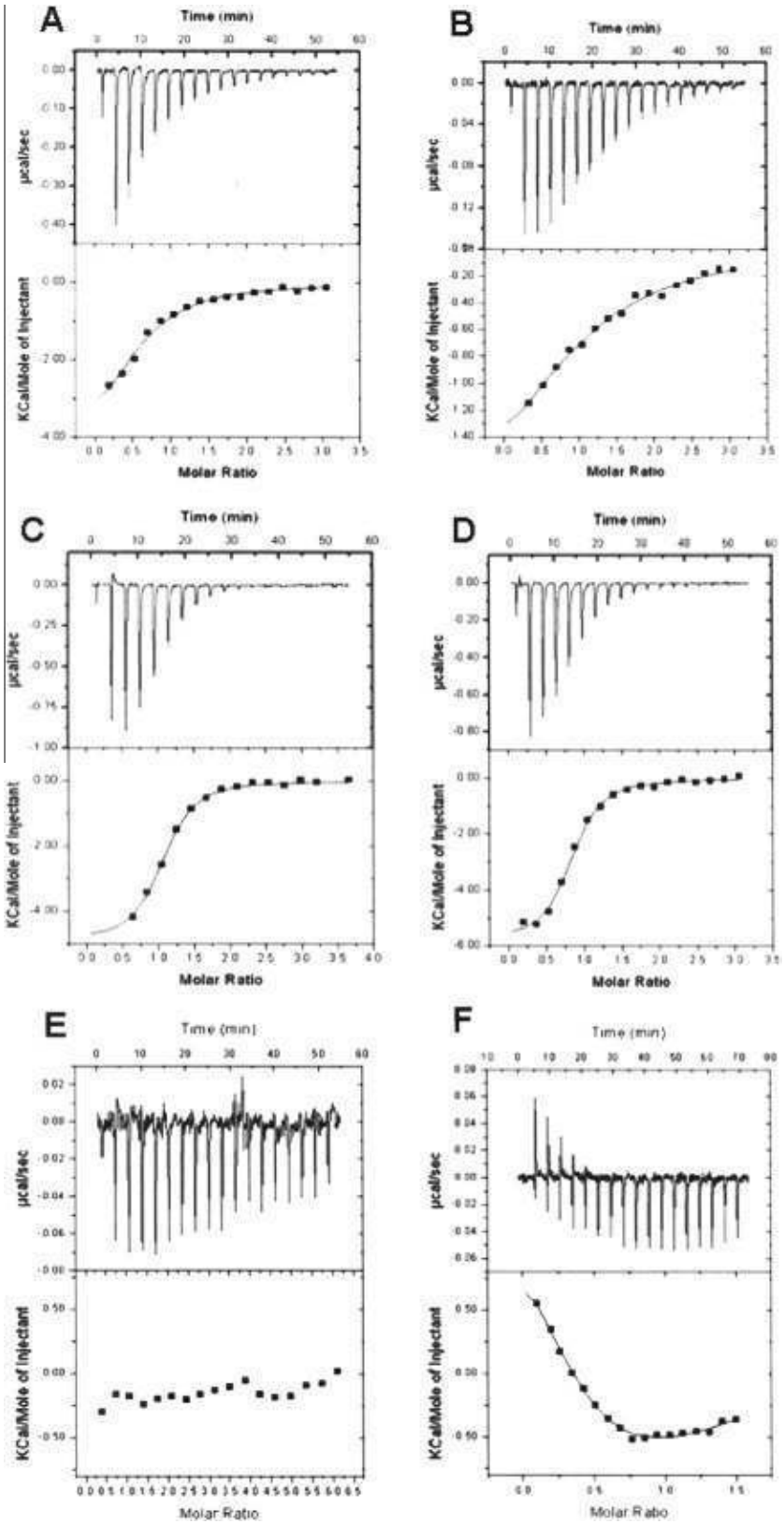

Fig. 7. Isothermal titration calorimetric curves of binding of ligands to *Mt*UMPK (100 µM). (A) Titration of the ATP substrate at a final concentration of 248 µM. (B) Titration of the ADP product at a final concentration of 248 µM. (C) Titration of the UDP product at a final concentration of 398 µM. (D) Titration of the allosteric effector GTP at a final concentration of 248 µM. (E) Titration of the UMP substrate at a final concentration of 497 µM. (F) Titration of the UMP substrate at a final concentration of 132 µM in the presence of the non-hydrolyzable ATP analog (AMP-PNP). The experiments were carried out at constant temperature and pressure.

Please cite this article in press as: D.C. Rostirolla et al., Arch. Biochem. Biophys. (2010), doi:10.1016/j.abb.2010.10.019

Table 4
Association constants and thermodynamic parameters of different ligands binding to *Mt*UMPK.

Ligands	n[a]	K_a[b] (M^{-1})	ΔH°[c] (kcal mol^{-1})	ΔG°[d] (kcal mol^{-1})	ΔS°[e] (cal mol^{-1} K^{-1})	K_d[f] (μM)
ATP	0.57 ± 0.06	$3.0e^4 \pm 5.7e^3$	−4.8 ± 0.6	−6.1 ± 1.2	4.3 ± 0.8	33.3 ± 6.3
ADP	1.0 ± 0.1	$1.5e^4 \pm 3.5e^3$	−2.1 ± 0.4	−5.7 ± 1.3	12.1 ± 2.8	66 ± 15
UDP	1.01 ± 0.01	$2.1e^5 \pm 2.4e^4$	−4.9 ± 0.1	−7.3 ± 0.8	7.9 ± 0.9	4.8 ± 0.5
GTP	0.80 ± 0.01	$2.0e^5 \pm 2.6e^4$	−5.8 ± 0.1	−7.2 ± 0.9	4.6 ± 0.6	5.0 ± 0.6
UMP		$2.4e^5 \pm 1.5e^5$	0.68	−7.34	26.9	4.2 ± 2.6
		$7.5e^4 \pm 3.8e^4$	−2.3	−6.63	14.6	13.3 ± 6.8
		$1.5e^5 \pm 9.3e^4$	−3.0	−7.03	13.4	6.7 ± 4.2
		$1.0e^5 \pm 5.3e^4$	7.9	−6.84	49.5	10 ± 5.3

[a] n = number of sites.
[b] K_a = association constant.
[c] ΔH° = binding enthalpy.
[d] ΔG° = Gibbs free energy.
[e] ΔS° = binding entropy.
[f] K_d = dissociation constant.

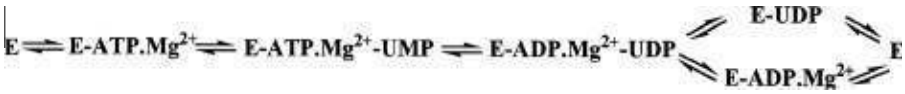

Fig. 8. Proposed kinetic mechanism for *Mt*UMPK.

The cooperative kinetics with respect to ATP, activation by GTP, and inhibition by UTP, showed that *Mt*UMPK is an allosteric enzyme that is subject to a complex control by these metabolites. The results here described also show that *Mt*UMPK belongs to the *K* system. This term was originally proposed by Monod et al. [47], in which the enzyme exists at equilibrium between two states with the same catalytic activities, but different substrate affinities (T of low affinity, and R of high affinity). In the absence of effectors, ATP has a positive heterotropic effect on UMP binding to *Mt*UMPK to form the catalytically competent ternary complex. This degree of cooperativity is decreased in the presence of GTP as there is a lowering of the Hill coefficient value, and a decrease in $K_{0.5}$ value for ATP, thereby suggesting increased ATP affinity for *Mt*UMPK. This model may also be applicable to UTP inhibition, in which binding of UTP displaces the equilibrium for the state with lower affinity for ATP with no effect on the Hill coefficient and maximum velocity. Moreover, as UTP is an uncompetitive inhibitor towards UMP, it appears that UTP can have a dual inhibitory effect on *Mt*UMPK enzyme activity depending on which substrate is varied. The results on *Mt*UMPK mode of action show that its cooperativity is more pronounced than that observed for other UMPKs (n values of 1.28–2.5) [19,21,43]. In general, the Hill coefficient does not represent the actual number of sites, unless the cooperativity is high [35]. Our findings show that the n value of ATP (3.9) for tetrameric *Mt*UMPK indicates strong positive cooperativity and it may correspond to the actual number of protomers. Activation of *Mt*UMPK by GTP and feedback inhibition by UTP imply a role for this enzyme in coordinating the synthesis of purine versus pyrimidine nucleoside triphosphates, and highlights the likely relevance of UMPK in the metabolism of *M. tuberculosis*.

The currently available repertoire of antimycobacterial agents reveals only a handful of comprehensively validated targets, namely RNA polymerase, DNA gyrase, NADH-dependent enoyl-ACP reductase, and ATP synthase [48]. The complete genome sequencing of *M. tuberculosis* H37Rv strain has accelerated the study and validation of molecular targets aiming at the rational design of anti-TB drugs [23]. The target-based rational design of new agents with anti-TB activity includes functional and structural efforts. However, the first step to enzyme target validation must include experimental data demonstrating that a gene predicted by *in silico* analysis to encode a particular protein catalyzes the proposed chemical reaction. Moreover, it has recently been pointed out that recognition of the limitations of high-throughput screening approaches in the discovery of candidate drugs has rekindled interest in rational design methods [8]. Understanding the mode of action of *Mt*UMPK will inform us on how to better design inhibitors targeting this enzyme with potential therapeutic application in TB chemotherapy. Accordingly, it is hoped that the results here described may be useful to the rational design of anti-TB agents and that they may contribute to our understanding of the biology of *M. tuberculosis*.

References

[1] C. Dye, S. Scheele, P. Dolin, V. Pathania, M.C. Raviglione, J. Am. Med. Assoc. 282 (1999) 677–686.
[2] World Health Organization, Global Tuberculosis Control: A Short Update to the 2009 Report, 2010.
[3] W.W. Yew, C.C. Leung, Respirology 13 (2008) 21–46.
[4] A.A. Velayati, P. Farnia, M.R. Masjedi, T.A. Ibrahim, P. Tabarsi, R.Z. Haroun, H.O. Kuan, J. Ghanavi, P. Farnia, M. Varahram, Eur. Respir. J. 34 (2009) 1202–1203.
[5] R.G. Ducati, L.A. Basso, D.S. Santos, Curr. Drug Targets 8 (2007) 423–435.
[6] J.G. Robertson, Biochemistry 44 (2005) 5561–5571.
[7] J.G. Robertson, Curr. Opin. Struct. Biol. 17 (2007) 674–679.
[8] J.E. Ladbury, G.K. Klebe, E. Freire, Nat. Rev. Drug Discov. 9 (2010) 23–27.
[9] C. Meier, L.G. Carter, S. Sainsbury, E.J. Mancini, R.J. Owens, D.I. Stuart, R.M. Esnouf, J. Mol. Biol. 381 (2008) 1098–1105.
[10] G.E. Shambaugh, Am. J. Clin. Nutr. 32 (1979) 1290–1297.
[11] C. Marco-Marín, F. Gil-Ortiz, V. Rubio, J. Mol. Biol. 352 (2005) 438–454.
[12] H. Yan, M.D. Tsai, Adv. Enzymol. Relat. Areas Mol. Biol. 73 (1999) 103–134.
[13] P. Briozzo, C. Evrin, P. Meyer, L. Assairi, N. Joly, O. Barzu, A. Gilles, J. Biol. Chem. 280 (2005) 25533–25540.
[14] H.J. Müller-Dieckmann, G.E. Schulz, J. Mol. Biol. 236 (1994) 361–367.
[15] J. Liou, G.E. Dutschman, W. Lam, Z. Jiang, Y. Cheng, Cancer Res. 62 (2002) 1624–1631.
[16] K. Scheffzek, W. Kliche, L. Wiesmüller, J. Reinstein, Biochemistry 35 (1996) 9716–9727.
[17] L. Serina, C. Blondin, E. Krin, O. Sismeiro, A. Danchin, H. Sakamoto, A.M. Gilles, O. Bârzu, Biochemistry 34 (1995) 5066–5074.
[18] C. Gagyi, N. Bucurenci, O. Sîrbu, G. Labesse, M. Ionescu, A. Ofiteru, L. Assairi, S. Landais, A. Danchin, O. Bârzu, A. Gilles, Eur. J. Biochem. 270 (2003) 3196–3204.
[19] F. Fassy, O. Krebs, M. Lowinski, P. Ferrari, J. Winter, V. Collard-Dutilleul, Biochem. J. 384 (2004) 619–627.
[20] K.S. Jensen, E. Johansson, K.F. Jensen, Biochemistry 46 (2007) 2745–2757.
[21] L. Egeblad-Welin, M. Welin, L. Wang, S. Eriksson, FEBS J. 274 (2007) 6403–6414.
[22] K.A. Kantardjieff, C. Vasquez, P. Castro, N.M. Warfel, B.S. Rho, T. Lekin, C.Y. Kim, B.W. Segelke, T.C. Terwilliger, B. Rupp, Acta Crystallogr. D: Biol. Crystallogr. 61 (2005) 355–364.
[23] S.T. Cole, R. Brosch, J. Parkhill, T. Garnier, C. Churcher, D. Harris, S.V. Gordon, K. Eiglmeier, S. Gas, C.E. Barry, F. Tekaia, K. Badcock, D. Basham, D. Brown, T. Chillingworth, R. Connor, R. Davies, K. Devlin, T. Feltwell, S. Gentles, N. Hamlin, S. Holroyd, T. Hornsby, K. Jagels, A. Krogh, J. McLean, S. Moule, L. Murphy, K.

Oliver, J. Osborne, M.A. Quail, M.A. Rajandream, J. Rogers, S. Rutter, K. Seeger, J. Skelton, R. Squares, S. Squares, J.E. Sulston, K. Taylor, S. Whitehead, B.G. Barrell, Nature 393 (1998) 537–544.
[24] D. Robertson, P. Carroll, T. Parish, Tuberculosis 87 (2007) 450–458.
[25] K. Yamanaka, T. Ogura, H. Niki, S. Hiraga, J. Bacteriol. 174 (1992) 7517–7526.
[26] J.C. Smallshaw, R.A. Kelln, Genetics (Life Sci. Adv.) 11 (1992) 59–65.
[27] J. Sambrook, D.W. Russel, Molecular Cloning: A Laboratory Manual, Spring Harbor Laboratory Press, New York, 2001.
[28] U.K. Laemmli, Nature 227 (1970) 680–685.
[29] M.M. Bradford, Anal. Biochem. 72 (1976) 248–254.
[30] B. Monson de Souza, M.S. Palma, Biochim. Biophys. Acta 1778 (2008) 2797–2805.
[31] H. Chassaigne, R. Lobinski, Analyst 123 (1998) 2125–2130.
[32] D.A. Benson, I. Karsch-Mizrachi, D.J. Lipman, J. Ostell, E.W. Sayers, Nucleic Acids Res. 37 (2009) D26–D31.
[33] J.D. Thompson, D.G. Higgins, T.J. Gibson, Nucleic Acids Res. 22 (1994) 4673–4680.
[34] J.S. Oliveira, C.A. Pinto, L.A. Basso, D.S. Santos, Protein Expr. Purif. 22 (2001) 430–435.
[35] I. Segel, Enzyme Kinetics, Behavior and Analysis of Rapid Equilibrium and Steady-State Enzyme Systems, John Wiley and Sons, New York, 1975.
[36] R.A. Copeland, Evaluation of Enzyme Inhibitors in Drug Discovery, John Wiley and Sons, Inc., New Jersey, 2005.
[37] R.G. Bates, H.B. Hetzer, J. Phys. Chem. 65 (1961) 667–671.
[38] H. Fukada, K. Takahashi, Proteins 33 (1998) 159–166.
[39] M.C. Pinna, A. Salis, M. Monduzzi, B.W. Ninham, J. Phys. Chem. B 109 (2005) 5406–5408.
[40] Y. Zhang, P.S. Cremer, Curr. Opin. Chem. Biol. 10 (2006) 658–663.
[41] P. Meyer, C. Evrin, P. Briozzo, N. Joly, O. Bârzu, A. Gilles, J. Biol. Chem. 283 (2008) 36011–36018.
[42] L. Serina, N. Bucurenci, A.M. Gilles, W.K. Surewicz, H. Fabian, H.H. Mantsch, M. Takahashi, I. Petrescu, G. Batelier, O. Bârzu, Biochemistry 35 (1996) 7003–7011.
[43] C. Evrin, M. Straut, N. Slavova-Azmanova, N. Bucurenci, A. Onu, L. Assairi, M. Ionescu, N. Palibroda, O. Bârzu, A. Gilles, J. Biol. Chem. 282 (2007) 7242–7253.
[44] S.E. Lee, S.Y. Kim, C.M. Kim, M. Kim, Y.R. Kim, K. Jeong, H. Ryu, Y.S. Lee, S.S. Chung, H.E. Choy, J.H. Rhee, Infect. Immun. 75 (2007) 2795–2801.
[45] C. Thum, C.Z. Schneider, M.S. Palma, D.S. Santos, L.A. Basso, J. Bacteriol. 191 (2009) 2884–2887.
[46] N. Bucurenci, H. Sakamoto, P. Briozzo, N. Palibroda, L. Serina, R.S. Sarfati, G. Labesse, G. Briand, A. Danchin, O. Bărzu, A.M. Gilles, J. Biol. Chem. 271 (1996) 2856–2862.
[47] J. Monod, J. Wyman, J.P. Changeux, J. Mol. Biol. 12 (1965) 88–118.
[48] T.S. Balganesh, P.M. Alzari, S.T. Cole, Trends Pharmacol. Sci. 29 (2008) 576–581.

Please cite this article in press as: D.C. Rostirolla et al., Arch. Biochem. Biophys. (2010), doi:10.1016/j.abb.2010.10.019

Anexo D

Recombinant *Escherichia coli* GMP reductase: Kinetic, catalytic and chemical mechanisms, and thermodynamics of enzyme-ligand binary complex formation

Leonardo Krás Borges Martinelli, Rodrigo Gay Ducati, Leonardo Astolfi Rosado, Ardala Breda, Bruna Pelegrim, Diógenes Santiago Santos, Luiz Augusto Basso

Artigo submetido para a publicação – *Molecular Biosystems, 2011*.

RSC Publishing Molecular BioSystems

Recombinant Escherichia coli GMP reductase: kinetic, catalytic and chemical mechanisms, and thermodynamics of enzyme-ligand binary complex formation.

Journal:	*Molecular BioSystems*
Manuscript ID:	MB-ART-10-2010-000245.R1
Article Type:	Paper
Date Submitted by the Author:	09-Dec-2010

Complete List of Authors:	Martinelli, Leonardo; PUCRS, CPBMF Ducati, Rodrigo; PUCRS, CPBMF Rosado, Leonardo; PUCRS, CPBMF Breda, Ardala; PUCRS, CPBMF Selbach, Bruna; PUCRS, CPBMF Santos, Diogenes; PUCRS, CPBMF Basso, Luiz; Pontificia Universidade Católica do Rio Grande do Sul - PUCRS, Centro de Pesquisas em Biologia Molecular e Funcional - CPBMF

PONTIFÍCIA UNIVERSIDADE CATÓLICA DO RIO GRANDE DO SUL - PUCRS
INSTITUTO NACIONAL DE CIÊNCIA E TECNOLOGIA EM TUBERCULOSE – INCT-TB
CENTRO DE PESQUISAS EM BIOLOGIA MOLECULAR E FUNCIONAL – CPBMF

December 8th, 2010
Ms. ID: MB-ART-10-2010-000245

Ms Vikki Bean, BSc
Publishing Editor
MOLECULAR BIOSYSTEMS

Dear Ms. Vikki Bean,

Our manuscript entitled "**Recombinant *Escherichia coli* GMP reductase: kinetic, catalytic and chemical mechanisms, and thermodynamics of enzyme-ligand binary complex formation.**" by Martinelli *et al*. was recently reviewed for publication in **MOLECULAR BIOSYSTEMS** as Full Paper. We, the authors, were pleased that the comments of the reviewers were positive. In particular, reviewer #1 was of opinion that our manuscript "is an interesting study which potentially will have a noticeable impact to the field", and reviewer #2 found that "this is an interesting study which potentially will have a noticeable impact to the field." However, the reviewers raised a number of issues that should be addressed for a revised version of our manuscript to be considered for publication in **MOLECULAR BIOSYSTEMS**. We were also pleased that you offered us an opportunity to deal with the issues raised by the reviewers. We have thus made a number of changes to our manuscript in response to the comments and suggestions made by the reviewers. Our responses to the issues raised by the reviewers and changes made to our manuscript are as follows:

Reviewer #1

Issue 1: "In the experiments of determination of apparent steady-state kinetic constants and initial velocity pattern (Fig 3), it need more concentration of GMP or NADPH."

Response: The accuracy of values estimated for steady-state kinetic parameters (K_M and V_{max}) depends on the range of substrate concentrations over which the initial velocity has been determined. Enzymologists usually make efforts to measure initial velocities using substrate concentrations from $0.25K_M$ to $5.0K_M$. However, there may be practical limits on the range of substrate concentrations over which these measurements can be performed. At low substrate concentrations, for small values of velocity (v) small errors in v lead to enormous error in $1/v$ in the double-reciprocal (or Lineweaver-Brurk) plot. On the other hand, for large values of v the same small errors in v lead to barely noticeable errors in $1/v$. However, the double-reciprocal plot is by far the most widely used in enzyme kinetics and there is a large body of data and graphical interpretation that can be used for comparisons. In addition, for an enzyme system that obeys the Michaelis-Menten equation, the advantage of including substrate concentrations values much higher than K_M is very slight and may well be outweighed by the added cost in materials. In any case, the K_M and V_{MAX} (k_{cat}) for both GMP and NADPH were determined in the experiments of apparent steady-state kinetics and initial velocity patterns using saturating substrate concentrations and at least one point below the K_M values for both substrates in every curve. Accordingly, we are of opinion that the data presented are reliable and more initial velocity measurements will neither change the interpretation nor increase accuracy of data.

Issue 2: "Mean square error should be presented in all the figure if possible".

Response: As requested, we added mean square errors to the following figures:
Figure 8: Temperature dependence of log k_{cat}
Figure 9: Primary deuterium kinetic isotope effects
Figure 10: Solvent isotope effects
Figure 11: Multiple kinetic isotope effects

Adding mean square errors to figures 1, 2, 4, 5, 6, 12 and 13 are not needed. We haven't added mean square errors to figure 3 because it would become somewhat "crowded". In addition, adding mean square errors to pH-rate profiles (figure 7) is not a common practice among enzymologists. At any rate, we have added mean square errors to all figures we deemed appropriate.

Issue 3: "It would help to understand the mechanism more easily if the incorporation of GMP and NADPH, and release of IMP and NADP+ was added in figure 11".

Avenida Ipiranga 6681, Tecnopuc, Prédio 92A
Tel/Fax: +55-51-33203629
Cep 90619-900, Porto Alegre,RS, Brasil

PONTIFÍCIA UNIVERSIDADE CATÓLICA DO RIO GRANDE DO SUL - PUCRS
INSTITUTO NACIONAL DE CIÊNCIA E TECNOLOGIA EM TUBERCULOSE – INCT-TB
CENTRO DE PESQUISAS EM BIOLOGIA MOLECULAR E FUNCIONAL – CPBMF

Response: Indeed. We have changed figure 13 (figure 11 of the previous version of our MS) so that it now shows GMP and NADPH sequential binding and sequential release of NADP and IMP products. We would like to thank this reviewer for bringing it to our attention.

Reviewer #2

Issue 1: "Since the main focus of this article is on the mechanism of GMPR it is not necessary to discuss the (standard) procedure used to purify E.c. GMPR or make it part of the results section (Moving it into the Materials and Methods will improve readability)."

Response: Indeed, we agree that discussing the standard purification method is not the main focus of the article and will not add much to the discussion. Accordingly, as requested, we have moved part of the discussion on the procedures used to purify *E. coli* GMP reductase to the Materials and Methods section (pages 28 and 29; "Purification of recombinant GMP reductase"). We have also transferred part of the discussion on the procedures used to purify recombinant *E. coli* GMP reductase to the Results section. In the previous version of our manuscript, we had two sections entitled: "**Expression of recombinant GMP reductase**" and "**Purification of recombinant GMP reductase**". These two section have been combined in the current version of our manuscript, and it is now entitled (Results section, page 5): "**Expression and purification of recombinant GMP reductase**". In the Discussion section (**Expression and purification of recombinant GMP reductase**; pages 13 and 14), we have kept the discussion on recombinant protein expression in the absence of IPTG induction as it is a surprising result that deserves due attention. Comments on the protein purification protocol was reduced just to the following sentence (page 14): "The recombinant *E. coli* GMP reductase was purified to homogeneity by a three-step purification protocol using standard anionic exchange and size exclusion columns."

Issue 2: "Including an ITC titration figure would be extremely beneficial"

Response: Indeed. A figure showing the ITC data for all four ligands (Figure 4) has been added to the current version of our manuscript. The legend of Figure 4 is as follows (page 46): "**Figure 4:** Isothermal titration calorimetry (ITC) analysis of *E. coli* GMP reductase titration with GMP (a), NADPH (b), IMP (c), and $NADP^+$ (d). The top panels show raw data of the heat pulses resulting from titration of *E. coli* GMP reductase. The bottom panels show the integrated heat pulses, normalized per mol of injectant as a function of the molar ratio (ligand concentration/*E. coli* GMP reductase concentration). These binding curves were best fitted to a sequential binding sites model equation."

Issue 3: "Figure legends need to be more descriptive in order to allow the reader to understand the figures (in particular Fig 10)".

Response: We are of opinion that the legends of figures 1 (chemical reaction), 2 (SDS-PAGE), 3 (double-reciprocal plots), 4 (ITC data), 5 (multiple sequence alignment), 6 (structural model), 9 (primary deuterium kinetic isotope effects), 11 (multiple kinetic isotope effects), and 12 (proposed chemical mechanism) are give appropriate description of data being shown. Notwithstanding, as suggested, the following figure legends were modified to be more descriptive:
- Figure 7 (it corresponds to figure 5 of the previous version of our MS): "Dependence of kinetic parameters on pH. (a) pH dependence of log k_{cat} data were fitted to Eq. 3; (b) log k_{cat}/K_{GMP} data were fitted to Eq. 4; (c) pH dependence of log k_{cat}/K_{NADPH} data was fitted to Eq. 5."
- Figure 8 (it corresponds to figure 6 of the previous version of our MS): "Temperature dependence of log k_{cat}. Saturating concentrations of NADPH and GMP substrates were employed to measure the maximum velocity as a function of temperature ranging from 15 to 35 °C. The data were fitted to Eq. 6. The linearity of the Arrhenius plot suggests that there is no change in the rate-limiting step over the temperature range utilized in the assay."
- Figure 10 (it corresponds to figure 8 of the previous version of our MS): "Solvent isotope effects for GMP reductase. (a) NADPH was used as the variable substrate (4 – 60 μM), with a saturating concentration of GMP (100 μM). (b) GMP was used as the variable substrate (4 – 60 μM), with a saturating concentration of NADPH (100 μM). Both reactions mix contained either 0 (●) or 90 (■) atom % D_2O. The inset of (b) represents the proton inventory (0, 20, 40, 60, and 90 atom % D_2O) measuring GMP reductase enzyme activity with both substrates at saturating concentrations (100 μM)."

Avenida Ipiranga 6681, Tecnopuc, Prédio 92A
Tel/Fax: +55-51-33203629
Cep 90619-900, Porto Alegre,RS, Brasil

PONTIFÍCIA UNIVERSIDADE CATÓLICA DO RIO GRANDE DO SUL - PUCRS
INSTITUTO NACIONAL DE CIÊNCIA E TECNOLOGIA EM TUBERCULOSE – INCT-TB
CENTRO DE PESQUISAS EM BIOLOGIA MOLECULAR E FUNCIONAL – CPBMF

- Figure 12 (it corresponds to figure 10 of the previous version of our MS): Representative stopped-flow trace for product formation, measuring the decrease in absorbance at 340 nm upon conversion of NADPH to $NADP^+$catalyzed by 10 μM of recombinant *E. coli* GMP reductase (mixing chamber concentration). The data were fitted to Eq. 10 for a single exponential decay, yielding a value of 0.204 s^{-1} for the apparent first-order constant of product formation.

Issue 4: "Include a structural model of the E.c. GMPR to illustrate the role of discussed amino acid residues based on the available human protein (discussed in the manuscript)".

Response: Indeed. We have added a structural model of *E. coli* GMP reductase (Figure 6) as suggested by this reviewer. We would like to thank the reviewer for raising this particular issue because it has added relevant data to our manuscript that should be useful to the readership of Molecular BioSystems, in case our manuscript is found appropriate for publication in this journal. The Figure 6 legend is as follows:

- "*E. coli* GMPR model superimposed on experimentally solved human type 2 GMPR (hGMPR2) structure. Amino acid residues involved in GMP binding and the GMP molecule are shown as sticks. Template corresponding amino acids are depicted as thin gray sticks. *E. coli* amino acids numbering are depict and amino acid replacement at position 288 is shown in italics (template). H-bonds are shown as dotted lines."

The following sentences were added to the "Results" section ("Multiple sequence alignment and *E. coli* GMPR structural analysis"; pages 9-10):

"The three-dimensional model of *E. coli* GMPR indicates high conservation of its tertiary structure as compared to hGMPR2 structural template, with RMSD value of 0.61 Å, which is in agreement with the 68 % identity at the amino acid level. The model presented no stereochemical parameters violation, as evaluated by PROCHECK package (data not shown), in which 99.2 % of *E. coli* GMP reductase amino acids are within allowed regions of the Ramachandran plot. Amino acids involved in GMP binding are almost all conserved in the bacterial homologue (Fig. 5). In addition, there are minor conformational deviations even for the conserved amino acid residues (Fig. 6). H-bond network of side chains and main chains of these amino acid residues to bound GMP is maintained in both human and *E. coli* GMP reductases. A noticeable exception is Gly290 amino acid residue that is displaced by 1.3 Å away from substrate binding site in *E. coli* GMP reductase (Fig. 6). Therefore, there is no H-bond between Gly290 and GMP O6 atom since its distance raised from 3.12 Å in the template to 4.4 Å in *E. coli* GMP reductase. The hGMPR2 template structure indicates that the conserved Asp219 residue makes two H-bonds between its carboxyl oxygen atoms and O2'and O3' atoms of the GMP ribose moiety. However, our proposed model showed just one H-bond to O2' atom of GMP. Although Glu289 *E. coli* GMP reductase substitutes for Ser288 in hGMPR2, there is either no gain or loss of H-bonds between the amino acid side chain at this position and GMP. The H-bond between N1 of guanine moiety of GMP and the main chain oxygen atom of Glu289 in *E. coli* GMP reductase replaces the same interaction made between the main chain oxygen atom of Ser288 in hGMPR2. The catalytic Cys186 residue that likely plays a critical role in *E. coli* GMP reductase catalysis makes an H-bond to C2 exocyclic amino group of the guanine moiety of GMP (Fig. 6). Another H-bond is made between Thr188 side chain and the C2 exocyclic amino group of GMP (Fig. 6). Interestingly, according to the PDB coordinates of hGMPR2, there is only one H-bond that is made between Thr188 side chain and the C2 exocyclic amino group of GMP, and Cys186 side chain is H-bonded to Thr188."

The sentences below were thus included in the current version of our manuscript in "Experimental Procedures" section ("*E. coli* GMP reductase comparative homology modeling"; page 27):

"*E. coli* three-dimensional model was built by comparative homology modeling using human type 2 GMP reductase structure as template (PDB ID: 2A7R; hGMPR2)[16], solved by X-ray crystallography at 3.0 Å in complex with GMP. Template structure was used for *E. coli* GMP reductase modeling, as well as to evaluate GMP binding mode to bacterial enzyme active site. Template selection was based on high primary sequence conservation (68.5% identity and 16.47% strong similarity), and presence of enzyme substrate bound to its active site. Target and template pair-wise sequence alignment required a single gap inclusion in human GMP reductase primary sequences. *E. coli* GMP reductase model was built by restrained-based homology modeling implemented in MODELLER9v1[47], with the standard protocol of the comparative protein structure modeling methodology, by satisfaction of spatial restrains[48,49]. Atomic coordinates of GMP heteroatoms were copied from template structure

PONTIFÍCIA UNIVERSIDADE CATÓLICA DO RIO GRANDE DO SUL - PUCRS
INSTITUTO NACIONAL DE CIÊNCIA E TECNOLOGIA EM TUBERCULOSE – INCT-TB
CENTRO DE PESQUISAS EM BIOLOGIA MOLECULAR E FUNCIONAL – CPBMF

into the *E. coli* GMP reductase model. The best model was selected according to MODELLER objective function[50] and subjected to energy minimization for amino acid side chain and main chain rearrangements with GROMACS package[51] using the 43a1 force-field. The system was submitted to an initial steepest descent energy minimization in vacuum with a maximum number of 400 minimization steps, followed by a maximum of 3000 steps of conjugate gradient energy minimization. The program PROCHECK[52] was employed to analyze the stereochemical quality of the model, as previously described [53]. Structural correspondence between *E. coli* model and human GMP reductase template was evaluated by their root-mean square deviation (RMSD). H-bond interactions were evaluated with LIGPLOT v4.4.2[54], considering an atomic distance cut off of 3.9 Å (program default values). Images were generated with PyMOL Molecular Graphic System V1.3 (Schrödinger, LLC)."

The following references were also added to the current version of our MS (page 42):
"47 A. Sali and T. L. Blundell. *Journal of Molecular Biology*, 1993, **234**, 779-815.
48 M. A. Martí-Renom, A. C. Stuart, A. Fiser, R. Sánchez, F. Melo and A. Sali. *Annu Review Biophysics and Biomolecular Structures*, 2000, **29**, 291-325.
49 A. Sali and J. P. Overington. *Protein Science*, 1994, **3**, 1582-1596.
50 M. Y. Shen and A. Sali. *Protein Science*, 2006, **15**, 2507-2524.
51 D. van der Spoel, E. Lindahl, B. Hess, G. Groenhof, A. E. Mark and H. J. C. Berendsen. *Journal of Computational Chemistry*, 2005, **26**, 1701-1718.
52 R. A. Laskowski, M. W. MacArthur, D. S. Moss and J. M. Thornton. *Journal of Applied Crystallography*, 1993, **26**, 283-291.
53 I. O. Fonseca, R. G. Silva, C. L. Fernandes, O. N. de Souza, L. A. Basso and D. S. Santos. *Archives of Biochemistry and Biophysics*, 2007, **457**, 123-133.
54 A. C. Wallace, R. A. Laskowski and J. M. Thornton. *Protein Engineering*, 1995, **8**, 127-134."

As appropriate, references were re-numbered and cited sequentially in the text.

Issue 5: "Replace Fig 11 with a model of GMPR mechanism (e.g. hydride transfer) derived from the reported data".

Response: This issue has been dealt with in response to issue #3 raised by reviewer #1. We deemed more appropriate to follow the suggestion made by reviewer #1 (issue #3) because site-directed mutagenesis results are currently being carried out in our research group to provide support for the amino acid residues suggested by the pH-rate profiles to be involved in catalysis/binding. In addition, a figure showing hydride transfer and a single proton solvent transfer involved in catalysis wouldn't add much to Molecular BioSystems readership because we still lack experimental data to demonstrate the involvement of GMP reductase amino acid side chains in, for instance, stabilization of an intermediate. We believe that the data presented in our MS provide solid support to the proposed *E. coli* GMP reductase enzyme mechanism. Although these same data suggest the catalytic and chemical mechanisms, we are of opinion that further experimental data should be provide (site-directed mutagenesis, measurements of activity of mutant enzymes, measurements of substrate binding to mutant enzymes, crystal structure or molecular model of mutants, etc).

Issue 6: "Avoiding the repeated use of phrases such as "it was pointed out" to start sentences will significantly increase the readability of the manuscript".

Response: Indeed. We thus avoided the repeated use of any phrase in the paper and all half sentences were corrected along with the typos.

Issue 7: "Provide a more detailed description of the equations used (and their respective justification)".

Response: We believe to have offered the readers not only detailed descriptions of the equations used to analyse the data presented in our manuscript, but also their justifications and relevant citations in the "Experimental Procedures" section (Data Analysis; pages 35-38). We hope you agree that giving a more detailed description of the equations in either the "Results" or "Discussion" section would be redundant and not improve readability of the paper.

Issue 8: "Naming of constants and variables needs to be consistent (e.g. in the current manuscript Ka is used to describe an equilibrium binding constant as well as the acid dissociation constant)".

Avenida Ipiranga 6681, Tecnopuc, Prédio 92A
Tel/Fax: +55-51-33203629
Cep 90619-900, Porto Alegre,RS, Brasil

PONTIFÍCIA UNIVERSIDADE CATÓLICA DO RIO GRANDE DO SUL - PUCRS
INSTITUTO NACIONAL DE CIÊNCIA E TECNOLOGIA EM TUBERCULOSE – INCT-TB
CENTRO DE PESQUISAS EM BIOLOGIA MOLECULAR E FUNCIONAL – CPBMF

Response: We have replaced "…association constant (K_a)…" with "…equilibrium binding constant (K_{eq})…" whenever ITC data were presented or analysed: Page 9 ("Results" section) and Page 39 ("Experimental Procedures" section). The term "…association constant (K_a)…" was reserved to describe the acid dissociation constant in pH-rate profiles.

Reviewer #3

Issue 1: "Procedure of the E. coli GMPR purification should be moved to the Materials and Methods section".

Response: This issue has been addressed in response to issue #1 raised by reviewer #2.

Issue 2: "Equations should be explained, described and discussed in the main text of the manuscript rather than in the materials and methods".

Response: This issue has been dealt with in response to issue #7 raised by reviewer #2.

Issue 3: "A figure with the *E. coli* GMPR structure is needed".

Response: This issue has been dealt with in response to issue #4 raised by reviewer #2.

Issue 4: "A figure with the ITC data should be added".

Response: This issue has been dealt with in response to issue #2 raised by reviewer #2.

I have included Ardala Breda as co-author of our manuscript because she did the *E. coli* GMP reductase *in silico* model and helped interpret pH-rate profiles in light of the proposed structural model. As new references have been added to the current version of our manuscript, they have been renumbered accordingly. As two new figures were added to the current version of our MS: Figure 4 (ITC data) and Figure 6 (*E. coli* GMP reductase structural model), figures were re-numbered accordingly (except figures 1, 2 and 3).

We thank the reviewers' valuable comments and suggestions that, we believe, have improved the current version of our manuscript. We would also like to thank you for having given us an opportunity to address the reviewers' comments. We hope that you are of opinion that we have properly addressed the issues raised by the reviewers and that the revised version of our manuscript is worthy of publication in MOLECULAR BIOSYSTEMS.

Sincerely,

Luiz A. Basso, Ph.D.

Avenida Ipiranga 6681, Tecnopuc, Prédio 92A
Tel/Fax: +55-51-33203629
Cep 90619-900, Porto Alegre,RS, Brasil

Recombinant *Escherichia coli* GMP reductase: kinetic, catalytic and chemical mechanisms, and thermodynamics of enzyme-ligand binary complex formation.

Leonardo Krás Borges Martinelli[1,2], Rodrigo Gay Ducati[1], Leonardo Astolfi Rosado[1,3], Ardala Breda[1,2], Bruna Pelegrim Selbach[1,2], Diógenes Santiago Santos[1,2*], Luiz Augusto Basso[1,2*]

[1]Centro de Pesquisas em Biologia Molecular e Funcional (CPBMF), Instituto Nacional de Ciência e Tecnologia em Tuberculose (INCT-TB), Pontifícia Universidade Católica do Rio Grande do Sul (PUCRS), 6681/92-A Av. Ipiranga, 90619-900, Porto Alegre, RS, Brazil.

[2]Programa de Pós-Graduação em Biologia Celular e Molecular, Pontifícia Universidade Católica do Rio Grande do Sul (PUCRS), Porto Alegre, RS, Brazil.

[3]Programa de Pós-Graduação em Medicina e Ciências da Saúde, Pontifícia Universidade Católica do Rio Grande do Sul (PUCRS), Porto Alegre, RS, Brazil.

[*]Corresponding authors. Telephone/Fax: +55-51-33203629.

E-mail addresses: luiz.basso@pucrs.br (Luiz A. Basso); diogenes@pucrs.br (Diógenes S. Santos).

Running title: Mode of action of recombinant of *E. coli* GMP reductase

Summary

Guanosine monophosphate (GMP) reductase catalyzes the reductive deamination of GMP to inosine monophosphate (IMP). GMP reductase plays an important role in the conversion of nucleoside and nucleotide derivatives of guanine to adenine nucleotides. In addition, as a member of the purine salvage pathway, it also participates in the reutilization of free intracellular bases. Here we present cloning, expression and purification of *Escherichia coli guaC*-encoded GMP reductase to determine its kinetic mechanism, as well as chemical and thermodynamic features of this reaction. Initial velocity studies and isothermal titration calorimetry demonstrated that GMP reductase follows an ordered bi-bi kinetic mechanism, in which GMP binds first to the enzyme followed by NADPH binding, and $NADP^+$ dissociates first followed by IMP release. The isothermal titration calorimetry also showed that GMP and IMP binding are thermodynamically favorable processes. The pH-rate profiles showed groups with apparent p*K* values of 6.6 and 9.6 involved in catalysis, and p*K* values of 7.1 and 8.6 important to GMP binding, and a p*K* value of 6.4 important for NADPH binding. Primary deuterium kinetic isotope effects demonstrated that hydride transfer contributes to the rate-limiting step, whereas solvent kinetic isotope effects arise from a single protonic site that plays a modest role in catalysis. Multiple isotope effects suggest that protonation and hydride transfer steps take place in the same transition state, lending support to a concerted mechanism. Pre-steady-state kinetic data suggest that product release does not contribute to the rate-limiting step of the reaction catalyzed by *E. coli* GMP reductase.

Keywords: GMP reductase; initial velocity; isothermal titration calorimetry; pH-rate profile; kinetic isotope effects; kinetic mechanism.

Introduction

Purine nucleoside and nucleotide biosynthesis is a fundamental and well-established pathway in the metabolism of avian, mammalian and microbial cells.[1] Guanosine monophosphate (GMP) reductase (NADPH:GMP oxidoreductase; EC 1.6.6.8) catalyzes the reductive deamination of GMP to inosine monophosphate (IMP)[2] (Fig 1). GMP reductase plays an important role in the conversion of nucleoside and nucleotide derivatives of guanine (Gua) to adenine (Ade) nucleotides, and in the maintenance of the intracellular balance between Gua and Ade nucleotides.[3] As part of the purine salvage pathway, it also participates in the reutilization of free intracellular bases.[2] In *Escherichia coli*, the *guaC*-encoded GMP reductase is induced by GMP,[4] and is also regulated by cyclic adenosine monophosphate (cAMP),[5] by the intracellular ratio of purine nucleotides, and by glutamine and its analogs.[6] In addition to its role as an enzyme for the interconversion of purine nucleotides, GMP reductase provides a nitrogen source via its deamination activity.[6] In addition, it is inhibited by adenosine triphosphate (ATP) and is reactivated by the presence of guanosine triphosphate (GTP).[3] GMP reductase is not normally necessary for efficient bacterial growth, since the lack of its activity leaves the *de novo* synthesis of purine nucleotides via IMP intact.[4] However, when the route of IMP is blocked, GMP reductase activity becomes necessary to provide AMP when Gua and its derivatives are the purine sources.[7] In purine auxotrophs mutants that are blocked prior to the formation of IMP, *guaC* mutations prevent the use of Gua or xanthine derivatives as sources of purine.[3]

GMP reductases have been found and characterized in a number of organisms, including *E. coli*,[3] *Salmonella typhimurium*,[6] *Artemia salina*,[8] *Leishmania donavani*,[9] and *Homo sapiens*.[10] The human homologue is responsible for the only known

metabolic step by which Gua nucleotides can be converted to the pivotal precursor of both Ade and Gua nucleotides.[11] Human deficiency of this enzyme has not been related to any known disease, which can be explained by several possibilities, the main one being that the lack of this enzyme is invariably lethal.[12] Human GMP reductase has been identified as two isoenzymes, hGMPR1[11] and hGMPR2[2] (the second, being shown to promote monocytic differentiation of HL-60 leukemia cells[13]). Salvatore and co-workers[14] studied the role of GMP reductase in non-shivering thermogenesis, a process required for the survival of rodents during cold stress, and determined that the enzyme plays a critical role in this process, evidenced by significant increases in its expression during cold exposure. GMP reductases have been shown to be involved in various biological functions, including maintenance of the balance of purine nucleotides,[3] as a possible target for antileishmanial[9] and anticancer drugs[15], and involvement in human cell differentiation.[13] Moreover, GMP reductases are similar across the species at the amino acid level.[16] Accordingly, the need to further investigate *E. coli* GMP reductase to elucidate the kinetic, catalytic and chemical mechanisms to provide a basis on which to design species-specific inhibitors is warranted. Understanding the mode of action of *E. coli* GMP reductase may also be useful to chemical biologists interested in designing function-based chemical compounds to elucidate the biological role of this enzyme in the context of whole *E. coli* cells. In addition, availability of recombinant *E. coli* GMP reductase may provide a tool for determination of substrate specificity of cyclic nucleotide phosphodiesterases (PDEs).

Results

Amplification and cloning of the *E. coli guaC* gene

A PCR amplification product consistent with the expected size for the *E. coli guaC* (1038 bp) coding sequence was detected by agarose gel electrophoresis (data not shown), purified, and cloned into pCR-Blunt vector. The cloned sequence was extracted from the cloning vector, purified and subcloned into pET-23a(+) expression vector. DNA sequence identity of the fragment cloned in the expression vector was confirmed by enzyme restriction analysis and automated DNA sequencing.

Expression and purification of recombinant GMP reductase

The recombinant pET-23a(+)::*guaC* plasmid was transformed into *E. coli* BL21(DE3) host cells by electroporation. Sodium dodecyl sulfate-polyacrylamide gel electrophoresis (SDS-PAGE) analysis revealed expression of a protein in the soluble fraction with an apparent subunit molecular mass of ~38 kDa, consistent with *E. coli* GMP reductase (37,383.6 Da). The expression of the recombinant protein was monitored at different periods of cell growth after an $OD_{600\ nm}$ value of approximately 0.4 - 0.6 was reached. The best result was achieved at 24 h of cell growth at 37 °C in LB medium without isopropyl-β-D-thio-galactopyranoside (IPTG) induction (data not shown). Recombinant GMP reductase was efficiently purified to homogeneity (Fig 2) by a three-step purification protocol yielding 45 mg of homogeneous recombinant GMP reductase from 2.8 g of cells (Table 1). Homogeneous enzyme was stored at –80 °C with no loss of activity.

Table 1: Purification protocol of recombinant *E. coli* GMP reductase (2.8 g wet cell paste).

Purification Step	*Total protein (mg)*	*Total enzyme activity (U)*	*Specific activity (U mg^{-1})*	*Purification fold*	*Yield (%)*
Crude extract	210	89	0.47	1.0	100
Q-Sepharose FF	81	68	0.84	2	76
Sephacryl S-200	47	20	0.44	1.1	23
Mono-Q	45	30	0.66	1.6	34

Quaternary structure analysis of *E. coli* GMP reductase

The subunit molecular mass of *E. coli* GMP reductase was determined as 37,382 Da by electrospray ionization mass spectrometry (ESI-MS) and suggests that there was no removal of the N-terminal methionine residue (theoretical molecular mass of 37,383.6 Da). Amino acid sequencing of *E. coli* GMP reductase confirmed approximately 85 % of the sequence.

The protein native molecular mass was determined by gel filtration chromatography and revealed a single peak with elution volume consistent with a molecular mass of 155.98 kDa (data not shown), indicating that *E. coli* GMP reductase is a tetramer in solution.

Determination of apparent steady-state kinetic constants and initial velocity pattern

The determination of the apparent steady-state kinetic constants were performed using either GMP or NADPH as the variable substrate, and the data were fitted to Eq. 1 (hyperbolic equation), which indicates that the GMP reductase catalyzed reaction follows Michaelis-Menten kinetics.[17] The apparent K_M and V_{max} values for GMP (at 100 μM NADPH fixed concentration) were, respectively, 6.9 (± 0.3) μM and 0.065 (± 0.001) U mg^{-1}; and the apparent K_M and V_{max} values for NADPH (at 100 μM GMP

fixed concentration) were, respectively, 11.1 (± 1.2) μM and 0.40 (± 0.01) U mg^{-1}. No *E. coli* GMP reductase activity could be detected for varying NADH concentrations (up to 200 μM) in the presence of saturating concentration of GMP. In addition, no enzymatic activity could be detected when, in the presence of saturating levels of NADPH, varying AMP concentrations (up to 1000 μM) was substituted for GMP.

To both determine the true steady-state kinetic parameters and GMP reductase enzyme mechanism, initial velocity as a function of substrate concentration (either GMP or NADPH) was plotted as a linear function of reciprocal of initial velocity against the reciprocal of substrate concentration (double-reciprocal or Lineweaver-Burk plot). The double-reciprocal plots showed a family of lines intersecting to the left of the *y*-axis (Fig 3), which is consistent with ternary complex formation and a sequential mechanism. Data were plotted in reciprocal form and fitted to the equation for a sequential initial velocity pattern (Eq. 2), yielding the following values for the true steady-state kinetic parameters: k_{cat} = 0.28 (± 0.02) s^{-1}, K_{GMP} = 5.5 (± 1.0) μM, K_{NADPH} = 14.7 (± 2.5) μM, k_{cat}/K_{GMP} = 5.1 (± 0.9) x 10^4 $M^{-1}s^{-1}$, and k_{cat}/K_{NADPH} = 1.9 (± 0.3) x 10^4 $M^{-1}s^{-1}$.

Isothermal titration calorimetry (ITC)

Isothermal titration calorimetry (ITC) experiments were carried out to both determine the relative affinities of substrate(s)/product(s) binding to *E. coli* GMP reductase and provide support for the proposed enzyme mechanism. ITC measurements of ligand equilibrium binding to the enzyme followed the amount of heat generated or consumed upon formation of the binary complex, at constant temperature and pressure. The measure of heat released (exothermic process) upon binding of a ligand provides the binding enthalpy (ΔH) of the process, an estimate for the stoichiometry of the

interaction (n) and the equilibrium binding constant (K_{eq}). These values allow the Gibbs free energy (ΔG) and the entropy (ΔS) of the process to be calculated.

The ITC data for binding of ligands to *E. coli* GMP reductase are summarized in Table 2. The ITC results showed significant heat changes upon binding of GMP to free *E. coli* GMP reductase enzyme (Fig 4a), and data fitting to the sequential binding sites model yielded a value of 4 for n, consistent with the quaternary structure determined by gel filtration. This model provides values of ΔH, ΔS, K_{eq} for the binding sites of each subunit. The binding of IMP to the free enzyme also showed significant heat changes (Fig 4c), and the best fit was also to the sequential binding sites model yielding an n value of 4. No heat change upon the addition of either NADPH or $NADP^+$ to *E. coli* GMP reductase could be detected, suggesting that neither ligand can bind to free enzyme (Fig 4b and Fig 4d).

Table 2: ITC measurements of either GMP or IMP binding to *E. coli* GMP reductase. ΔG = Gibbs free energy changes; ΔS = Entropy changes; ΔH = Enthalpy changes; K_d = Dissociation constants.

GMP				
	Subunit 1	**Subunit 2**	**Subunit 3**	**Subunit 4**
ΔG (kcal. mol^{-1})	-5.5	-6.6	-6.2	-5.1
ΔS (cal.mol^{-1}deg^{-1})	-35.1	133	-53	-4.06
ΔH (cal.mol^{-1})	-1.6 x 10^4	3.3 x 10^4	-2.2 x 10^4	-6.3 x 10^3
K_d (µM)	82.6	49.7	14.8	159.7
IMP				
	Subunit 1	**Subunit 2**	**Subunit 3**	**Subunit 4**
ΔG (kcal. mol^{-1})	-5.6	-5.3	-6.9	-6.2
ΔS (cal.mol^{-1}deg^{-1})	-22.5	99.7	-115	-5.36
ΔH (cal.mol^{-1})	-1.2 x 10^4	2.4 x 10^4	-1.04 x 10^4	-7.8 x 10^3
K_d (µM)	60.9	142.2	7.8	25.7

Multiple sequence alignment and *E. coli* GMPR structural analysis

Sequence alignment of GMP reductases from *E. coli* strain K12 (GMPR NC_010473.1) and both human isoforms (hGMPR1 NP_006868.3 and hGMPR2 NP_001002000.1) was performed using the CLUSTALW program.[18] The sequence alignment reveals that the homologues present high similarity (Fig 5). At the amino acid level, *E. coli* GMP reductase is 65 % identical with hGMPR1 and 68 % identical with hGMPR2. The proposed catalytic site loop that acts as a lid that closes upon GMP binding is comprised by the conserved residues 179-187[16] (Fig 5). Based on structural comparison and model building for hGMPR2, it has been suggested that the amino acid residues 129-133 are involved in NADPH binding.[16] These residues are all conserved in *E. coli* GMP reductase (Fig 5). In addition, the residues involved in GMP binding, which are located in a flexible binding region of hGMPRs,[16] are all conserved in *E. coli* GMP reductase (residues 268-290). Moreover, the N7 of the guanine moiety of GMP makes hydrogen bonds with Met269 and the O6 atom with Ser270 and Gly290, which are all conserved (Fig 5). It has been shown for hGMPR1 that Ser288 makes hydrogen bonds with N1 and N2 atoms of guanine base.[16] However, this residue is not conserved in *E. coli* GMP reductase, being replaced by Ala288 (Fig 5). Amino acid residues involved in interactions with the ribose (Asp219 and Arg286) and phosphate (Ser184, Gly221, Gly242, and Gly243) moieties of GMP are all conserved. A disulfide bond between Cys68 and Cys95 side chains has been observed in the crystal structure of hGMPR2, and it has been proposed that it may play a role in stabilization of the tetramer. Interestingly, there are no corresponding residues in *E. coli* GMP reductase indicating that such disulfide bridge plays no part in stabilization of the tetramer.

The three-dimensional model of *E. coli* GMPR indicates high conservation of its tertiary structure as compared to hGMPR2 structural template, with RMSD value of

0.61 Å, which is in agreement with the 68 % identity at the amino acid level. The model presented no stereochemical parameters violation, as evaluated by PROCHECK package (data not shown), in which 99.2 % of *E. coli* GMP reductase amino acids are within allowed regions of the Ramachandran plot. Amino acids involved in GMP binding are almost all conserved in the bacterial homologue (Fig. 5). In addition, there are minor conformational deviations even for the conserved amino acid residues (Fig. 6). H-bond network of side chains and main chains of these amino acid residues to bound GMP is maintained in both human and *E. coli* GMP reductases. A noticeable exception is Gly290 amino acid residue that is displaced by 1.3 Å away from substrate binding site in *E. coli* GMP reductase (Fig. 6). Therefore, there is no H-bond between Gly290 and GMP O6 atom since its distance raised from 3.12 Å in the template to 4.4 Å in *E. coli* GMP reductase. The hGMPR2 template structure indicates that the conserved Asp219 residue makes two H-bonds between its carboxyl oxygen atoms and O2'and O3' atoms of the GMP ribose moiety. However, our proposed model showed just one H-bond to O2' atom of GMP. Although Glu289 *E. coli* GMP reductase substitutes for Ser288 in hGMPR2, there is either no gain or loss of H-bonds between the amino acid side chain at this position and GMP. The H-bond between N1 of guanine moiety of GMP and the main chain oxygen atom of Glu289 in *E. coli* GMP reductase replaces the same interaction made between the main chain oxygen atom of Ser288 in hGMPR2. The catalytic Cys186 residue that likely plays a critical role in *E. coli* GMP reductase catalysis makes an H-bond to C2 exocyclic amino group of the guanine moiety of GMP (Fig. 6). Another H-bond is made between Thr188 side chain and the C2 exocyclic amino group of GMP (Fig. 6). Interestingly, according to the PDB coordinates of hGMPR2, there is only one H-bond that is made between Thr188 side chain and the C2 exocyclic amino group of GMP, and Cys186 side chain is H-bonded to Thr188.

pH-rate profiles

To probe for acid-base catalysis, pH dependence studies of k_{cat}, and k_{cat}/K_M for GMP and NADPH were performed. The the pH-rate profiles are shown in Fig 7. The bell-shaped pH-rate data for k_{cat} were fitted to Eq. 3, yielding apparent pK values of 6.6 (± 0.6) and 9.6 (± 1.2) (Fig 7a), with slopes of +1 for the acidic limb and -1 for the basic limb. These results indicate participation of a single ionizable group in each limb, in which protonation of a group with apparent pK value of 6.6 and deprotonation of another group with pK value of 9.6 play critical roles in *E. coli* GMP reductase enzyme catalysis. The pH-rate data for of k_{cat}/K_{GMP} were fitted to Eq. 4 and indicate that both protonation of two groups with apparent pK values of 7.1 (± 0.8) and deprotonation of two groups with apparent pK values of 8.6 (± 1.1) (Fig 7b) are required for binding of GMP. The data of pH-rate profile for k_{cat}/K_{NADPH} were fitted to Eq. 5, which suggests that protonation of two groups with apparent pK values of 6.2 (± 1.0) abolish NADPH binding to *E. coli* GMP reductase (Fig 7c).

Energy of activation

The energy of activation for the enzyme-catalyzed chemical reaction was assessed by measuring the dependence of k_{cat} on temperature (Fig 8). These data were fitted to Eq. 6, yielding a value of 4.4 kcal mol^{-1}, which represents the minimal amount of energy necessary to initiate the chemical reaction catalyzed by *E. coli* GMP reductase. The linearity of the Arrhenius plot (Fig 8) also suggests that there is no change in the rate-limiting step over the temperature range utilized in the assay.

Deuterium kinetic isotope effects and proton inventory

To probe for rate-limiting steps and determine the stereospecificity of hydride transfer, measurements of primary deuterium kinetic isotope effects were carried out (Fig 9). The data were fitted to Eq. 7 for kinetic isotope effects on both *V* and *V*/*K*, yielding values of 2.50 (± 0.04) for $^{D}V_{NADPH}$ and 0.40 (± 0.04) for $^{D}V/K_{NADPH}$ (Table 3). The corresponding values for GMP were 1.05 (± 0.06) for $^{D}V_{GMP}$ and 1.03 (± 0.07) for $^{D}V/K_{GMP}$ (Table 3).

To evaluate the contribution of proton-transfer from the solvent to the GMP reductase catalyzed reaction, solvent kinetic isotope effects were determined and the data fitted to Eq. 7. The following values were found for the solvent kinetic isotope effects (Table 3): $^{D2O}V_{NADPH}$ = 0.99 (± 0.03) and $^{D2O}V/K_{NADPH}$ = 0.67 (± 0.09) (Fig 10a), and $^{D2O}V_{GMP}$ = 1.30 (± 0.01) and $^{D2O}V/K_{GMP}$ = 0.82 (± 0.03) (Fig 10b). In an attempt to determine the number of protons transferred during the solvent isotope-sensitive step, a proton inventory experiment was conducted. It was found a linear relationship between *V* and the mole fraction of D_2O for GMP reductase (Fig 10b - inset), suggesting that a single proton is transferred during this step.

Multiple isotope effects are capable of discriminating if two different isotopic substitutions affect the same or distinct chemical steps. Accordingly, solvent kinetic isotope effects were measured using NADPD as the varied substrate. Isotope effects values on $^{D2O}V_{NADPD}$ and $^{D2O}V/K_{NADPD}$ were, respectively, 1.00 (± 0.02) and 1.50 (± 0.17) (Fig 11; Table 3). The isotope effect on the equilibrium constant, $^{D}K_{eq}$, was determined in order to assess whether the deuterium substitution could affect the internal equilibrium of the reaction. A value of 0.82 was determined for the equilibrium isotope effect ($^{D}K_{eq}$; Table 3).

Table 3: Kinetic Isotope Effects for *E. coli* GMP Reductase[a]

Parameter	*Isotope Effect*
$^{D}V/K_{NADPH}$	0.40 ± 0.04
$^{D}V_{NADPH}$	2.50 ± 0.04
$^{D}V/K_{GMP}$	1.03 ± 0.07
$^{D}V_{GMP}$	1.05 ± 0.06
$^{D2O}V/K_{NADPH}$	0.67 ± 0.09
$^{D2O}V_{NADPH}$	0.99 ± 0.03
$^{D2O}V/K_{GMP}$	0.82 ± 0.03
$^{D2O}V_{GMP}$	1.30 ± 0.01
$^{D2O}V/K_{NADPD}$	1.50 ± 0.17
$^{D2O}V_{NADPD}$	1.00 ± 0.02
$^{D}K_{eq}$	0.82

[a] value ± standard error obtained upon data fitting to the appropriate equations.

Pre-steady-state kinetics

In an attempt to determine whether product release contributes to some extent to the rate limiting step, pre-steady-state analysis of the reaction catalyzed was performed. Fitting the pre-steady-state data to Eq. 10, which describes a single exponential decay, yielded a value of 0.204 (± 0.002) s^{-1} for the apparent first-order rate constant (Fig 12). This result in agreement with the value of 0.28 (± 0.02) s^{-1} for the catalytic rate constant (k_{cat}) determined by initial velocity study measurements.

Discussion

Amplification and cloning of *E. coli guaC* gene

The *guaC* gene was successfully amplified from the *E. coli* genome, cloned into pCR-Blunt vector, and subcloned into pET-23a(+) expression vector. The automatic DNA sequencing confirmed the integrity of the gene and the absence of mutations, which enabled the expression of the recombinant enzyme.

Expression and purification of recombinant GMP reductase

E. coli GMP reductase was expressed after 24 h of cell growth in the absence of IPTG induction. It is noteworthy that hGMPR2 was produced only in the presence of IPTG, after a growth period of only 4 h at 30 °C.[2] The pET expression system makes use a powerful T7 polymerase, under control of IPTG-inducible *lacUV5* promoter to transcribe genes of interest, which are positioned downstream of the bacteriophage T7 late promoter.[19] Expression of recombinant GMP reductase showed that even in the absence of the inducer, high levels of protein production could be obtained in stationary phase, as has been previously reported for other enzymes.[20,21,22] It has been proposed that uninduced expression of *lac*-controlled genes occurs when cells approach stationary phase in complex medium and that cAMP, acetate and low pH are required to produce high level expression in the absence of IPTG induction, which perhaps is part of a general response to carbon-limiting conditions.[23] Nevertheless, more recently, it has been shown that unintended induction in the pET system is due to the presence of as little as 0.0001 % of lactose in the medium.[24] The recombinant *E. coli* GMP reductase was purified to homogeneity by a three-step purification protocol using standard anionic exchange and size exclusion columns.

Quaternary structure analysis of *E. coli* GMP reductase

The results of mass spectrometry analysis combined with the amino acid sequencing demonstrated, unequivocally, that the homogeneous protein is, indeed, recombinant *E. coli* GMP reductase. The gel filtration chromatography showed that the enzyme from *E. coli* has the same tetrameric quaternary structure of hGMPR2, demonstrated by X-ray diffraction.[16]

Determination of apparent steady-state kinetic constants and initial velocity pattern

The results of the apparent steady-state kinetic data for *E. coli* GMP reductase indicate a K_M value for GMP of 6.9 μM, which is 2.5-fold lower than that for hGMPR2 (17.4 μM),[2] and 3-fold lower than the enzyme from *L. donovani* (21.2 μM).[9] The same pattern occurs for NADPH, with a K_M value of 11.1 μM, which is 2.3-fold lower than that for hGMPR2 (26.6 μM).[2] As for its human counterparts, *E. coli* GMP reductase cannot catalyze conversion of GMP to IMP using NADH as the hydride donor up to 200 μM concentration (data not shown).

Lineweaver-Burk analysis (Fig 3) suggests that ping-pong and rapid equilibrium ordered mechanisms can be ruled out for *E. coli* GMP reductase. The former mechanism gives double reciprocal plots displaying parallel lines and the latter a family of lines intersecting on the *y*-axis. These data are consistent with ternary complex formation and a sequential mechanism. A sequential mechanism was also reported for hGMPR1[11] and hGMPR2.[2]

It has been shown that the true K_M values for erythrocyte hGMPR1 are 2.6 μM for GMP and 16.9 μM for NADPH,[11] which are in the same concentration range as *E. coli* GMP reductase true steady-state kinetic parameters. These results suggest that *E. coli* GMP reductase possesses a similar overall dissociation constant for both substrates when compared to hGMPR1. However, the erythrocyte human enzyme presents a bimodal GMP substrate saturation curve,[11] which is usually attributed to the existence of independent isoenzymes with different kinetic constants or to a single multisubunit enzyme with multiple sites that can interact in a negatively cooperative manner.[25] Deng and co-workers[2] identified the hGMPR2 isoenzyme, making the bimodal substrate-

saturation kinetic found in hGMPR likely to be a result of a mixture of both isoenzymes. At any rate, a sequential addition of substrates to form a ternary complex has also been proposed for hGMPR2 enzyme.[2]

Isothermal titration calorimetry

ITC is an important and well-established technique for the study of thermodynamics of macromolecular interactions, and is unique in that it is capable of measuring simultaneously the association and thermodynamic constants of binding.[26] Binding experiments using ITC combined with the initial velocity study demonstrated that the reaction catalyzed by *E. coli* GMP reductase follows an ordered bi-bi kinetic mechanism, in which GMP is the first substrate to bind to free enzyme, followed by the binding of NADPH to form the ternary complex capable of undergoing catalysis; and $NADP^+$ is the first product to dissociate from the enzyme, followed by the dissociation of IMP (Fig. 13). This mechanism is in agreement with both human GMP reductases, for which a sequential kinetic mechanism has been reported.[2,11] Notwithstanding, the results reported here provide, to the best of our knowledge, the first experimental evidence for both order of addition of substrate and release of products.

The ITC measurements of GMP binding provided dissociation constant values (K_d), one for each subunit, where $K_{d1} > K_{d2} > K_{d3}$, suggesting a positive homotropic cooperativity, since the binding of one molecule of GMP increases the affinity for the next molecule which will bind to the next subunit. The K_{d4} value is higher though than the others, indicating a lower affinity for the last subunit to bind GMP. Interestingly, this finding is consistent with the crystal structure of hGMPR2, as no GMP binding could be observed for one of the subunits of this enzyme.[16] The ΔG values for all four subunits are negative, which demonstrate that GMP binding to *E. coli* GMP reductase is

a thermodynamically favorable process. The thermodynamic analysis revealed different types of interactions between the ligand and the enzyme subunits, ranging from favorable hydrogen bonds and/or van der Waals interactions (negative ΔH), release of "bound" water molecules to bulk solvent (positive ΔS) to conformational changes in either or both of the molecules (negative ΔS).[27] As can be seen in Table 2, with the exception of subunit 2, the analyses of ΔH and ΔS reveal that the binding of GMP is coupled with favorable hydrogen bonds (negative ΔH) and conformational changes (negative ΔS).[28] This finding appears to be consistent with the hGMPR2 structure,[16] in which GMP was located on the top of the α/β barrel surrounded by a hydrophilic surface formed by the active site loop and the flexible binding loop that would close upon GMP binding to the enzyme.

The IMP binding to *E. coli* GMP reductase yielded four different K_d values (Table 2). However, no evident relationships could be observed between the constants that would suggest either positive or negative cooperativity among the subunits. The analysis of the Gibbs free energy revealed that the binding of IMP is thermodynamically favorable for all subunits of *E. coli* GMP reductase (negative ΔG), and the analysis of ΔH and ΔS for IMP follows a similar pattern as observed for GMP. The determination of the crystal structure of *E. coli* GMP reductase in complex with IMP may shed light on these thermodynamic features.

pH-rate profiles

The Cys186 amino acid side chain has been shown to play a key role in catalysis for hGMPR2 since the Cys186Ala mutant displayed less than 5 % activity as compared to wild-type enzyme.[16] The pH dependence of k_{cat} and sequence alignment analyses suggest that the conserved Cys186 is likely the residue with apparent pK value of 9.6

that plays a critical role in *E. coli* GMP reductase catalysis. The cysteine thiol group usually ionizes at slightly alkaline pH values, and the resulting thiolate anion is the reactive species that acts as a nucleophile, which is one of the most reactive functional groups found in proteins.[29] It is possible that the Cys186 side chain, which has been shown to interact with GMP in the crystal structure of hGMPR2,[16] interacts with the exocyclic amino group bound to C2 of the guanine moiety of GMP thereby facilitating both hydride transfer to C2 and the amino leaving group. In addition, the proposed model of *E. coli* GMP reductase indicates that this residue makes an H-bond to C2 exocyclic amino group of the guanine moiety of GMP (Fig. 6). Notwithstanding, site-directed mutagenesis studies are in progress to confirm the role of Cys186, if any, in *E. coli* GMP reductase enzyme catalysis. The bell-shaped pH profile for k_{cat} (Fig 7a) also showed participation of single ionizable group with apparent p*K* value of 6.6 that has to be deprotonated for catalysis. Sequence alignment showed conservation of Asp129 in *E. coli* GMP reductase (Fig 7) that has been shown to be located in the active site loop in hGMPR2.[16] Although the p*K* value of the β-carboxyl group of Aspartate residues are usually in the 3.9 – 4.0 range, it is not unlikely that this p*K* value may be displaced by a neighbouring chemical group. However, assigning a definite catalytic role to Asp129 in *E. coli* GMP reductase is not warranted and site-directed mutagenesis studies should be carried out. Although the apparent p*K* value of 6.6 that plays a role in catalysis could tentatively be ascribed to the imidazole side chain of a Histidine residue (p*K* usually in the 6.0 – 7.0 range), His278 is located in the GMP binding site of *E. coli* GMP reductase whereas it is not present in hGMPR2 (Fig 7).

The pH-rate data for of k_{cat}/K_{GMP} indicate that both protonation of two groups with apparent p*K* values of 7.1 and deprotonation of two groups with apparent p*K* values of 8.6 (Fig 7b) are required for GMP binding. These dissociation constants can

be in the ligand and the other in the enzyme, or both can be in one or the other. The crystal structure of hGMPR2 in complex with GMP demonstrated that this substrate is surrounded by a hydrophilic surface formed by the active site loop (residues 179-187 in hGMPR2) and the flexible GMP binding region (residues 268-290 in hGMPR2).[16] Sequence alignment of GMP reductases (Fig 5) shows a relatively good conservation of these two regions in *E. coli* GMP reductase (active site loop: residues 179-187; GMP binding region: 268-290). The p*K* value for N7 atom of the guanine moiety of GMP is 3.6, and the ribose 2',3'-diol only loses a proton above pH 12. The guanine base becomes protonated on one of the ring nitrogens rather than on the exocyclic amino group since this does not interfere with delocalization of the NH_2 electron lone pair into the aromatic system. In the case of monoesters, the phosphate group of GMP loses one proton at pH 1 and a second proton at pH 7. The proximity of negative charge on the phosphate residues has a secondary effect, making the ring nitrogens more basic ($\Delta pK \approx +0.4$) and the amine protons less acidic ($\Delta pK \approx +0.6$). It is thus likely that the pH-rate profile does not reflect any ionization of the guanine moiety of GMP. On the other hand, it is possible that the apparent p*K* values reflect change in ionization of His278 in the GMP binding site, and change in ionization of the phosphate group of GMP and, for instance, Asp219 that makes H-bonds with the ribose hydroxyl groups of the pentose.

The pH-rate profile for k_{cat}/K_{NADPH} indicated that protonation of two groups with apparent p*K* values of 6.2 abolish NADPH binding to *E. coli* GMP reductase (Fig 7c). Although the there was no diffraction pattern to allow identification of NADPH binding site in hGMPR2, structural comparison and model building has been employed to suggest that the amino acid residues 129-133 are involved in NADPH binding.[16] These residues are conserved in *E. coli* GMP reductase (Fig 5). The adenine-C2'-ribose phosphate group has a p*K* value of 6.1. It is thus tempting to suggest that protonation of

NADPH phosphate and the putative Asp129 residue located in the NADPH binding site can account for the k_{cat}/K_{NADPH} pH-rate profile.

Deuterium kinetic isotope effects and proton inventory

Measurements of kinetic isotope effects in enzyme catalyzed reactions aim at examining the contribution of proton transfer(s) to rate-limiting step(s). However, the maximal velocity may be dependent of several rate-contributing or partially rate-limiting steps instead of one rate-determining step.[30]

Isotope effects on *V* report on events following the ternary complex formation capable of undergoing catalysis (fully loaded enzyme), which include the chemical steps, possible enzyme conformational changes, and product release (leading to regeneration of free enzyme). Isotope effects on *V*/*K* report on steps in the reaction mechanism from binding of isotopically labeled substrate to the first irreversible step, usually considered to be the release of the first product (that is, all rate constants from reactant binding until the first irreversible step).[30] Any substrate can be varied; it does not need to the labeled one, but one obtains $^{D}V/K$ effect for the varied substrate rather than for the labeled one. Although the apparent classical limit for primary deuterium kinetic isotope effects on *V* is approximately 8, values as low as 2 have sometimes been accepted as evidence of a rate-determining step.[30,31] For reactions involving NAD(P)H oxidation, primary deuterium isotope effects ranging from 1 to 3 have been found.[32] The magnitude of primary deuterium isotope effect depends on the chemical nature of the transition state.[33] This isotope effect reaches a maximum value when the hydrogen is symmetrically placed between the donor atom from which cleavage occurs and the acceptor atom to which a new bond is formed, and decreases for reactant- or product-like transition states. The value of 2.5 for the observed primary deuterium kinetic

isotope effect on *V* for *E. coli* GMP reductase using either NADPH or [4*S*-^{2}H]-NADPH ($^DV_{NADPH}$) as variable substrate indicates that hydride transfer is involved in a rate-limiting step and that the transition state may be either substrate- (early) or product-like (late). However, the symmetry of the transition state can only be inferred from the magnitude of a deuterium kinetic isotope effect if it is for the specific step in an enzymatically catalyzed reaction at which the isotopically substituted bond is broken by passing through a single transition state (that is, the intrinsic kinetic isotope effect). Enzyme-catalyzed chemical reactions proceed through many steps and the rate constants for several steps are usually consequential to the composite rate constant for the overall reaction, consequently the observed deuterium kinetic isotope effect is less than or equal to the intrinsic deuterium isotope effect for the step in which the hydrogen is transferred. In any case, the observed primary deuterium kinetic isotope effect on *V* for *E. coli* GMP reductase indicates that hydride transfer is from C4-*proS* hydrogen of NADPH and that it is partially rate-limiting. On the other hand, the inverse primary deuterium kinetic effect on *V*/*K* for NADPH ($^DV/K_{NADPH} = 0.4$) is somewhat puzzling. Incidentally, there have been numerous reports of inverse isotope effects on *V*/*K* of unknown origin.[34,35] The expression of deuterium kinetic isotope effect on *V*/*K* includes the intrinsic isotope effect, commitment factors (forward and reverse) and equilibrium isotope effect.[33] An equilibrium isotope effect may be invoked to account for the inverse effect on *V*/*K*, providing that the reverse commitment factor is large and the forward commitment factor is small. The inverse deuterium isotope effect on the equilibrium constant ($^DK_{eq} = 0.82$) suggest that the deuterated product is more stiffly bonded than the deuterated substrate[36] and the internal equilibrium might dominate the observed kinetic isotope effect. The inverse isotope effect indicates that once the hydride is transferred it becomes more tightly bonded to the corresponding product (IMP) when

compared to the substrate. The magnitude of this isotope effect is a direct consequence of the difference in the bonds of the substrate and product, with deuterium becoming enriched in the stiffest bond and the hydrogen in the looser one (deuterium accumulates where binding is tighter).[37] In addition, isotope effects on *V*/*K* are a combination of binding and catalytic events. Binding isotope effects can contribute in the opposite direction of kinetic isotope effects that arise from transition state chemistry. An inverse binding isotope effect may arise when binding of the molecule containing the heavier isotope atom (NADPD) is increased as bonds to the isotopic label are tighter in the bound complex. Although it is conceivable that the inverse $^{D}V/K_{NADPH}$ value reflects inverse binding isotope effect, it cannot be experimentally assessed as NADPH (enzyme mechanism proposed here) binds to the *E. coli* GMP reductase:GMP binary complex to form the catalytic competent ternary complex. Accordingly, the inverse $^{D}V/K_{NADPH}$ value is likely due to the inverse deuterium isotope effect on the equilibrium constant. Isotope effects can provide further experimental evidence for a specific enzyme mechanism. In the case of an ordered mechanism, the *V*/*K* for the first substrate (GMP) to bind (at saturating concentrations of the second substrate: NADPH) is the on-rate for the reactant binding to enzyme, a non-isotope sensitive step.[33] The value of 1.03 (± 0.07) for $^{D}V/K_{GMP}$ (Table 3) provides further support for an ordered enzyme mechanism as suggested by the initial velocity pattern and ITC data.

To evaluate the contribution of proton transfer from solvent to a rate-limiting step, measurements of solvent isotope effects on *V* and *V*/*K* were carried out. As rule of thumb, deuterium accumulates where binding is tighter (that is, fractionation factor is larger than one). Transition state proton contributes the reciprocal of its respective fractionation factor to the solvent isotope effect, whereas the contribution of a reactant state proton to the solvent isotope effect is equal to its fractionation factor.[32] Reactant

state fractionation by enzyme cysteine thiol groups (S-H group of cysteine) can make large inverse contributions to solvent isotope effects.[32,33] It is thus conceivable that the value of 0.82 for $^{D2O}V/K_{GMP}$ reflects participation of Cys186 of free enzyme, which has been shown to interact with GMP in hGMPR2 crystal structure,[16] and the value of 0.67 for $^{D2O}V/K_{NADPH}$ reflects an inverse contribution of conserved Cys127 of free enzyme, located near the NADPH binding site of *E. coli* GMP reductase (Fig 5). The value of 0.99 for $^{D2O}V_{NADPH}$ suggests no participation of proton solvent in catalysis. On the other hand, solvent proton transfer appears to play a modest role in catalysis since a value of 1.30 was found for $^{D2O}V_{GMP}$. In addition, proton inventory data (Fig 10b – inset) suggest that this modest solvent kinetic isotope effect arises from a single protonic site. The difference found between the primary deuterium and solvent kinetic isotope effects suggests that the hydride and proton transfer may occur in distinct reaction steps, as found in other NADPH-dependent reductive reactions.[34] Nevertheless, it is not possible to ascertain whether or not hydride transfer and protonation steps occur in a single transition state (concerted mechanism) or in distinct transition states (stepwise mechanism) based solely on primary and solvent isotope effects.

Multiple isotope effects (double isotope effects) allow to determine whether two different isotopic substitutions affect the same (concerted) or different (stepwise) chemical steps.[38] This method uses the normal effect of deuterium to slow down one step of a reaction mechanism while observing changes in the expression of another isotope effect,[38] the effects in question being the protonation and the hydride transfer. If the protonation and hydride transfer occur in the same transition state, the solvent isotope effect will be larger or unchanged with the deuterium substitution (NADPD) when compared with NADPH. However, if the effects take place in different steps, the solvent isotope effect will decrease with NADPD, once the hydride transfer will become

more rate-limiting.[34,35,38] As can be seen in Table 3, the results of the multiple isotope effects showed similar values for $^{D2O}V_{NADPD}$ (1.00) and $^{D2O}V_{NADPH}$ (0.99), suggesting that hydride transfer and solvent proton transfer steps take place in the same transition state (concerted mechanism). In addition, the value for the solvent isotope effect on *V*/*K* with NADPD (1.50) is larger than with NADPH (0.67), thereby lending support to a concerted mechanism.

Pre-steady-state kinetics

In the study of the transient phase of enzyme reactions, the data obtained is generally expressed by a single exponential curve for first order reaction[39]. The analysis of the data allows determining the apparent first order rate constant, which was in the same range as the first order in the steady-state kinetics. The observation of burst during a time course in the transient phase is evidence of significant build-up of product formation along the reaction pathway.[39] If a burst is observed during the transient phase, and the concentration of $NADP^+$ produced is approximately equal to the initial *E. coli* GMP reductase subunit concentration, it would indicate that the chemical step of the reaction is much faster than the release of the first product ($NADP^+$). The absence of burst suggests that both steps have similar rates and the product release is not the rate-limiting step of the reaction.

Conclusion

Rational inhibitor design relies on mechanistic and structural information on the target enzyme. Enzyme inhibitors make up roughly 25 % of the drugs marketed in United States.[40] Enzymes catalyze multistep chemical reactions to achieve rate accelerations by

stabilization of transition state structure(s).[40] Accordingly, mechanistic analysis should always be a top priority for enzyme-targeted drug programs aiming at the rational design of potent enzyme inhibitors. Moreover, ITC has been used as an important technique for the direct determination of thermodynamic and kinetic parameters of enzymatic reactions.[41] The recognition of the limitations of high-throughput screening approaches in the discovery of candidate drugs has rekindled interest in rational design methods.[42] Understanding the mode of action of *E. coli* GMP reductase will inform us on how to better design inhibitors targeting this enzyme. In addition, understanding the mode of action of an enzyme can be used to inform functional annotation of newly determined sequences and structures, to select appropriate enzyme scaffolds for engineering new functions, and to refine definitions in the current EC classifications.[43] The elucidation of the mode of action of *E. coli* GMP reductase and its availability in recombinant form may also provide a tool for determination of substrate specificity of cyclic nucleotide phosphodiesterases (PDEs). PDEs belong to a superfamily of proteins with medical relevance that play a major role in cell signaling by catalyzing the hydrolysis of cyclic AMP (cAMP) and cyclic GMP (cGMP).[44] PDE enzymes are distinguished by their substrate specificity. The PDE activity cannot be directly assayed, being necessary to couple an accessory enzyme. As recombinant *E. coli* GMP reductase is specific for GMP, it may be employed to determine the substrate specificity of PDE enzymes. Among the 11 families of PDEs, only PDE 5, PDE 6 and PDE 9 are specific for cGMP, which are targets for, respectively, treatment of erectile dysfunction (sildenafil), visual alterations, and behavioral state regulations and learning.[45] The results here presented may also help chemical biologists to design function-based chemical compounds to carry out either loss-of-function (inhibitors) or gain-of-function (activators) experiments to reveal the biological role of GMP reductase in the context of

whole *E. coli* cells.[46] It is also hoped that the results presented here may be useful to understand the role that GMP reductase plays in *E. coli* salvage pathway.

Experimental Procedures

Materials

All chemicals were of analytical or reagent grade and were used without further purification, unless stated otherwise. 5'GMP, NADPH, IMP, and $NADP^+$ along with lysozyme and streptomycin sulfate were purchased from Sigma-Aldrich. Deuterium oxide (99.9 atom % D_2O) was from Cambridge Isotope Laboratories. Fast performance liquid chromatography (FPLC) protein purification (4 °C) was carried out using an Äkta Purifier from GE Healthcare; all chromatographic columns and the LMW and HMW Gel Filtration Calibration Kit were also from GE Healthcare. Bovine serum albumin and Bradford reagent were from Bio-Rad Laboratories. All steady-state activity assays were performed in an UV-2550 UV/Visible Spectrophotometer (Shimadzu). Dithiothreitol (DTT) was from Acros Organics. *Pfu* DNA polymerase was from Stratagene. Restriction enzymes and T4 DNA ligase and pCR-Blunt cloning vector were from Invitrogen and pET-23a(+) expression vector and *E. coli* BL21(DE3) were from Novagen The mass spectrometer LTQ-XL and LTQ Orbitrap Discovery were from Thermo and the nanoLC Ultra 1D plus was from Eksigent. iTC_{200} Microcalorimeter was from MicroCal Inc (Northampton, MA). Pre-steady-state measurements were carried out using an Applied Photophysics SX.18MV-R stopped-flow spectrofluorimeter on absorbance mode.

E. coli GMP reductase comparative homology modeling

E. coli three-dimensional model was built by comparative homology modeling using human type 2 GMP reductase structure as template (PDB ID: 2A7R; hGMPR2)[16], solved by X-ray crystallography at 3.0 Å in complex with GMP. Template structure was used for *E. coli* GMP reductase modeling, as well as to evaluate GMP binding mode to bacterial enzyme active site. Template selection was based on high primary sequence conservation (68.5% identity and 16.47% strong similarity), and presence of enzyme substrate bound to its active site. Target and template pair-wise sequence alignment required a single gap inclusion in human GMP reductase primary sequences. *E. coli* GMP reductase model was built by restrained-based homology modeling implemented in MODELLER9v1[47], with the standard protocol of the comparative protein structure modeling methodology, by satisfaction of spatial restrains[48,49]. Atomic coordinates of GMP heteroatoms were copied from template structure into the *E. coli* GMP reductase model. The best model was selected according to MODELLER objective function[50] and subjected to energy minimization for amino acid side chain and main chain rearrangements with GROMACS package[51] using the 43a1 force-field. The system was submitted to an initial steepest descent energy minimization in vacuum with a maximum number of 400 minimization steps, followed by a maximum of 3000 steps of conjugate gradient energy minimization. The program PROCHECK[52] was employed to analyze the stereochemical quality of the model, as previously described [53]. Structural correspondence between *E. coli* model and human GMP reductase template was evaluated by their root-mean square deviation (RMSD). H-bond interactions were evaluated with LIGPLOT v4.4.2[54], considering an atomic distance cut off of 3.9 Å (program default values). Images were generated with PyMOL Molecular Graphic System V1.3 (Schrödinger, LLC).

Amplification and cloning of the *E. coli guaC* gene

The oligonucleotide primer sequences of *E. coli guaC* structural gene were 5'-AACATATGCGTATTGAAGAAGATCTGAAGTTAGGTTTTAAAGACG-3' (forward) and 3'-AAGGATCCTCATTACAGGTTGTTGAAGATGCGG TTTTCTTGTTCC-5' (reverse). The primers were designed to contain, respectively, *Nde*I and *Bam*HI restriction sites (underlined). The DNA fragment (1038 bp) was amplified using *Pfu* DNA polymerase, ligated into pCR-Blunt cloning vector, and transformed into *E. coli* DH10B cells. Plasmid DNA recovered from these cells was digested with the restriction enzymes *Nde*I and *Bam*HI, and the isolated insert was ligated into pET-23a(+) expression vector, previously treated with the same restriction enzymes. The sequence of *E. coli guaC* gene was determined by automated DNA sequencing to confirm the identity, integrity, and absence of PCR-introduced mutations in the cloned fragment.

Expression of recombinant GMP reductase

The recombinant plasmid pET-23a(+)::*guaC* was transformed into *E. coli* BL21(DE3) cells, and these were selected on Luria-Bertani (LB) agar plates containing 50 μg mL^{-1} ampicillin. LB medium (60 mL) containing 50 μg mL^{-1} ampicillin was inoculated with a single colony and cells were grown overnight. The culture (10 mL) was inoculated in LB medium (500 mL) with the same antibiotic concentration, and, as soon as $OD_{600\ nm}$ reached a value of 0.6, culture was grown for additional 24 h at 180 rpm and 37 °C without IPTG induction. Cells (15 g) were harvested by centrifugation at 7,690 *g* for 30 min at 4 °C and were stored at –20 °C. Soluble and insoluble fractions were analyzed by 12 % SDS-PAGE and Coomassie staining.

Purification of recombinant GMP reductase

Approximately 2.8 g of frozen cells were resuspended in 14 mL of 100 mM tris(Hydroxymethyl)aminomethane (Tris; buffer A) pH 7.8, and incubated with lysozyme (0.2 mg mL^{-1}) for 30 min with stirring. Cells were disrupted by sonication, and centrifuged at 38,900 *g* for 30 min to remove cells debris. Streptomycin sulfate was added to the supernatant up to 1 % (wt/vol), stirred for 30 min to precipitate nucleic acids, and centrifuged at 38,900 *g* for 30 min. The resulting supernatant was dialyzed against buffer A (2 x 2 L; 2 h each) using a dialysis tubing with molecular weight exclusion limit of 12 - 14 kDa. The sample was clarified by centrifugation at 38,900 *g* for 30 min and loaded on a FPLC 2.6 cm x 8.2 cm Q-Sepharose Fast Flow anion exchange column, pre-equilibrated with buffer A, washed with 5 column volumes of buffer A, and the adsorbed material was eluted with a linear gradient (0 - 40 %) of 20 column volumes of 100 mM Tris pH 7.8 containing 500 mM NaCl (buffer B) at 1 mL min^{-1}. The adsorbed recombinant GMP reductase was eluted at approximately 145 mM NaCl concentration, with substantial removal of contaminants. All fractions were analyzed by SDS-PAGE electrophoresis, and the ones containing the target protein were pooled and concentrated to 8.5 mL using an Amicon ultrafiltration cell (molecular weight cutoff 30 kDa). The soluble sample was loaded on a 2.6 cm x 60 cm HiPrep Sephacryl S-200 High Resolution size exclusion column, which was previously equilibrated with buffer A, and isocratically eluted with buffer A at a flow rate of 0.25 mL min^{-1}. This step was employed to further purify the recombinant protein and to remove salt from the sample, thereby allowing protein preparation for the next chromatographic step. Fractions containing the target protein were pooled and the soluble sample was loaded on a 1.6 cm x 10 cm Mono Q High Resolution anion

exchange column, pre-equilibrated with buffer A. The column was washed with 5 column volumes, and the adsorbed proteins were eluted with a linear gradient (0 - 40 %) of 20 column volumes of buffer B, and the target protein eluted at approximately 155 mM NaCl concentration. The active fractions containing the target protein were pooled and dialyzed against buffer A (2 x 2 L; 2 h each) in order to remove the remaining salt. Protein concentration was determined by the Bradford's method using bovine serum albumin as standard.[55]

Quaternary structure analysis of *E. coli* GMP reductase

The homogeneous sample was submitted to ESI-MS in order to confirm the identity of *E. coli* GMP reductase. The protein was also digested with trypsin and the resulting peptides were separated and analyzed by liquid chromatographic associated with mass spectrometry with fragmentation collision induced, and the results were used to identify the amino acid sequence through a search software (Protein Discoverer, Thermo).

The molecular mass of recombinant GMP reductase was determined by gel filtration chromatography using a 1.0 cm x 30 cm High Resolution Superdex 200 column pre-equilibrated with 50 mM Tris pH 7.5 containing 200 mM NaCl at a flow rate of 0.4 mL min^{-1}. The LMW and HMW Gel Filtration Calibration Kit were used as the protein molecular mass standards in the calibration curve, measuring the elution volumes of several standards (ferritin, catalase, aldolase, ovalbumin, coalbumin, ribonuclease A, and blue dextran 2000), calculating their partition coefficients (K_{av}), and plotting these values against the logarithm of their molecular mass. The K_{av} values were determined as $K_{av} = (V_e - V_o)/(V_t - V_o)$, where V_e is the sample elution volume, V_t is the total bed volume of the column, and V_o is the column void volume, which had

been determined by loading blue dextran 2000 into the column. Protein elution was monitored at 215, 254, and 280 nm.

Synthesis of [4*S*-^{2}H]-NADPH

[4*S*-^{2}H]-NADPH was synthesized according to the method of Ottolina and co-workers[56] and purified on a 1.0 cm x 10 cm Mono Q High Resolution anion exchange column. The column was washed with 1 column volume of 100 mM *N*-2-hydroxyethylpiperazine-*N'*-2-ethanesulfonic acid (Hepes) pH 7.0, and the material was eluted with a linear gradient (0 - 100 %) of 5 column volumes of 100 mM Hepes containing 1.0 M NaCl pH 7.0 at a flow rate of 0.5 mL min^{-1}. The fractions with $A_{260\ nm}/A_{340\ nm} \leq 2.3$ were pooled.

Enzyme activity assay of *E. coli* GMP reductase

The recombinant GMP reductase activity was determined by a continuous spectrophotometric assay monitoring the conversion of NADPH to NADP$^+$ at 340 nm. The standard assay was performed at 25 °C in 100 mM Tris pH 7.8 with 10 mM DTT, unless stated otherwise.

Determination of apparent steady-state kinetic constants and initial velocity pattern

In order to determine the apparent steady-state kinetic constants, GMP reductase activity was measured (in duplicates) in the presence of varying concentrations of GMP (5 – 80 μM) and fixed NADPH concentration (100 μM), and varying concentrations of NADPH (5 – 120 μM) and fixed GMP concentration (100 μM), in 100 mM Tris pH 7.8 buffer containing 10 mM DTT in a total volume of 500 μL. The enzyme specificity for

NADPH was evaluated measuring the enzymatic activity in the presence of varying concentrations of NADH (20 – 200 μM) at a fixed-saturating concentration of GMP (100 μM). To determine the true steady-state kinetic parameters and initial velocity patterns, enzymatic activity was measured in the presence of varying concentrations of GMP (1 - 60 μM) and several fixed-varied NADPH concentrations (1 - 60 μM). Enzyme activity was determined in an UV-2550 UV/Visible spectrophotometer (Shimadzu) by monitoring the decrease in absorbance at 340 nm (ε_{340nm} = 6220 $M^{-1}cm^{-1}$) upon GMP reductase-catalyzed conversion of NADPH to $NADP^+$. One unit of enzyme activity was defined as the amount of protein that catalyzes the consumption of 1 μmol of NADPH/min at 25 °C.

Isothermal titration calorimetry

ITC experiments were carried out using the iTC_{200} Microcalorimeter. The reference cell (200 μL) was loaded with water during all experiments and the sample cell (200 μL) was filled with *E. coli* GMP reductase at a concentration of 122 μM in buffer A. The injection syringe (39.7 μL) was filled with substrates or products at different concentrations, GMP at 0.75 mM, NADPH at 3.5 mM, $NADP^+$ at 1.0 mM, and IMP at 1.0 mM, and the ligand binding isotherms were measured by direct titration (ligand into macromolecule). The same buffer was used to prepare all ligand solutions. The stirring speed was 500 rpm at 25 °C with constant pressure for all ITC experiments. Titration first injection (0.5 μL) was not used in data analysis and was followed by 17 injections of 2.2 μL each at 180 s intervals. Control titrations (ligand into buffer) were performed in order to subtract the heats of dilution and mixing for each experiment prior to data analysis. All data were evaluated utilizing the Origin 7 SR4 software (Microcal, Inc.).

pH-rate profiles

The dependence of kinetic parameters on pH was determined by measuring initial velocities in the presence of varying concentrations of one substrate and saturating levels of the other, in a buffer mixture of 500 mM 2-(*N*-morpholino)ethanesulfonic acid (MES) / Hepes / 2-(*N*-cyclohexylamino)ethanesulfonic acid (CHES) over the following pH values: 6.0 (10 – 160 μM varying GMP concentration and fixed concentration of NADPH at 240 μM, and 10 – 160 μM varying NADPH concentration and fixed concentration of GMP at 240 μM), 6.5 (2 – 60 μM varying GMP concentration and fixed concentration of NADPH at 100 μM, and 2 – 60 μM varying NADPH concentration and fixed concentration of GMP at 100 μM), 7.0 (2 – 60 μM varying GMP concentration and fixed concentration of NADPH at 100 μM, and 2 – 60 μM varying NADPH concentration and fixed concentration of GMP at 100 μM), 7.5 (5 – 80 μM varying GMP concentration and fixed concentration of NADPH at 100 μM, and 5 – 80 μM varying NADPH concentration and fixed concentration of GMP at 100 μM), 8.0 (5 – 80 μM varying GMP concentration and fixed NADPH concentration at 100 μM, and 5 – 80 μM varying NADPH concentration and fixed concentration of GMP at 100 μM), 8.5 (5 – 60 μM varying GMP concentration and fixed concentration of NADPH at 100 μM, and 5 – 60 μM varying NADPH concentration and fixed concentration of GMP at 100 μM), 9.0 (5 – 60 μM varying GMP concentration and fixed concentration of NADPH at 100 μM, and 5 – 60 μM varying NADPH concentration and fixed concentration of GMP at 100 μM), and 9.5 (2 – 60 μM varying GMP concentration and fixed concentration of NADPH at 100 μM, and 2 – 60 μM varying NADPH concentration and fixed concentration of GMP at 100 μM). Prior to performing the pH-rate profiles, the recombinant enzyme was incubated over a broader pH range and

assayed under standard conditions to identify denaturing pH values and to ensure enzyme stability at the tested pH range.

Energy of activation

In order to determine the energy of activation of the GMP reductase-catalyzed reaction, initial velocities were measured in the presence of varying concentrations of one (GMP 1 – 60 μM) (NADPH 1 – 80 μM) substrate and saturating levels of the other (100 μM), at temperatures ranging from 15 to 35 °C. GMP reductase was incubated for several minutes in all temperatures tested and assayed under standard conditions to ensure enzyme stability under all temperatures.

Deuterium kinetic isotope effects and proton inventory

Primary deuterium kinetic isotope effects were determined by measuring initial rates using a saturating level of GMP (100 μM) and varying concentrations of either NADPH (4 – 60 μM) or [4*S*-^{2}H]-NADPH (1 – 60 μM).

Solvent kinetic isotope effects were determined by measuring initial velocities using a saturating level of one substrate (100 μM) and varying concentrations of the other (GMP: 4 – 60 μM; NADPH: 4 – 60 μM) in either H_2O or 90 atom % D_2O. The proton inventory was determined using saturating concentrations of both substrates (100 μM) at various mole fractions of D_2O.

Multiple kinetic isotope effects were measured by determining the solvent isotope effects using [4*S*-^{2}H]-NADPH (NADPD) as the varied substrate.

Equilibrium isotope effect ($^DK_{eq}$) was determined by measuring the equilibrium constant in the presence of either NADPH or [4*S*-^{2}H]-NADPH. These equilibrium constants were measured as described by Leu and Cook.[57] In short, the ratio of

[NADPH]/[$NADP^+$] was fixed at 1 and the ratio of [IMP]/[GMP] were varied from 0.1 to 30 at fixed concentration of NH_4Cl. A plot of change in NADPH concentration versus [IMP]/[GMP] ratio crosses the abscissa at a value equal to K_{eq}.[57]

The notation utilized to express isotope effects is that of Northrop[33] as extended by Cook and Cleland.[58]

Pre-steady-state kinetics

Pre-steady-state kinetic measurements of the reaction catalyzed by *E. coli* GMP reductase were performed to determine whether product release is part of the rate-limiting step. The decrease in absorbance was monitored at 340 nm (1 mm split width = 4.65 nm spectral band), at 25 °C, using a split time base (2 – 50 s; 400 data points for each time base). The experimental conditions were 10 μM *E. coli* GMP reductase, 10 mM DTT, 250 μM GMP and 250 μM NADPH in 100 mM Tris-HCl pH 7.8 (mixing chamber concentrations). The dead time of the stopped-flow equipment is 1.37 ms.

Data analysis

Values of the kinetic parameters and their respective errors were obtained by fitting the data to the appropriate equations by using the nonlinear regression function of SigmaPlot 9.0 (SPSS, Inc.). Initial rate data at single concentration of the fixed substrate and varying concentrations of the other were fitted to Eq. 1.

$$v = \frac{VA}{K + A} \qquad \text{Eq. 1}$$

The family of lines intersecting to the left of the *y*-axis in double-reciprocal plots was fitted to Eq. 2, which describes a mechanism involving ternary complex formation and a sequential substrate binding.

$$v = \frac{VAB}{K_{ia}K_b + K_aB + K_bA + AB} \qquad \text{Eq. 2}$$

For Eq. 1 and Eq. 2, v is the initial velocity, V is the maximal initial velocity, A and B are the concentrations of the substrates (GMP and NADPH), K_a and K_b are their respective Michaelis constants, and K_{ia} is the dissociation constant for enzyme-substrate A binary complex formation.

pH-rate profiles data were fitted to Eqs. 3, 4 or 5, where y is the kinetic parameter, C is the pH-independent value of y, H is the proton concentration, and K_a and K_b are, respectively, the apparent acid and base dissociation constants for ionizing groups, and K_0 is the product of two apparent dissociation constants.[59]

$$\log y = \log\left(\frac{C}{1 + \frac{H}{K_a} + \frac{K_b}{H}}\right) \qquad \text{Eq. 3}$$

$$\log y = \log\left(\frac{C}{1 + \frac{H}{K_a} + \frac{H^2}{K_0} + \frac{K_b}{H} + \frac{K_0}{H^2}}\right) \qquad \text{Eq. 4}$$

$$\log y = \log\left(\frac{C}{1+\left(\frac{H}{K_{a1}}\right)\left(1+\frac{H}{K_{a2}}\right)}\right) \qquad \text{Eq. 5}$$

Eq. 3 describes a bell-shaped pH profile for a group that must be protonated for binding/catalysis and another group that must be unprotonated for binding/catalysis, and participation of a single ionizing group for the acidic limb (slope value of +1) and participation of a single ionizing group for the basic limb (slope value of -1). Eq. 4 describes a bell-shaped pH-rate profile that starts with a slope of +2 in the acidic limb and goes to an eventual slope of -2 in the basic limb, suggesting participation of two ionizing groups in each limb. Eq. 5 describes a pH-rate profile for two groups that need to be unprotonated for binding (slope of +2 for the acidic limb). Unless the p*K*s of the groups are at least 3 pH units apart, there will not be a linear region with a slope of +1.

The data for temperature effects were fitted to Eq. 6, where k is the maximal reaction rate, E_a is the energy of activation, T is the temperature in Kelvin, R is the gas constant (1.987 cal K^{-1} mol^{-1}), and A is a pre-exponential factor that correlates collision frequency and the probability of the reaction occurring when reactant molecules collide.

$$\log k = -\left(\frac{E_a}{2.3R}\right)\left(\frac{1}{T}\right) + \log A \qquad \text{Eq. 6}$$

Kinetic isotope effects data were fitted to Eq. 7, which assumes isotope effects on both V/K and V. In this equation, $E_{V/K}$ and E_V are the isotope effects minus 1 on V/K and V, respectively, and F_i is the fraction of isotopic label in the substrate A.

$$v = \frac{VA}{K(1 + F_i E_{V/K}) + A(1 + F_i E_V)} \quad \text{Eq. 7}$$

ITC data were fitted to Eq. 8, where ΔH is the enthalpy of process given by the ITC experiment, ΔG is the Gibbs free energy changes, ΔS is the entropy changes, T is the temperature of the experiment in Kelvin, R is the gas constant (1.987 cal K^{-1} mol^{-1}), and K_{eq} is the equilibrium binding constant. The dissociation constant, K_d, is the inverse of the equilibrium binding constant, K_{eq}, described in Eq. 9.

$$\Delta G = \Delta H - T\Delta S = -RT \ln K_{eq} \quad \text{Eq. 8}$$

$$K_d = \frac{1}{K_{eq}} \quad \text{Eq. 9}$$

The pre-steady-state time course of the reaction was fitted to Eq. 10 for a single exponential decay, in which A is the absorbance at time t, A_0 is the absorbance at time zero, and k is the apparent first-order rate constant for product formation.

$$A = A_0 e^{-kt} \quad \text{Eq. 10}$$

Acknowledgements

This work was supported by funds of Millennium Initiative Program (CNPq) and National Institute of Science and Technology on Tuberculosis (INCT-TB), MCT-CNPq, Ministry of Health - Department of Science and Technology (DECIT) - Secretary of Health Policy (Brazil) to D.S.S. and L.A.B. D.S.S. (CNPq, 304051/1975-06) and L.A.B. (CNPq, 520182/99-5) are Research Career Awardees of the National Research Council

of Brazil (CNPq). R.G.D. is a postdoctoral fellow of CNPq. L.A.R. acknowledges an MSc scholarship awarded by CAPES, A. B. acknowledges her PhD scholarship awarded by BNDES, and L.K.B.M. a PhD scholarship awarded by CNPq.

References

1 H. J. J. Nijkamp and P. G. DeHaan, *Biochim. Biophys. Acta*, 1967, **147**, 31-40.

2 Y. Deng, Z. Wang, K. Ying, S. Gu, C. Ji, Y. Huang, X. Gu, Y. Wang, Y. Xu, Y. Li, Y. Xie and Y. Mao, *Int. J. Biochem. Cell Biol.*, 2002, **34**, 1035-1050.

3 S. C. Andrews and J. R. Guest, *Biochem. J*., 1988, **255**, 35-43.

4 R. E. Roberts, C. I. Lienhard. C. G. Gaines, J. M. Smith and J. R. Guest, *J. Bacteriol.*, 1988, **170**, 463-467.

5 C. E. Benson, B. A. Brehmeyer and J. S. Gots, *Biochem. Biophys. Res. Commun*., 1971, **403**, 1089-1094.

6 B. B. Garber, B. U. Jochimsen and J. S. Gots, *J. Bacteriol.*, 1980, **143**, 105-111.

7 A. I. Kessler and J. S. Gots, *J. Bacteriol.*, 1985, **164**, 1288-1293.

8 M. F. Renart and A. Silero, *Biochim. Biophys. Acta*, 1976, **341**, 178-186.

9 T. Spector and T. E. Jones, *Biochem. Pharmacol.*, 1982, **31**, 3891-3897.

10 J. J. Mackenzie and L. B. Sorensen, *Biochim. Biophys. Acta*, 1973, **327**, 282-294.

11 T. Spector, T. E. Jones and R. L. Miller, *J. Biol. Chem*., 1979, **254**, 2308-2315.

12 S. Henikoff and J. M. Smith, *Cell*, 1989, **58**, 1021-1022.

13 J. Zhang, W. Zhang, D. Zou, G. Chen, T. Wan, M. Zhang and X. Cao, *J. Cancer Res. Clin. Oncol*., 2003, **129**, 76-83.

14 D. Salvatore, T. Bartha and P. R. Larsen, *J. Biol. Chem*., 1998, **273**, 31092-31096.

15 T. Page, S. J. Jacobsen, R. M. Smejkal, J. Scheele, W. L. Nyhan, J. H. Magnun and R. K. Robbins, *Cancer Chemother. Pharmacol*., 1985, **15**, 59-62.

16 J. Li, Z. Wei, M. Zheng, X. Gu, Y. Deng, R. Qiu, F. Chen, C. Ji, W. Gong, Y. Xie and Y. Mao, *J. Mol. Biol*., 2006, **355**, 980-988.

17 V. Henri, L. Michaelis and M. L. Menten, *Biochem. Zeitschr.*, 1913, **49**, 333-369.

18 J. D. Thompson, D. G. Higgins and T. J. Gibson, *Nucleic. Acids Res*., 1994, **22**, 4673-4680.

19 K. C. Kelley, K. J. Huestis, D. A. Austen, C. T.Sanderson, M. A. Donohue, S. K. Stickel, E. S. Kawasaki and M. S.Osburne, *Gene*, 1995, **156**, 33-36.

20 C. Rizzi, J. Frazzon, F. Ely, P. G. Weber, I. O. Fonseca, M. Gallas, J. S. Oliveira, M. A. Mendes, B. M. Souza, M. S. Palma, D. S. Santos and L.A. Basso, *Protein Expr. Purif*., 2005, **40**, 23-30.

21 G. Biazus, C. Z. Schneider, M. S. Palma, L. A. Basso and D. S. Santos, *Protein Expr. Purif*., 2009, **66**, 185-190.

22 Z. A. Sanchez-Quitian, C. Z. Schneider, R. G. Ducati, W. F. de Azevedo Junior, C. Bloch Junior, L. A. Basso and D. S. Santos, *J. Struct. Biol*., 2010, **169**, 413-423.

23 T. H. Grossman, E. S. Kawasaki, S. R. Punreddy and M. S. Osburne, *Gene*, 1998, **209**, 95-103.

24 F. W. Studier, *Protein Expr. Purif*., 2005, **41**, 207-234.

25 A. Levitzki and D. E. Koshland, Jr, *Proc Natl. Acad. Sci.*, **62**, 1969, 1121-1128.

26 A. Velazquez-Campoy and E. Freire, *Biophys. Chem*., **115**, 2005, 115-124.

27 J. E. Ladbury and M. L. Doyle, in *Biocalorimetry II*, ed. Wiley, London, 1st ed., 2004, 259.

28 P. Kwong, M. L. Doyle, D. J. Casper, C. Cicala, S.A. Leavitt, S. Majeed, T. D. Steenbeke , M. Venturi, I. Chaiken, M. Fung, H. Katinger, P. W. Parren, J. Robinson,

D. Van Ryk, L. Wang, D. R. Burton, E. Freire, R. Wyatt, J. Sodroski, W. A. Hendrickson and J. Arthos., *Nature*, **2002**, 420, 678-682.

29 G. Bulaj, T. Kortemme and D. P. Goldenberg, *Biochemistry*, 1998, **37**, 8965-8972.

30 D. B. Northrop, *Biochemistry*, 1975, **14**, 2644-2651.

31 J. H. Richards, in *Enzymes*, ed. Academic Press, New York, 2nd ed., 1970, 321.

32 P. F. Cook, in *Enzyme Mechanism from Isotope Effects*, ed. CRC Press, Boca Raton, 1991, 203-228.

33 P. F. Cook, *Isotopes Environ. Health Stud.*, 1998, **34**, 3-17.

34 M. P. Patel, W. Liu, J. West, D. Tew, T. D. Meek and S. H. Thrall, *Biochemistry*, 2005, **44**, 16753-16765; R. G. Silva, L. P. S. de Carvalho, J. S. Blanchard, D. S. Santos and L. A. Basso, *Biochemistry*, 2006, **45**, 13064-13073.

35 D. B. Northrop, *Methods*, 2001, **24**, 117-124.

36 P. F. Cook and W. W. Cleland, in *Enzyme Kinetics and Mechanism*, Garland Science Publishing, New York, 2007, ch. 9, pp. 251-273.

37 P. F Cook, J. S. Blanchard and W. W. Cleland, *Biochemistry*, 1980, **19**, 4853-4858.

38 J. G. Belasco, W. J. Albery and J. R. Knowles, *J. Am. Chem. Soc.*, 1983, **105**, 2475-2477.

39 K. Hiromi, in *Kinetics of Fast Enzyme Reactions: Theory and Practice*, ed. Kodansha Ltd., Tokyo, 1979, ch. 4, pp. 188-253.

40 J. G. Robertson, *Biochemistry*, 2005, **44**, 5561-5571; J. G. Robertson, *Curr. Opin. Struct. Biol.*, 2007, **17**, 674-679.

41 M. L. Bianconi, *Biophys. Chem.*, 2007, **126**, 59-64.

42 J. E. Ladbury, G. K. Klebe and E. Freire, *Nat. Rev. Drug Discov.*, 2010, **9**, 23-27.

43 D. E. Almonacid, E. R. Yera, J. B. O. Mitchell and P. C. Babbitt, *PLoS Comput. Biol.*, 2010, **6(3)**, e10000700.

44 C. Lugnier, *Pharmacol. Ther*., 2006, **109**, 366-398.

45 H. T. Zhang, *Curr. Pharm. Des*., 2009, **15**, 1688-1698.

46 A. C. Bishop and V. L. Chen, *J. Chem. Biol*., 2010, **2**, 1-9.

47 A. Sali and T. L. Blundell. *Journal of Molecular Biology*, 1993, **234**, 779-815.

48 M. A. Martí-Renom, A. C. Stuart, A. Fiser, R. Sánchez, F. Melo and A. Sali. *Annu Review Biophysics and Biomolecular Structures*, 2000, **29**, 291-325.

49 A. Sali and J. P. Overington. *Protein Science*, 1994, **3**, 1582-1596.

50 M. Y. Shen and A. Sali. *Protein Science*, 2006, **15**, 2507-2524.

51 D. van der Spoel, E. Lindahl, B. Hess, G. Groenhof, A. E. Mark and H. J. C. Berendsen. *Journal of Computational Chemistry*, 2005, **26**, 1701-1718.

52 R. A. Laskowski, M. W. MacArthur, D. S. Moss and J. M. Thornton. *Journal of Applied Crystallography*, 1993, **26**, 283-291.

53 I. O. Fonseca, R. G. Silva, C. L. Fernandes, O. N. de Souza, L. A. Basso and D. S. Santos. *Archives of Biochemistry and Biophysics*, 2007, **457**, 123-133.

54 A. C. Wallace, R. A. Laskowski and J. M. Thornton. *Protein Engineering*, 1995, **8**, 127-134.

55 M. M. Bradford, R. A. Mcroire and W. L.Williams, *Anal. Biochem*., 1976, **72**, 248-254.

56 G. Ottolina, S. Riva, G. Carrea, B. Danieli and A. F. Buckman, *Biochim. Biophys Acta*, 1989, **998**, 173-178.

57 L. S. Leu and P. F. Cook, *Biochemistry*, 1994, **33**, 2667-2671.

58 P. F. Cook and W. W. Cleland, *Biochemistr*y, 1981, **20**, 1790-1796.

59 P. F. Cook and W. W. Cleland, in *Enzyme Kinetics and Mechanism*, Garland Science Publishing, New York, 2007, ch. 10, pp. 325-366.

Figure Legends

Figure 1: Chemical reaction catalyzed by GMP reductase.

Figure 2: SDS-PAGE (12%) analysis for the three chromatographic steps of purification of recombinant *E. coli* GMP reductase that yielded homogeneous protein. Lane 1, Molecular Weight Protein Marker (Fermentas); lane 2, crude extract; lane 3, Q-Sepharose anion exchange column; lane 4, Sephacryl S-200 size exclusion; lane 5 MonoQ High Resolution anion exchange column.

Figure 3: Intersecting initial velocity patterns for GMP reductase using either GMP (a) or NADPH (b) as the variable substrate. Each curve represents varied-fixed levels of the cosubstrate.

Figure 4: Isothermal titration calorimetry (ITC) analysis of *E. coli* GMP reductase titration with GMP (a), NADPH (b), IMP (c), and $NADP^+$ (d). The top panels show raw data of the heat pulses resulting from titration of *E. coli* GMP reductase. The bottom panels show the integrated heat pulses, normalized per mol of injectant as a function of the molar ratio (ligand concentration/*E. coli* GMP reductase concentration). These binding curves were best fitted to a sequential binding sites model equation.

Figure 5: Multiple sequence alignment of *E. coli* GMP reductase with both human enzymes (GMPR1_Hsapiens and GMPR2_Hsapiens) using the program CLUSTAL W. (*), (:), (.) and (-) indicate, respectively, identity, strong similarity and weak similarity among the residues. The residues in the proposed catalytic site (active site loop that acts

as a lid that closes upon GMP binding) were shaded in light gray, the amino acid residues in the proposed NADPH binding site were shaded in dark gray, and amino acid residues in the GMP binding site were boxed by a dashed line. Conserved amino acid residues that are important for catalysis or binding were boxed by a solid line. Black dots above the conserved residue indicate residues involved in catalysis, and black arrows indicate residues involved in substrate binding.

Figure 6: *E. coli* GMP reductase model superimposed on experimentally solved human type 2 GMP reductase (hGMPR2) structure. Amino acid residues of *E. coli* GMP reductase involved in GMP binding (light gray) and the GMP molecule (dark gray) are shown as sticks. The corresponding amino acids of hGMPR2 template are depicted as thin gray sticks. It is noteworthy that Glu289 *E. coli* GMP reductase substitutes for Ser288 in hGMPR2 (italics). H-bonds between amino acid residues of *E. coli* GMP reductase and GMP are shown as dotted lines.

Figure 7: Dependence of kinetic parameters on pH. (a) pH dependence of log k_{cat} data were fitted to Eq. 3; (b) log k_{cat}/K_{GMP} data were fitted to Eq. 4; (c) pH dependence of log k_{cat}/K_{NADPH} data were fitted to Eq. 5.

Figure 8: Temperature dependence of log k_{cat}. Saturating concentrations of NADPH and GMP substrates were employed to measure the maximum velocity as a function of temperature ranging from 15 to 35 °C. The data were fitted to Eq. 6. The linearity of the Arrhenius plot suggests that there is no change in the rate-limiting step over the temperature range utilized in the assay

Figure 9: Primary deuterium kinetic isotope effects using either NADPH (●) or NADPD (■) as the variable substrate in the presence of saturating concentration of GMP (100 μM). The data were fitted to Eq. 7.

Figure 10: Solvent isotope effects for GMP reductase. (a) NADPH was used as the variable substrate (4 – 60 μM), with a saturating concentration of GMP (100 μM). (b) GMP was used as the variable substrate (4 – 60 μM), with a saturating concentration of NADPH (100 μM). Both reactions mix contained either 0 (●) or 90 (■) atom % D_2O. The inset of (b) represents the proton inventory (0, 20, 40, 60, and 90 atom % D_2O) measuring GMP reductase enzyme activity with both substrates at saturating concentrations (100 μM).

Figure 11: Multiple kinetic isotope effects using NADPD as the variable substrate in the presence of saturating concentration of GMP (100 μM) and either 0 (●) or 80 (■) atom % D_2O. The data were fitted to Eq. 7.

Figure 12: Representative stopped-flow trace for product formation, measuring the decrease in absorbance at 340 nm upon conversion of NADPH to $NADP^+$catalyzed by 10 μM of recombinant *E. coli* GMP reductase (mixing chamber concentration). The data were fitted to Eq. 10 for a single exponential decay, yielding a value of 0.204 s^{-1} for the apparent first-order constant of product formation.

Figure 13: Proposed enzyme mechanism for *E. coli* GMP reductase.

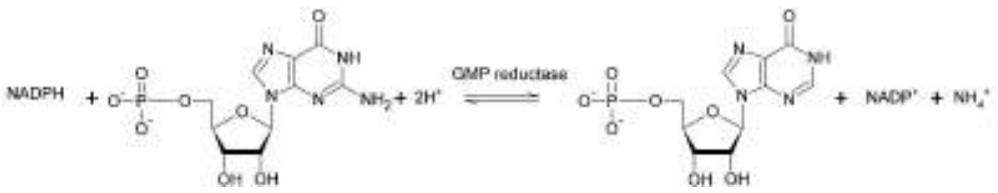

254x46mm (600 x 600 DPI)

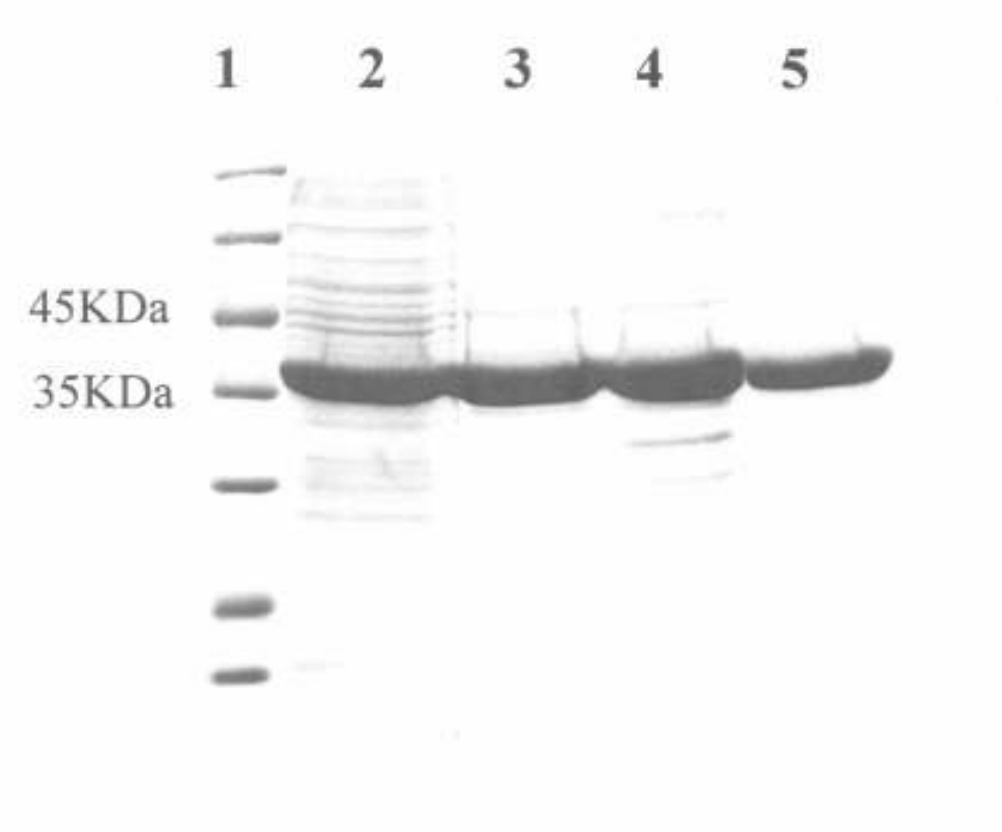

70x59mm (600 x 600 DPI)

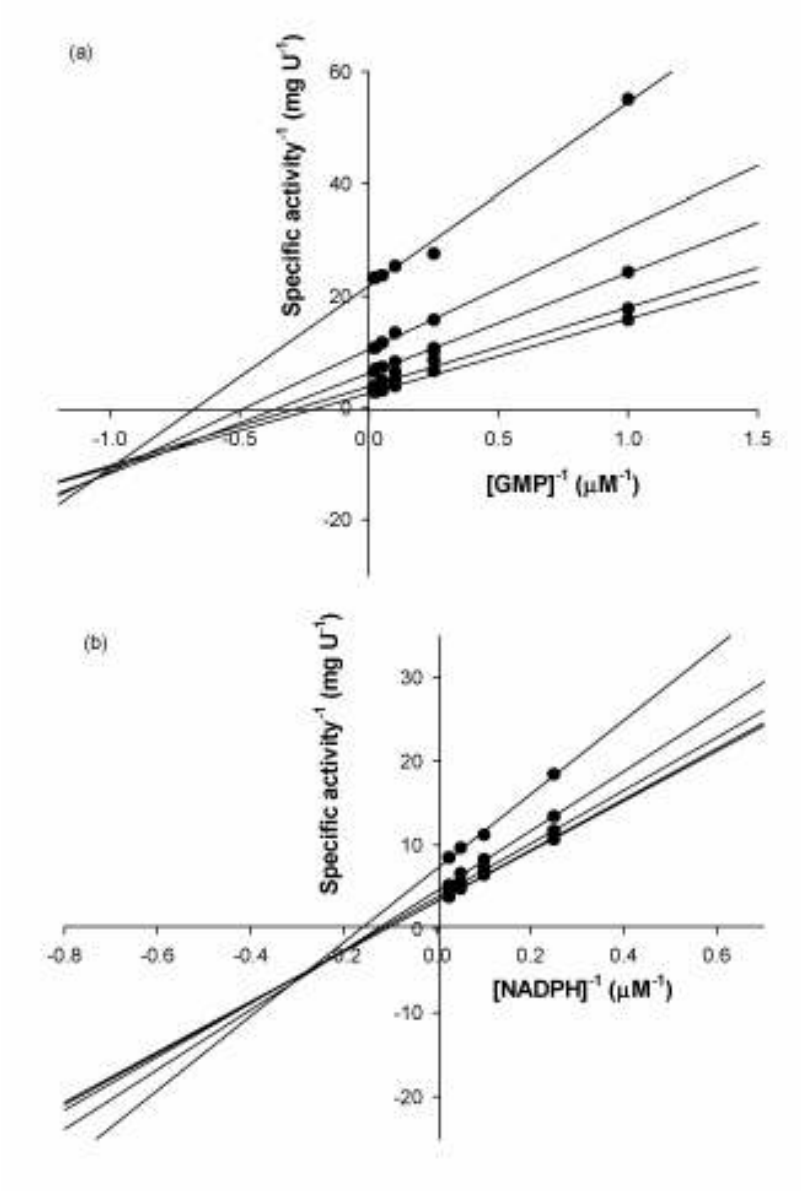

331x494mm (150 x 150 DPI)

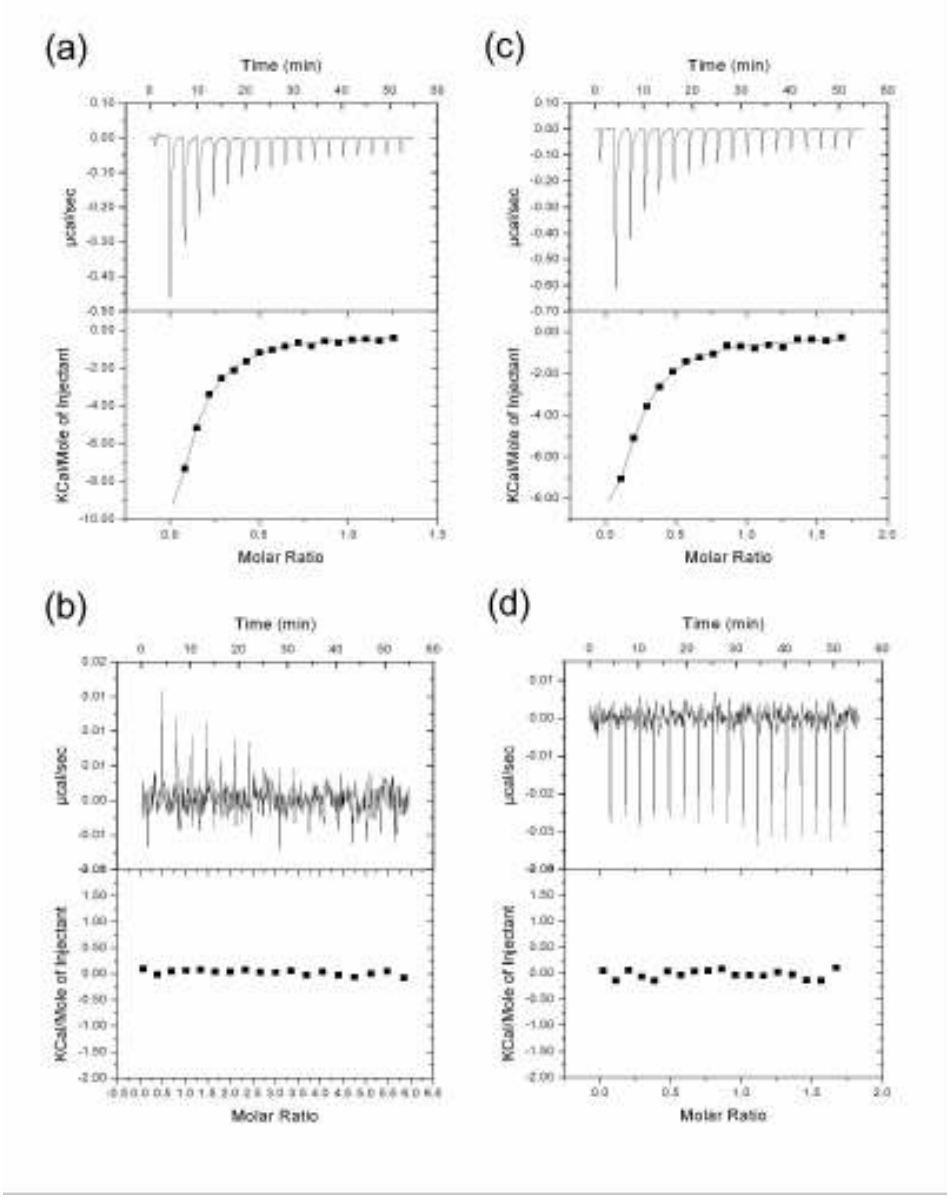

170x215mm (600 x 600 DPI)

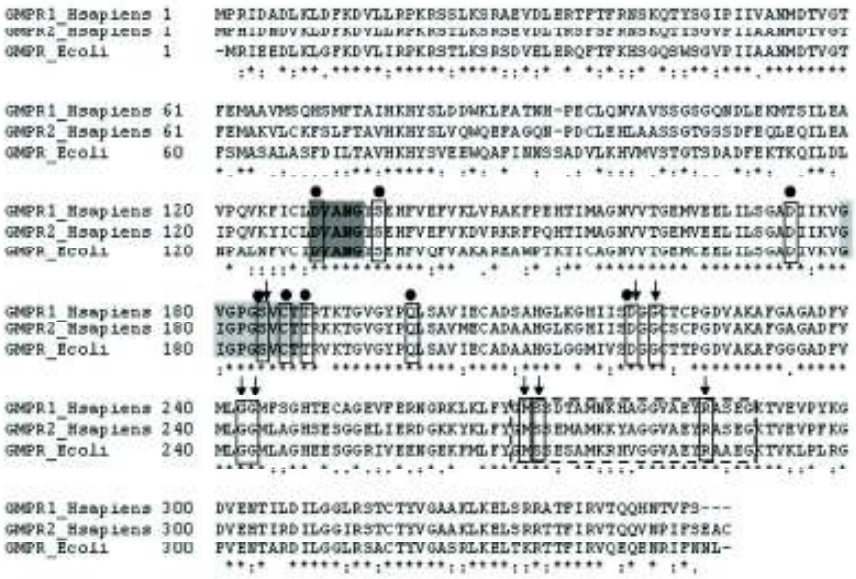

154x102mm (600 x 600 DPI)

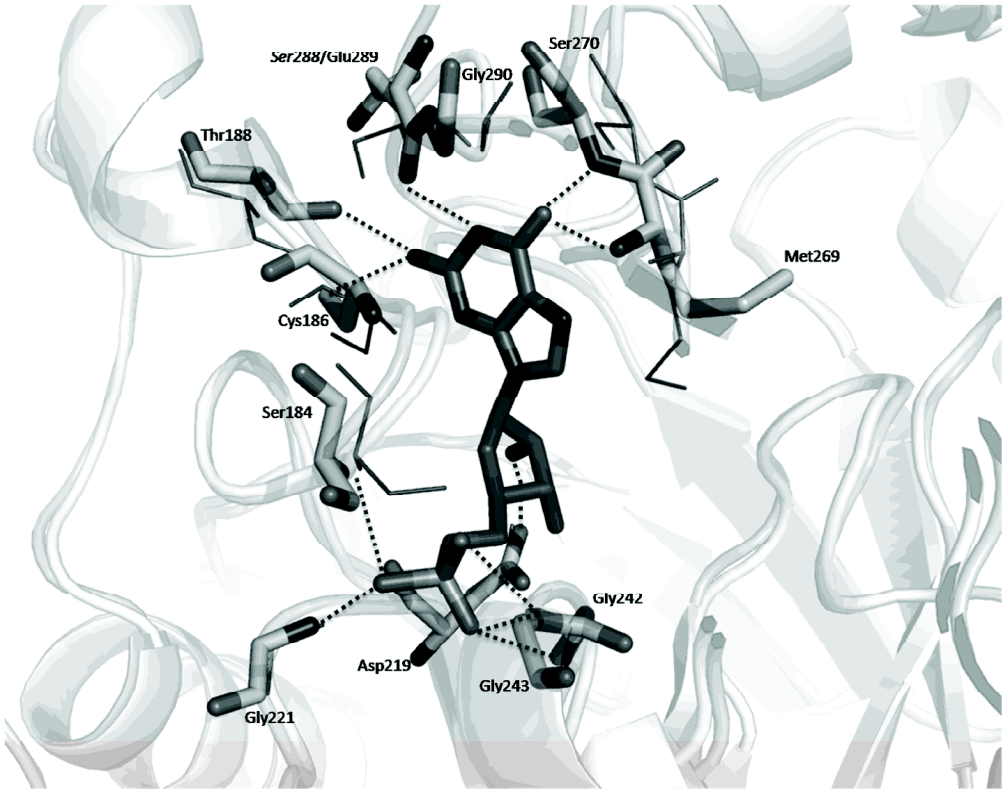

190x149mm (600 x 600 DPI)

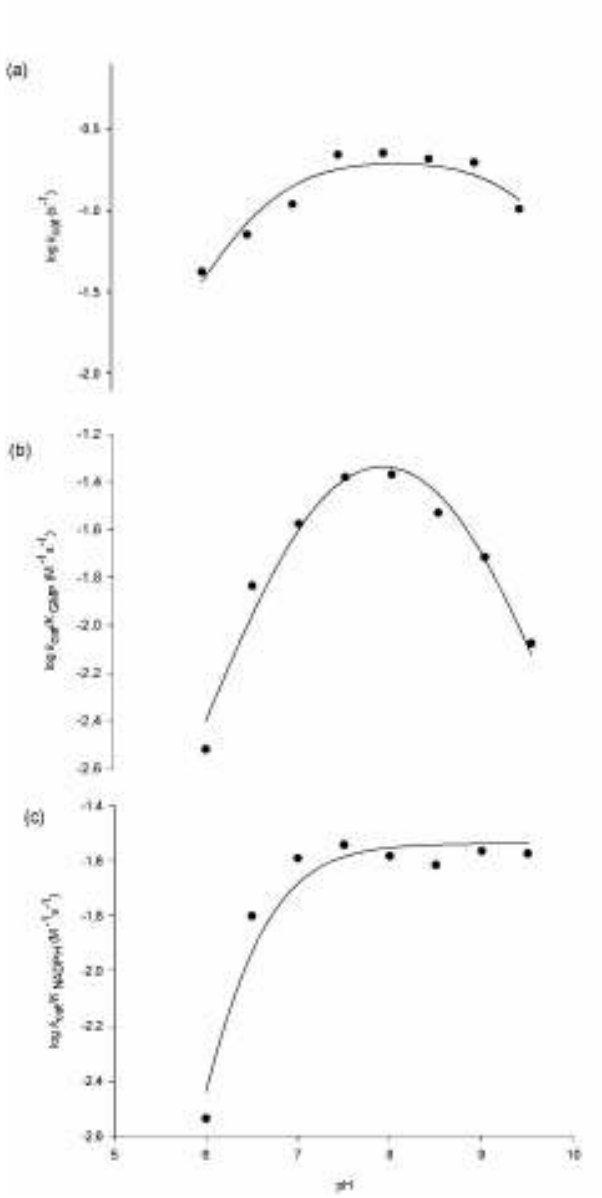

331x652mm (150 x 150 DPI)

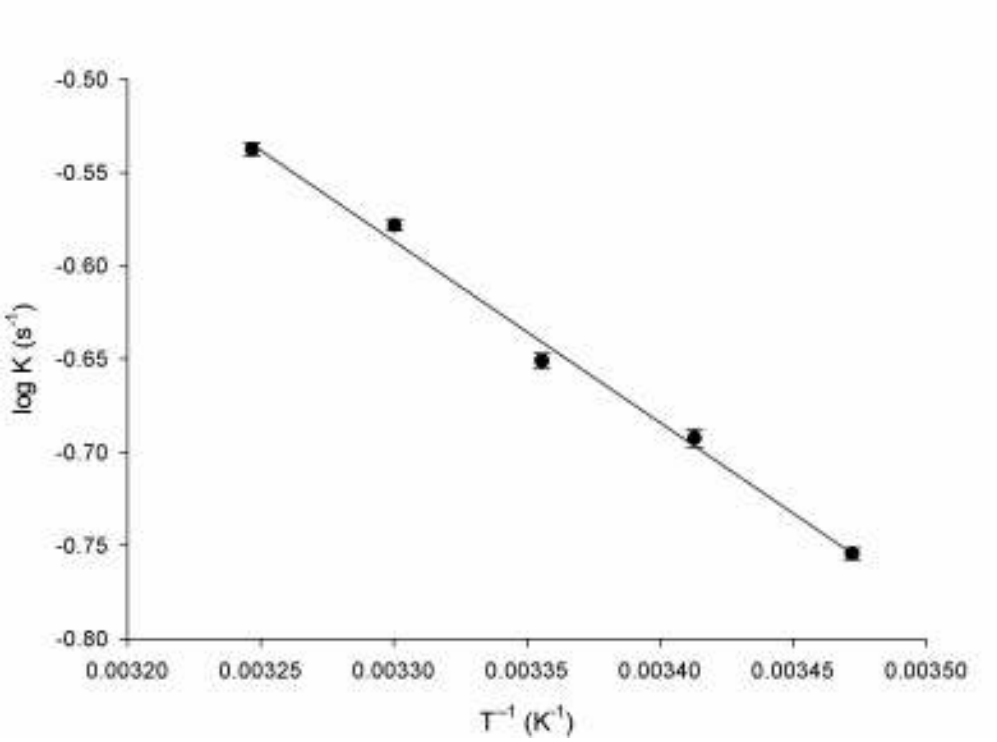

331x246mm (150 x 150 DPI)

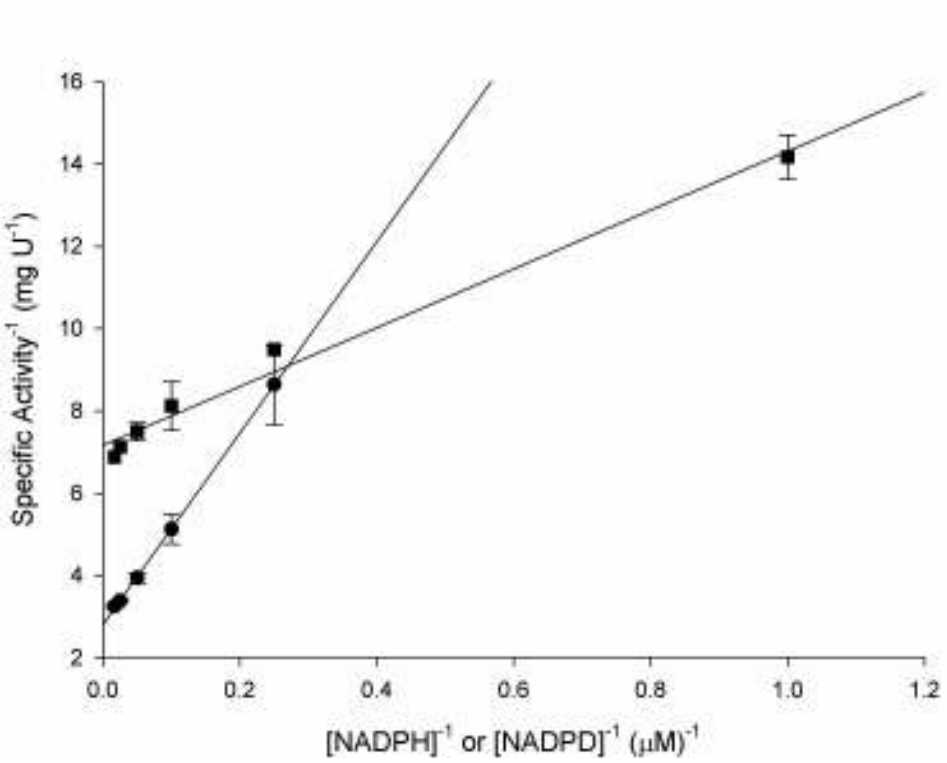

331x252mm (150 x 150 DPI)

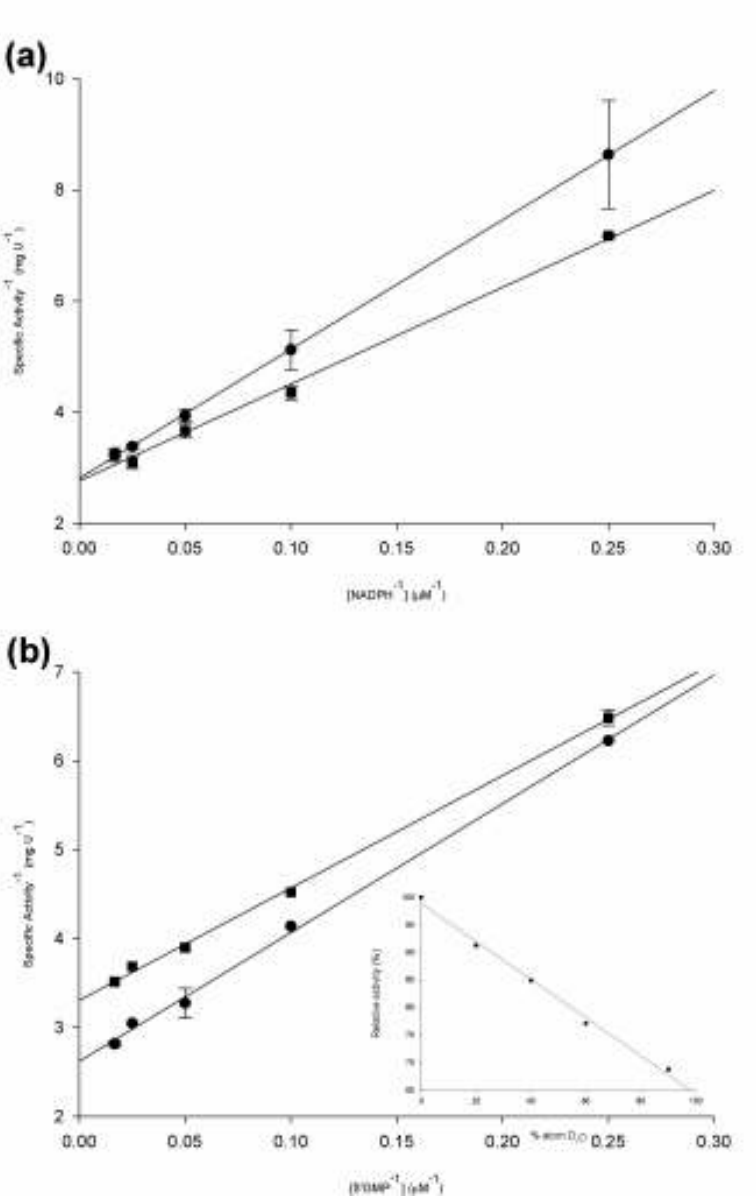

331x524mm (150 x 150 DPI)

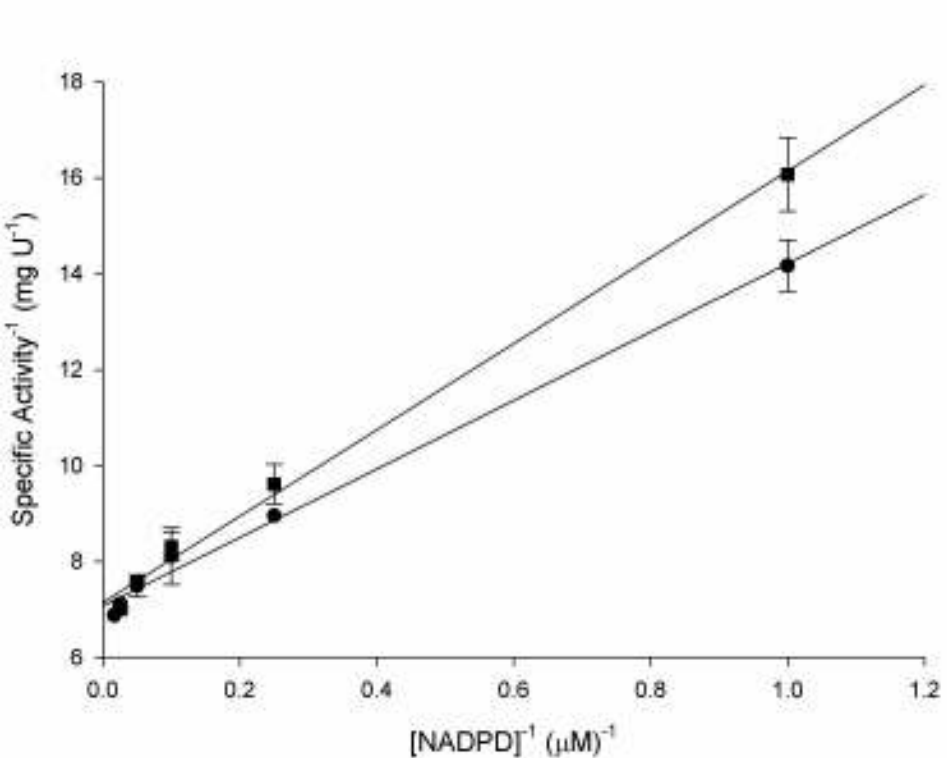

331x252mm (150 x 150 DPI)

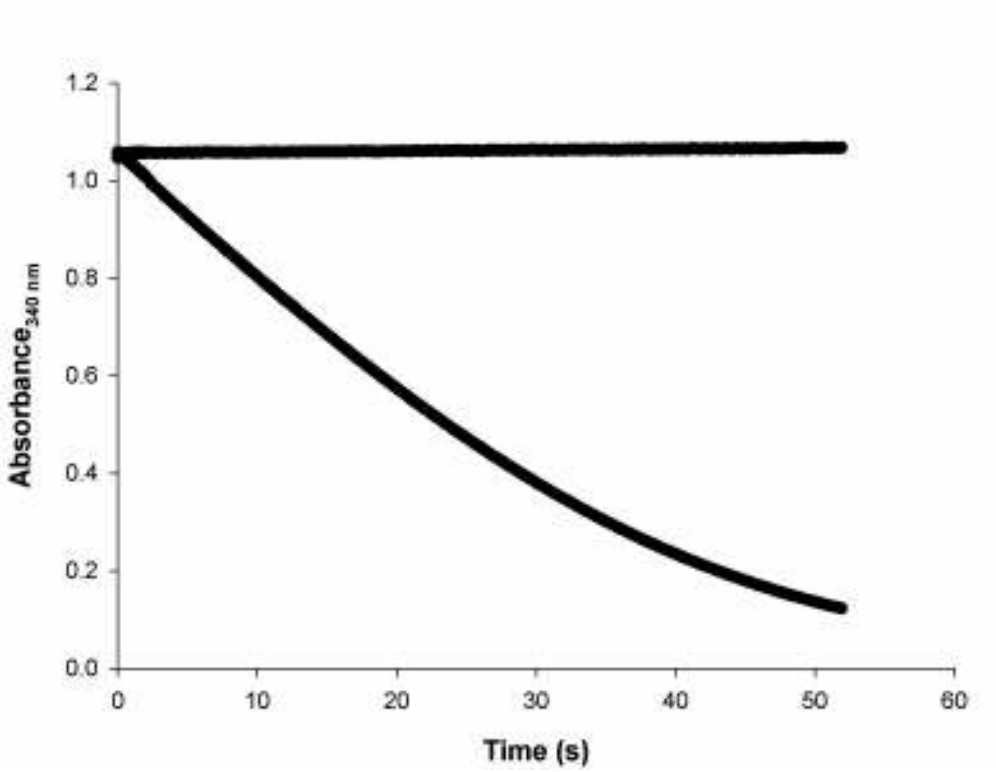

331x256mm (150 x 150 DPI)

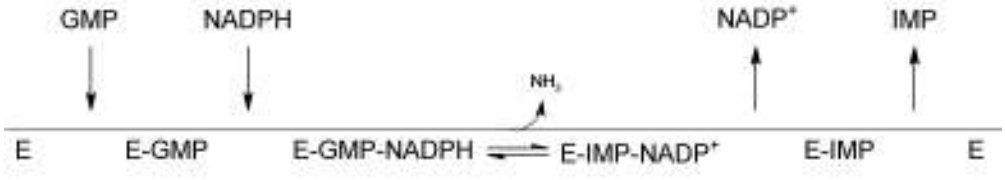

165x31mm (600 x 600 DPI)

The mode of action is described for recombinant *Escherichia coli* GMP reductase.